PHYSICAL VOLCANOLOGY AND FUTURE VOLCANIC RISK FROM TE MAARI CRATERS, TONGARIRO

A thesis
submitted in partial fulfilment
of the requirements for the Degree

of

Master of Science

at the University of Waikato
by

Ruth Basher

THE UNIVERSITY OF
WAIKATO
Te Whare Wānanga o Waikato

University of Waikato
2005

Abstract

The Te Maari Craters on the northern side of the Tongariro Cone Complex represent one of at least seven vent systems that have been active on Tongariro since the last glacial maximum. Activity at Te Maari had begun by at least 14 ka and has continued through historic times, making it one of the most long-lived of the young eruptives on Tongariro. The older lower crater is a wide (500 m), inclined, flat-floored structure up to 60 m deep, which exposes multiple layers of jointed andesite lava. The morphology of this structure implies some shallow collapse probably associated with withdrawal of a shallow magma chamber. The upper crater is a steep-sided, funnel-shaped feature constructed from weakly consolidated, very coarse, monolithic andesite breccia, and is largely the product of explosive eruptions through a pre-existing fan of thick, very coarse autobreccia. The most recent lava flow (probably around 1500 AD) and explosive ash eruptions (notably in 1892 and 1896) have been sourced from this upper crater. There are 4 older northern lava flows sourced from vents in the vicinity of the craters. From historic observations and analysis of the erupted products in the field, the typical eruptive style of these craters range from phreatic – phreatomagmatic to vulcanian. There is no evidence for more explosive sub-plinian eruptions from the Te Maari crater system.

The explosive eruption of 1896 was of sufficient intensity to disperse ash at least as far as the Hawkes Bay, and up to 50 mm of ash accumulated on the Desert Road. A repeat of this eruption today would cause severe disruption to agriculture and forestry operations, as well as critical transport and utility networks in the central North Island. The Tongariro Power Scheme would also be affected, as ash fall over Lake Rotoaira would cause damage to hydroelectric power facilities. A lava flow from these craters today on the scale of the 1500 AD flow would also have a major impact on transport networks if it reaches the State Highway, and outgassing would cause local acid rain and health problems in nearby communities such as Turangi and Taumarunui. The location of these craters close to the boundary of the national park also presents a unique hazard, as it would be difficult to prevent members of the public from gaining access to the area following an eruption and endangering their lives through curiosity.

Recent seismicity beneath the craters is a reminder that further eruptions are likely from the Te Maari system. Work on these craters to characterise the mechanisms, timing and magnitudes of typical eruptive activity contributes valuable information in the assessment of the probability and impacts of future eruptions.

Acknowledgements

Field work was a big part of this thesis and as such I spent a large chunk of 2004 on the mountain staying in Ketetahi Hut. Not only did I get to stay in beautiful surroundings but I met a lot of different people from all over the world and I have to thank the Department of Conservation, especially Jimmy Johnson, for allowing me to use this hut, and the various hut wardens for making my life much easier (and interesting!).

HUGE thanks to all the people who assisted me in the field. It was a mission every time I went up, but you made it so much easier and more enjoyable. So thanks Janine, Sarah M., Annett, Dad, Tim, but especially Daniel, who came up virtually every time and endured my more insane moments when things weren't going right. Also thanks to the people who helped me at Uni in the lab, Xu, Scott, Hadley, Dave, Annette and Debs, in sample preparation, analysis and general helpfulness.

Thank you to the Tongariro Natural History Society and the Waikato Graduate Women's Society for the much needed financial assistance. It was greatly appreciated and put to very good use.

Thank you to the Earth Science Department staff who all contributed to my learning and reaffirmed my decision to study in this field, but especially Richard and Roger, who reawakened a childhood fascination for volcanoes and inspired me to do something about it. Thanks Richard for being a fantastic supervisor and keeping me on the right track, providing help and encouragement for the many times when I needed it.

When you work for so long with a group of people you get to know them pretty well (both good and bad sides!) and I don't think I could have chosen a better group than my fellow thesis-writers. I wouldn't have been able to do this without you guys. You are my "rocks".

I would finally like to thank my long-suffering family and friends for keeping me sane during some of the harder times over the past six and a half years. I doubt I would have been able to keep it together without the help and support you gave me. Mum, Dad, Ellen, Nana, Nana and Grandad, (thanks for the use of your house!) Neville, Ben and Laree, you have all been amazing, giving advice and encouragement, or just being someone to vent to. Daniel, you not only helped physically (you are a great packhorse!) but also emotionally. Unfortunately this meant you usually bore the brunt of my worst days. Thank you for being there. And to everyone else I may have forgotten, it doesn't mean I don't appreciate you, it means I've just finished writing a thesis! Thankyou.

Table of Contents

List of Tables

List of Figures

CHAPTER ONE

Photo by Craig Potton (1995).

INTRODUCTION

1.1 Introduction

The Te Maari Craters are located on the northern flanks of Mount Tongariro, in the Tongariro Volcanic Centre (TgVC) (Fig. 1.1). They represent one of at least seven vent systems that have been active on Tongariro since the last glacial maximum. Activity at Te Maari probably had began by at least 14 ka and has continued through historic times, making it one of the most long-lived of the young eruptives on Tongariro (Hobden, 1997).

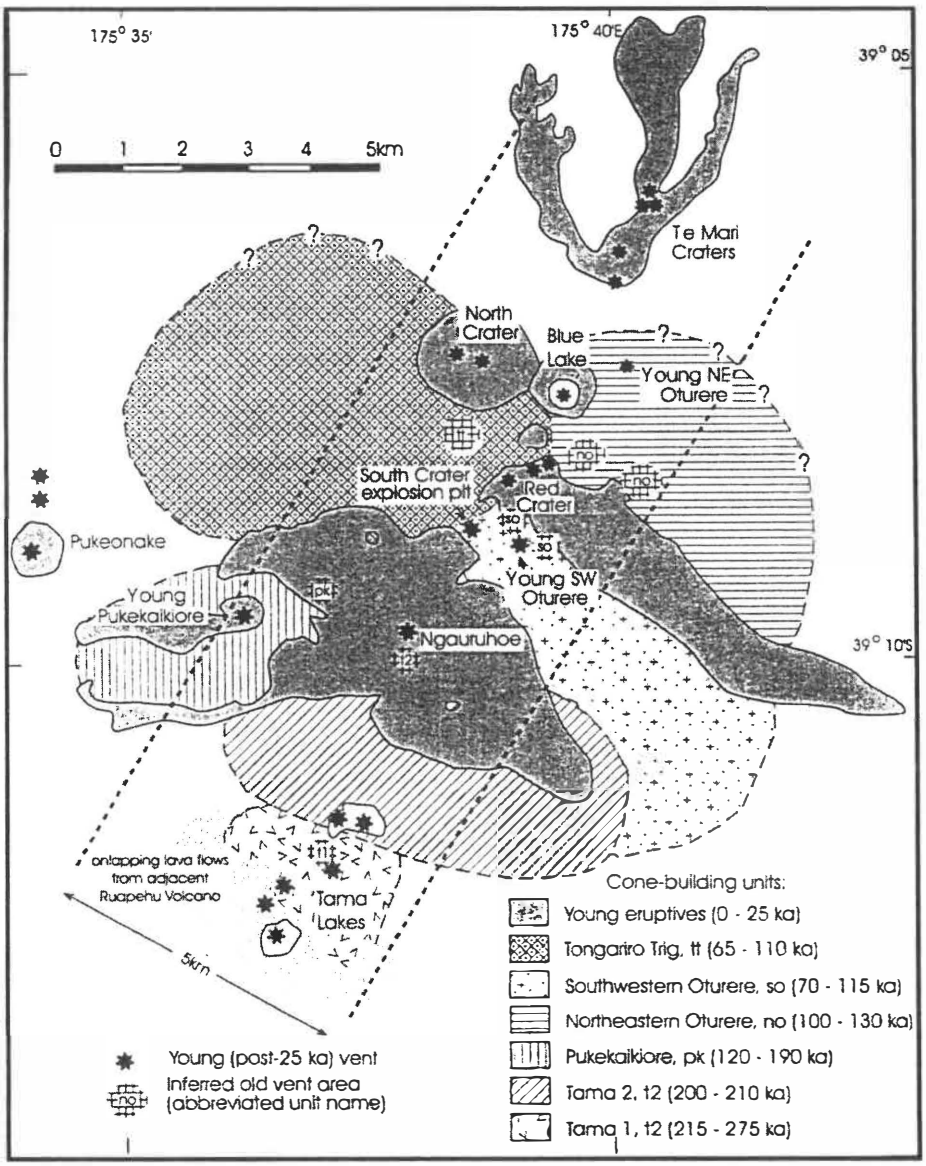

Figure 1.1: Map of Tongariro Volcanic Complex with location of Te Maari Craters, regional geology and main (< 50 ka) vents. After Hobden *et al.*, (2002).

The Te Maari Craters were first called Puia Hou, or New Puia when they erupted with Ngauruhoe in 1868-69. They were renamed Te Maari after the sister of Matuahu, chief of Otukau, whose death was supposed to have been hastened by the eruption of these craters (Hill, 1891).

There have been numerous observations made of the Te Maari Craters, both in eruption and during time of quiescence, but they have previously only been studied in conjunction with larger investigations of the Tongariro massif.

This chapter outlines the objectives of the thesis, the geological setting of the Te Maari Craters and previous work that has been done.

1.2 Study Objectives

The general aim of this study is to characterise the nature, timing and magnitude of past eruptions at Te Maari. A particular focus has been examination of the volcanic geology of the craters themselves and the associated eruptive products. An accessory objective has been to attempt to constrain aspects of the physical volcanology of the historic ash-producing eruptions, providing a likely future eruption scenario for modelling ash impacts on infrastructure and agriculture in the central North Island.

1.3 Geological Setting

The Te Maari Craters are located within the TgVC, which forms the southern most point of the Taupo Volcanic Zone (TVZ).

The TVZ is a NNE-SSW trending continental rifted volcanic arc which is the dominant location for volcanic activity during the late Pliocene to Quaternary in New Zealand, producing >90% of eruptives in this period. This TVZ is a manifestation of subduction

of the Pacific plate beneath the North Island (Fig. 1.2) (Wilson *et al.,* 1995) along the Hikurangi Trench.

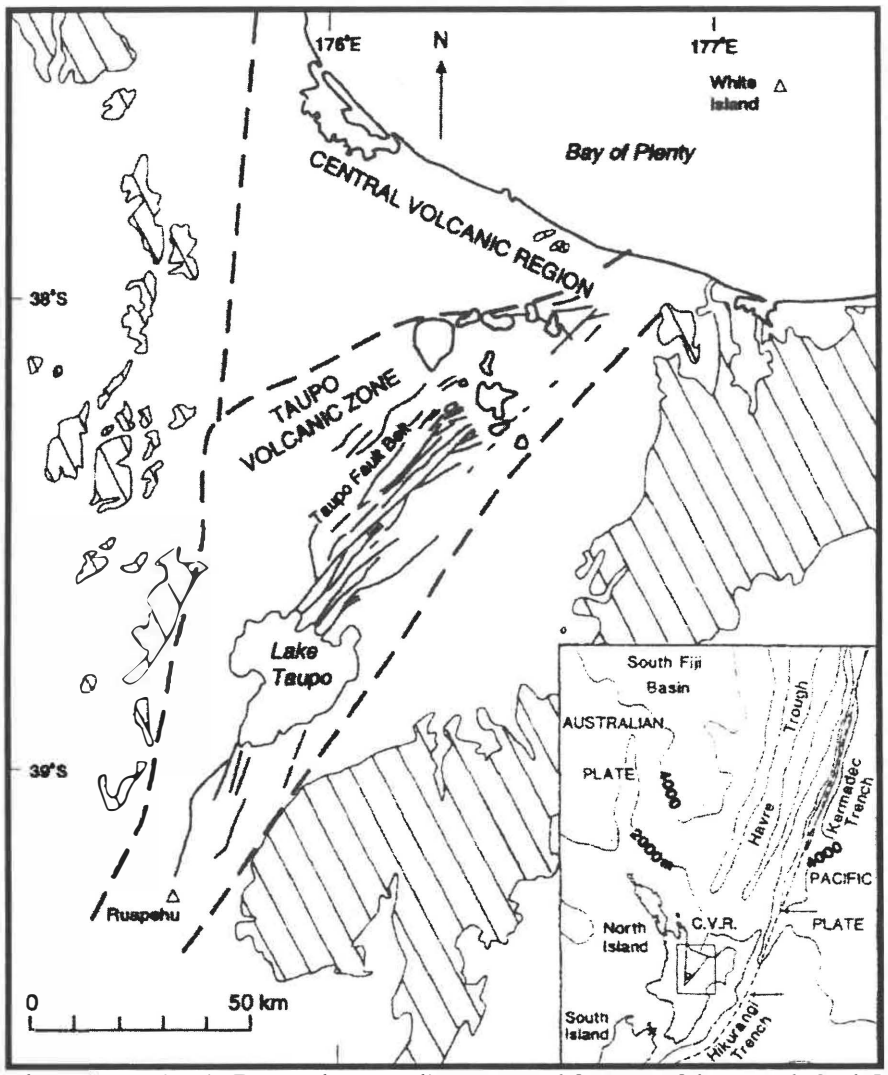

Figure 1.2: The Taupo Volcanic Zone and surrounding structural features of the central North Island. Insert shows bathometric contours, which outline offshore structure. Hatched regions show greywacke outcrops. After Bibby *et al.,* (1995).

The TgVC is an andesite-dominated cluster of volcanoes at the southern end of the TVZ. The TgVC includes the four large, andesite volcanoes of Kakaramea, Pihanga, Tongariro and Ruapehu; two smaller eroded centres, Mangakatote and Hauhungatahi; a satellite cone and associated flows, Pukeonake; and four craters near Ohakune (Cole, 1990). The vents for the young (post-glacial) eruptives are considered to lie in a NNE-trending alignment over a major basement fracture within a graben that has been defined by

normal faults (Nairn *et al.,* 1998). Mount Tongariro is a young, active dacite-andesite cone complex, the exposed portion of which has been growing steadily since at least 275 ka. Intervals of rapid cone growth have occurred at 210-200, 130-70 and 25 ka to the present (Hobden *et al.,* 1996, Hobden *et al.,* 2002). The Te Maari Craters are the northernmost vents on this complex, and are located above a concealed fracture zone within the same (NNE) regional trend (Walsh *et al.,* 1998). Underlying Tongariro there is also a substantial geothermal reservoir, which has been pierced by magma feeding flank eruptions at Red Crater and Te Maari Craters during the last century. A cross-section derived from magnetotelluric and DC resistivity measurements suggests a substantial, vapour-dominated reservoir capped by a 100-300 m thick condensate layer (Walsh *et al.,* 1998). The vapour reservoir can be linked to surface manifestations at Ketetahi Hot Springs and minor steam discharges at Red, Central and Te Maari Craters (Hagerty and Benites, 2003).

The morphology of the craters today consists of an older lower crater, which is a wide (500 m), inclined, flat-floored structure up to 60 m deep, which exposes multiple layers of jointed andesite lava. The upper crater is a steep-sided, funnel-shaped feature constructed from weakly consolidated, very coarse, monolithic andesite breccia. There is a cluster of craters located directly north of the Lower Crater and large lava flows sourced from Te Maari can be seen on the northern slopes of Tongariro.

1.4 Previous Work

There have been a number of historical observations and accounts of eruptions at the Te Maari Craters. Hill (1891) describes the volcanoes of the TgVC, which includes a description of Te Maari presenting "special features both curious and suggestive to the student of vulcanology". At the time his paper was published there were three craters in the location of Upper Crater, with circular shafts at the centre of each, from which steam, "containing a good deal of sulphuretted hydrogen is constantly rising". He concluded that the shafts were of great depth after rolling boulders into them and listening to the rebounds. It was also noted that dense clouds of black smoke, but no eruption, was sent

out by these craters at the time of the Tarawera eruption and rumblings were heard for days before. Hill (1891) proposed that the craters were formed by a "gyrating process from below", causing the overlying mass to give way and form the irregular-shaped craters. He also thought further consideration should be given to whether the opening of the shafts was a precursor to further volcanic activity or a phase of decay.

Hill (1894) gives a description of the craters following eruptions in 1892. This paper provides more detail about Te Maari, including the lower crater, which is described as being "quite extinct" with "banding in the walls of different lava-streams". There is also an outline of the planning and preparation of the ascent, eventually finding a route that was comparatively easy, "so much so, in fact, that ladies could ascend the mountain by this track without much difficulty". Evidence of an eruption was apparent from the camp site, located on the south shore of Lake Rotoaira and the "gut" that was used to ascend the mountain had evidently been washed out by water, sand, mud and stones that were ejected from Te Maari (Hill, 1894). When the party reached the lower crater the extent of the eruption was seen, with an "enormous fissure" having been opened through the shafts of Upper Te Maari Crater and along the slope of the mountain. Gases and fumaroles made it too dangerous to get close to the rift, however mud and water were observed on the northeast side of the crater. It was observed near the rift that water, sand and small stones were the only ejecta from the eruption, but higher up Tongariro a thin deposit of pumice was found. From eyewitness accounts of the eruption and his own observations Hill concluded that two eruptions took place at Te Maari, the first ejecting water and sand while the wind was from the southwest, the second explosion ejecting pumice and taking place when the wind had changed direction.

The most detailed eyewitness account of an eruption at Te Maari is included in a paper produced by Friedlander (1898). On December 11th, 1896 Friedlander was camped about an hours distance below Ketetahi Springs when his camp was awakened by a thundering noise. A gigantic pillar of ash was observed from Te Maari along with a "wonderful display of different kinds of light phenomena". Later Friedlander summarised these phenomena into four groups: the reflection of the incandescent matter on the steam;

"sparks", which turned out to be large red-hot boulders that were shot into the air; electric lightning and blue flames. He got an impression of relatively cool, viscous magma, although he could not explain why it was only visible at intervals. Friedlander goes on to compare this eruption with activity witnessed from Vulcano, the island from which the term "vulcanian eruption" was derived.

Gregg (1960) again provided a description of the craters as part of a survey on the Tongariro Subdivision. This included a transcript of the only description of the lower crater before the eruption of 1869, which is when the upper crater is thought to have been formed (Gregg, 1960). The account is from the field notebook of Sir James Hector, who visited Te Maari on 23 November 1867. He called the lower crater the "great Ngawha" and described a lake of brown-coloured water, in the centre of which there was a conical mound of white sinter about 200 ft across. Subsequent descriptions (>1890) do not mention this sinter mound, implying that it was destroyed in the 1869 eruption. Observation was difficult due to the amount of steam that was being discharged. The slopes were covered in sinter fragments but no scoria was evident (Gregg, 1960). Gregg also summarised a number of observations that were made on eruptions occurring at Te Maari throughout the 1800's, the final being Friedlander's account in 1896. He concludes by briefly describing the young lava flow from the Upper Crater and a cluster of explosion craters directly north of Lower Crater.

Topping (1973,1974) studied the quaternary history of the TgVC and looked at the tephrostratigraphy of these eruptives. He identified the Tongariro Sub-group as all tephras from the present day to 13 000 years B.P. that have originated from within the TgVC. This includes source vents of Mount Ruapehu and Ngauruhoe, Tama Lakes, Blue Lake, Red Crater, North Crater and Upper and Lower Te Maari Craters. The tephra formations within the Tongariro Sub-group that were sourced from the Te Maari Craters include Ngauruhoe Tephra, possibly Papakai Tephra and Rotoaira Lapilli (Fig. 1.3) (Topping, 1973).

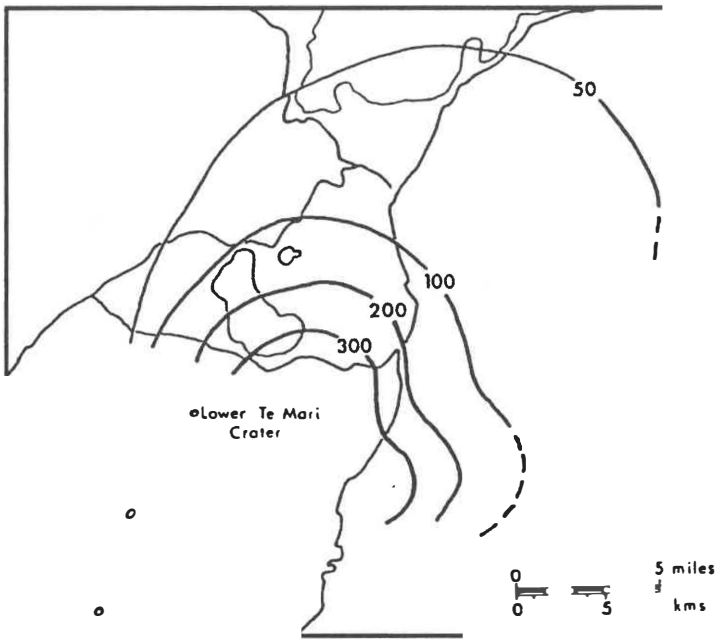

Figure 1.3: Isopachs (mm) of Rotoaira Lapilli Formation. Was not mapped further south due to lack of deep sections. After Topping (1973).

Topping (1974) summarised reports of eruptions from the craters in 1855, 1869, June 1886, November 1892 to January 1893, November-December 1896 and possibly in 1928. He identified andesite gravel and sand deposits on the National Park-Taupo Road (SH47a) as being probably sourced from the Te Maari Craters. These deposits occur above and below Taupo Pumice and above basal Mangawai Tephra, which suggested at least one of the craters has been active for 2,500 years (Topping, 1974). Deposits found beneath the 1895 AD Mangatipua Mudflow, sourced from Ketetahi Springs, and above a paleosol overlying the young aa flow from the upper crater were also sourced as tephras from the Te Maari Craters. One conclusion reached for the reduction in tree-ring width from cores taken for the dating of the Mangatipua Mudflow was that it could be attributed to eruptions from the Te Maari Craters during August 1869 (Topping, 1974). The Rotoaira Lapilli Formation was identified as most probably sourced from Lower Te Maari Crater about 13,800 years BP., using titanomagnetite analysis to compare the Rotoaira Lapilli with two lavas exposed in the Lower Crater (Topping, 1974). New mapping in this study and by Tetsuo Kobayashi (Univ. of Kuyoshima) suggest North Crater is a more likely source for the 13.8 ka Rotoaira event.

Topping was the first to describe in detail the large lava flow directly north of the Lower Crater as a large, levéed aa flow approximately 90 m thick, which probably began as a cumulodome as suggested by the topography across the northern cluster of pit craters. He describes two large collapse features and five younger explosion craters at the distal end of the flow, and uses the position of Papakai Tephra above the lava to estimate an age of between 9,700 and 6,000 years B.P. (Topping, 1974).

Topping identified the source of the youngest lava flows as the Upper Te Maari Crater, one flowing into the lower crater and others flowing northwest down into Okahukura Bush. The flows are younger than the Taupo Pumice and radiocarbon dating of wood collected from beneath the lava led to an assertion that they were erupted within the last 1819 years B.P. Topping cored four trees from the margins of the flow in an effort to determine its age. One of the trees cored (Podocarpus hallii) was apparently tilted by a block of the lava flow, through either having physically been tilted by the flow or growing towards the light from a nursery position close under the block. Using tree-ring dating on these cores it was estimated that if the tree was not tilted by the flow, then the lava was probably extruded before 1542-1514. If the tree was tilted by the flow then the age is slightly more recent than 1528 AD. Topping concluded that activity from the Te Maari Craters probably began 14,000 years B.P. and has continued through to the present (Topping, 1974).

Hobden (1997) described the volcanic stratigraphy of the Te Maari Craters, stating that at least 15 lava flows and pyroclastic units could be recognised from the northernmost vents. The flows sampled in this study were all identified as andesitic with SiO_2 ranging from 57.5 to 60.2 wt%. The lava flows on the northern and eastern slopes and those exposed in the Lower Crater were described as 2-8 m thick, blocky to platy-jointed with some flows displaying levée development. Good exposure in the Upper Crater revealed a sequence of an upper, bedded tuff breccia, a lower, massive block tuff breccia and a central hydrothermally altered vertical vent structure infilled with blocky tuff breccia (Hobden, 1997). The Te Maari breccia unit was found to cover 6 km^2, and represent a small volume of c.0.2 km^2. The eruptive style of the craters was thought to range from

effusive to phreatic and phreatomagmatic explosions, to subplinian lapilli fall events (Hobden, 1997).

Hobden (1997) also analysed the magma composition of the 1500 AD lava flow from Upper Crater samples taken in the field as part of a larger study into the petrogenesis and time-space relationships of magma batches at Tongariro. The Te Maari Craters flow was found to occupy the highest SiO_2 section of the MgO-SiO_2 diagram, which discounted them as parental to any other eruptives. Based on geochemical analysis and the lack of consistent AFC trends, it was concluded that the plumbing systems for Ngauruhoe, Red Crater and Te Maari Craters were not closely inter-connected over the last thousand years or so. This presents the probability that several spatially separate reservoirs coexisted, feeding vents a few kilometres apart (Hobden, 1997).

Hobden *et al.,* (1999, 2000) expanded on this, including a schematic representation of the growth of the Tongariro cone complex (Fig. 1.4) and further geochemical analysis of the young eruptives, separating them into five groups from Ngauruhoe and two from Red Crater and Te Maari Craters (Fig. 1.5). This again provided support for numerous small, short-lived magma chambers frequently erupting from a complex plumbing system beneath Tongariro (Hobden *et al.,* 1999).

Other geochemical results also showed the close spatial and temporal proximity of the young northern andesite cones and eruptives, including similar K/Rb and Rb/Zr, and $^{87}Sr/^{86}Sr$ ranging 0.705126-0.705700 (Hobden *et al.,* 2000).

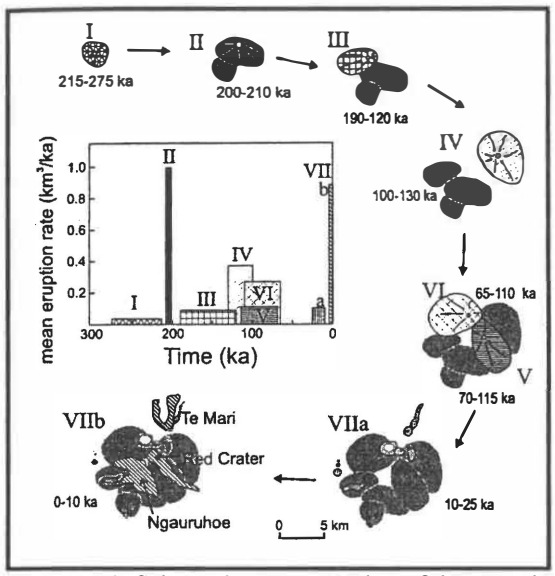

Figure 1.4: Schematic representation of the growth Tongariro cone complex. I-VII = main periods of cone-building. After Hobden *et al.*, 1999.

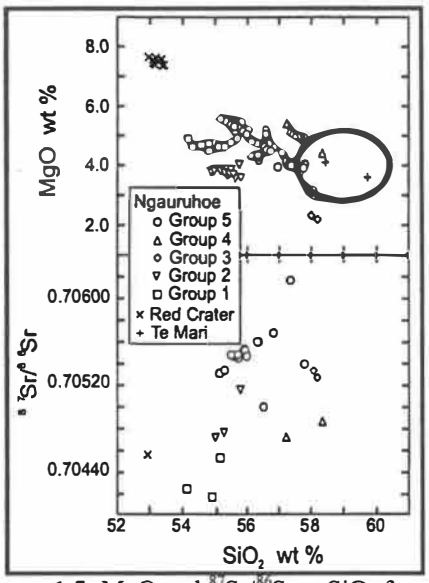

Figure 1.5: MgO and $^{87}Sr/^{86}Sr$ v. SiO_2 for of the young eruptives in a 1000 year time window. After Hobden *et al.*, 1999. Te Maari eruptives circled.

Nairn *et al.*, (1998) identified a period of uniquely intense activity at Tongariro at ~10 ka. This andesitic/dacitic sequence was named Pahoka-Mangamate (PM) and includes six named tephras (PM1-PM6) and two unnamed tephras erupted from multiple vents that were active during this period (Nairn *et al.*, 1998).

From mapping the PM deposits, Nairn *et al.*, (1998) established that there are two possible phases in the PM sequence where the Te Maari Crater vents may have had minor involvement. The main PM2 source location was identified as a now buried vent under Ngauruhoe cone. This deposit was found preserved beneath an explosion breccia erupted from Te Maari, leading to the conclusion that immediately after the PM2 event there were small explosive eruptions at Te Maari (Nairn *et al.*, 1998). The PM6 eruption was sourced from the Tama Lakes area. A poorly exposed coarse breccia containing arcuate-fractured magmatic bombs was found locally intercalated within Te Maari-sourced explosion breccias. These breccias were thought to have resulted from small eruptions probably during the PM6 episode (Nairn *et al.*, 1998). The large lava flow directly north of the Lower Crater, described and dated at ~10 ka to 6 ka by Topping (1974), is also thought to have been extruded at the end of the PM eruptions (Nairn *et al.*, 1998).

Hagerty and Benites (2003) investigated unusual seismic activity beneath Tongariro volcano. The low-frequency seismic events (tornillos) appeared to have similar waveforms to those recorded at Galeras Volcano, Colombia, which were found to precede small to medium-sized ash eruptions (Hagerty and Benites, 2003). The tornillos were first detected in June 2001 as part of a routine monitoring surveillance, but were found to have been occurring since at least January 2001, their small amplitude and infrequency proving difficult to identify. Further investigation using temporary seismic monitoring stations showed a complex mixture of seismic waves and identified the epicentre as below the Te Maari Craters area at a shallow depth (Hagerty and Benites, 2003). The tornillos were found to consist of two parts, a low-frequency and a high-frequency. By combining data from several deployments it was found that a spatial separation between these two components existed, with the low-frequency region near the top of a vapour dominated geothermal reservoir and the high-frequency region located at depth below the vapour zone within brittle rock (Fig. 1.6).

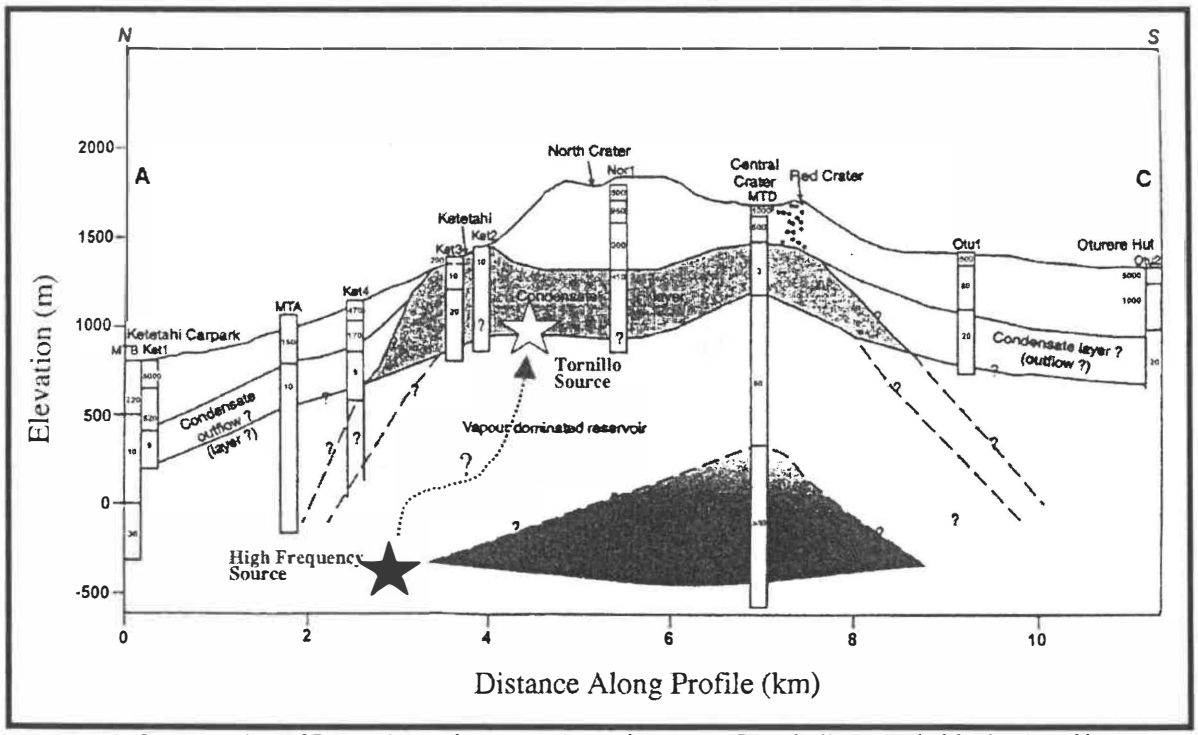

Figure 1.6: Cross-section of Tongariro Volcano geothermal system. Stars indicate probable depths of low-frequency and high-frequency components of the tornillo waveforms. After Hagerty and Benites (2003).

Because of the apparent depth of the low-frequency energy, samples were taken from fumaroles and springs in the area and analysed for evidence of magmatic input. While there is magmatic influence on this geothermal system, there was no significant change in chemistry that may have indicated fresh magmatic intrusion (Hagerty and Benites, 2003).

CHAPTER TWO

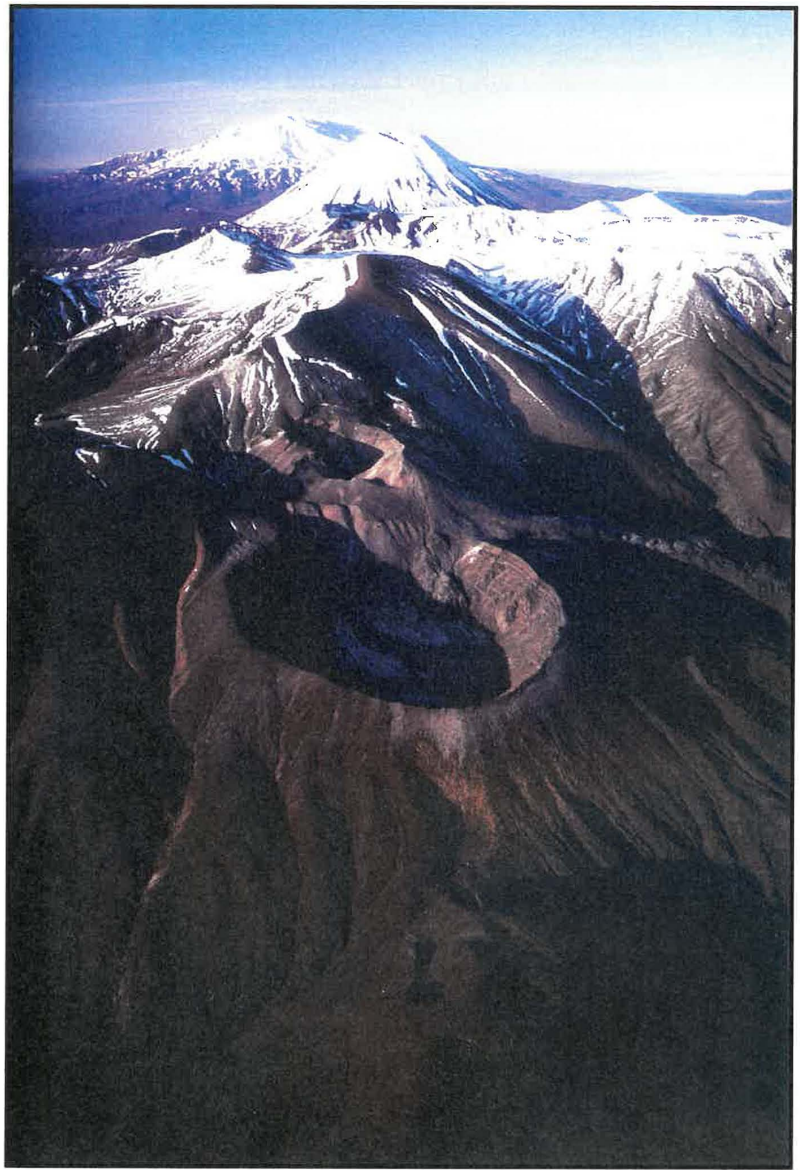

PRODUCTS AND STYLES

2.1 Introduction

The Te Maari Craters are a multiple crater system on the north eastern flank of Tongariro, excavated by predominantly vulcanian to phreatic activity but also the source of recent voluminous lava flows. They are the northernmost vents of the highly active Tongariro composite volcano that has evolved through vent migration into a complex of discrete, nested and overlapping cones and craters.

Vulcanian eruptions are characteristically small, violent outbursts with non-sustained eruption columns. This generally corresponds with historic eyewitness accounts of activity for Te Maari and products found in field at Te Maari. Ash deposits and block fields attest to this minor explosive activity.

Many of the deposits found in the Te Maari Craters are typical of andesitic composite volcanoes. Lithologies include massive and bedded mega-breccia within the Upper Te Maari Crater, pre-glacial andesitic lavas exposed in the wall of the Lower Te Maari Crater, and several large post-glacial aa lava flows erupted from multiple vents in the Te Maari Crater system.

The products resulting from eruptions of the Te Maari Craters are discussed in this chapter, including the processes and types of eruptive activity that formed them.

2.2 Composite Cones

Composite cones are the most obvious and recognisable types of large volcanic edifice. They have produced the most well known historic eruptions and are the sources of a wide range of volcanic products. They generate fertile volcanic soils that are renewed through frequent eruptions, creating hazards for human populations that have settled close to the surrounding ring plain (Davidson, 2000). The term "composite" has been used to describe many volcanic cones. They are large volcanoes that consist of multiple volcanic

landforms such as interlayered pyroclastic rocks, lava flows, domes and volcanic sediments (Wohletz & Heiken, 1992). This classification overlaps with many other edifice types and may incorporate smaller volcano types. Compound volcanoes also fall within this classification and denote an edifice comprising multiple cones, which has resulted from vent migration over time (Davidson, 2000).

2.2.1 Distribution

Although composite volcanoes can be found in nearly all regions of volcanism, they are most commonly found overlying subduction zones forming island arcs or volcanic chains (Wohletz & Heiken, 1992). Magma compositions at plate margins are largely the result of differentiation and volatile concentration. By the time they reach the surface they tend to have differentiated to basaltic andesites and andesites (Davidson, 2000). In areas where there is prolonged differentiation, large volumes of rhyolite may be also be produced, leading to explosive, caldera-forming events. This is the case in the TVZ where composite volcanoes and calderas are contemporaneous, varying slightly in location and zones of magmatism (Davidson, 2000).

2.2.2 Morphology

Most composite volcanoes have the classic concave-upward profile, indicating an equilibrium or steady-state profile of an active volcano (e.g. Mt. Ngauruhoe, Tongariro) (Davidson, 2000). On average a composite cone is about 2 km high but the structure may contain a complex history (Francis, 1993), with slopes made of up innumerable layers derived from secondary volcanic deposits interspersed with explosively produced pyroclastic layers and lava flows (Fig. 2.1) (Fisher *et al.,* 1998).

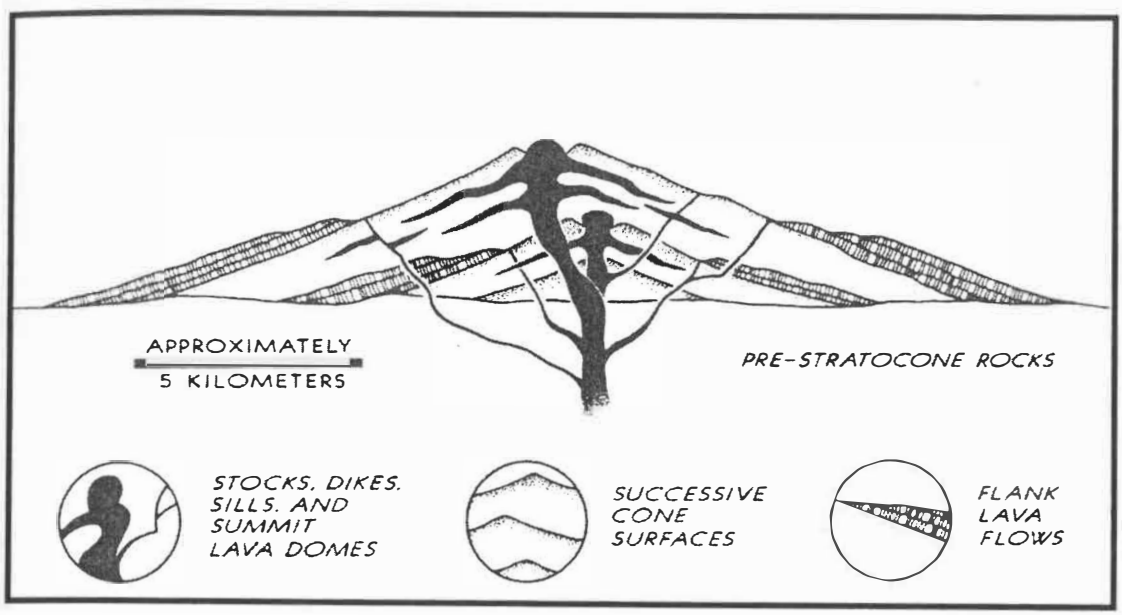

Figure 2.1: Conceptual diagram of a composite volcano showing multiple layers and magma intrusions. After Fisher *et al.*, (1998).

As the volcano grows the upper slopes become steeper, and so gravitationally unstable. This is enhanced with dome intrusion and hydrothermal alteration (Schmincke, 2004). Debris avalanches are occasional events on these inherently unstable structures, resulting from a number of triggers, probably most frequently earthquakes (e.g. Mt. St. Helens, 1980) (Davidson, 2000). There is evidence on the ring plain of many composite volcanoes of past debris avalanches (e.g. Taranaki, New Zealand).

The classic cone profile (Fig. 2.1) is formed through the constancy of vent location over time. However, composite cones in volcanic arcs usually evolve, growing from simple cones into multiple cones, domes and craters (Fig. 2.2) (Wohletz & Heiken, 1992).

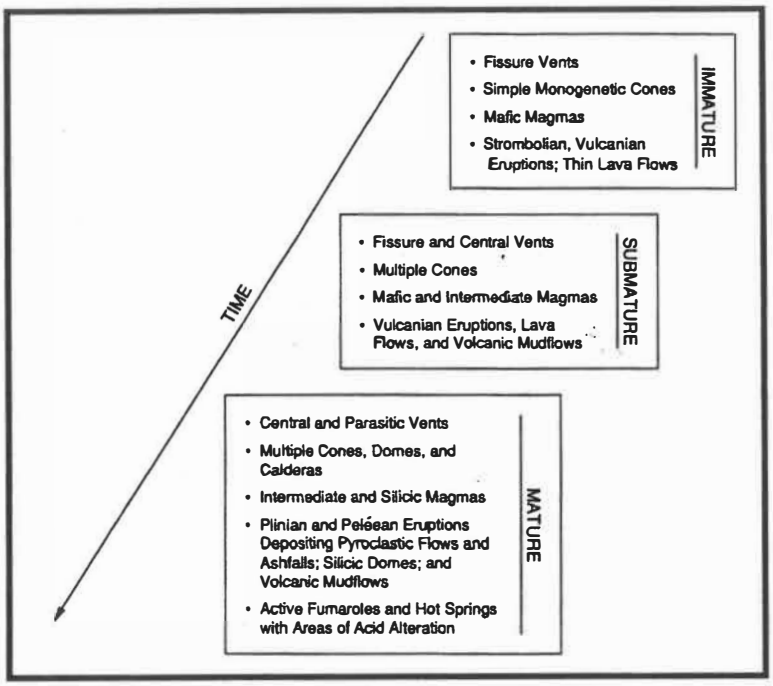

Figure 2.2: The evolution of composite cone volcanoes. After Wohletz & Heiken (1992).

The compound volcano of Tongariro is a good example of this, resulting from the migration of volcanic activity within a 5 km wide, 13 km long corridor. This process typically forms an elongated ridge or large massif with a migrating summit complex. Tongariro is an extreme example, as it has a cluster of as many as 30 small discrete or overlapping edifices (Fig. 2.3) (Davidson, 2000). The geology of compound volcanoes is difficult to unravel as the nested and overlapping cones make individual volume determination and rates of cone growth almost impossible. Stratigraphic analysis is also problematic, as there are a number of potential source vents in close proximity (Davidson, 2000).

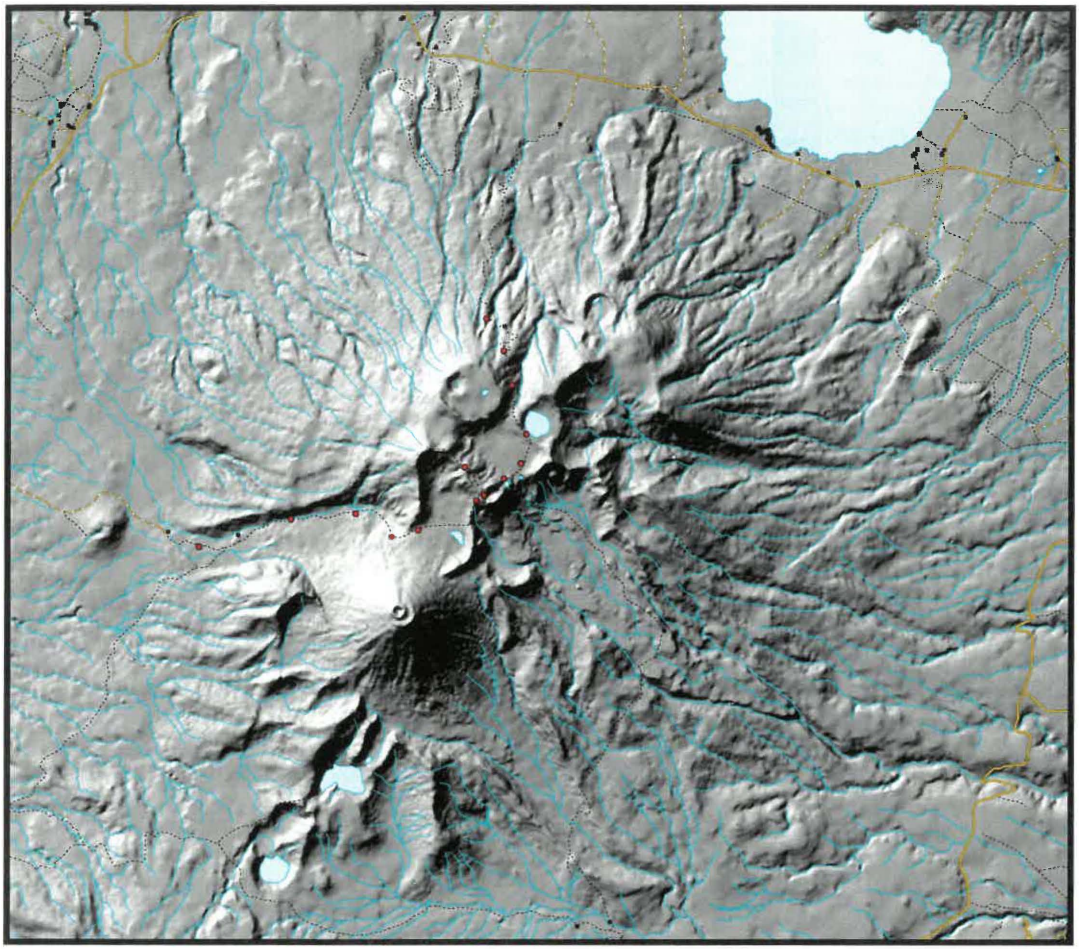

Figure 2.3: DEM of Tongariro volcano showing multiple craters and cones with linear alignment parallel to the local tectonic grain (NE-SW). DEM by Arne Pallentin, University of Waikato.

2.2.3 Product Characteristics

The materials produced by composite volcanoes can be grouped into three main facies groups or associations, relating to their proximity to the vent (Fig. 2.4) (Davidson, 2000).

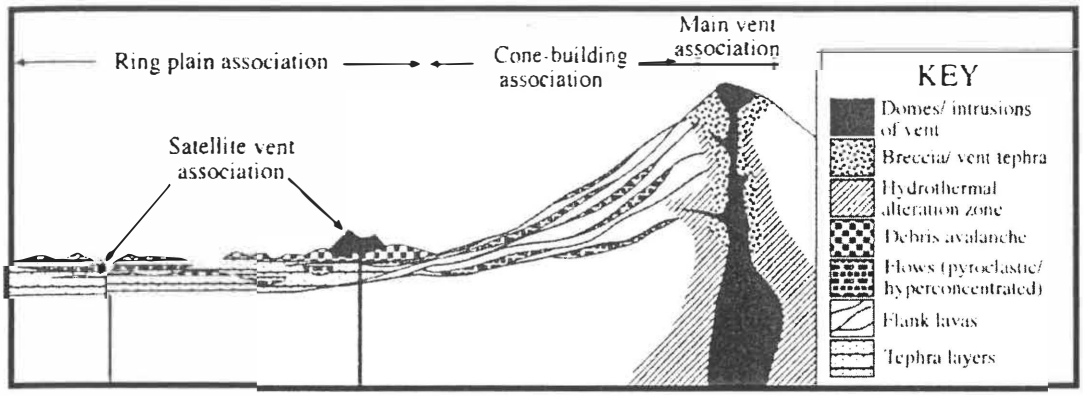

Figure 2.4: Schematic diagram of lithofacies associated with composite cone volcanoes showing types and distributions of deposits. After Davidson (2000).

Main Vent Facies Association

This is defined as "lithologies related to long-term vents at which volcanic products are erupted to the surface". For compound volcanoes the vent would change location a number of times in its history (Davidson, 2000).

There are two main lithofacies found in this area. Vent filling breccia comprised of wall rock material from the vent and coarse tephra commonly welded close to the vent (Davidson, 2000). However, not all of the rising magma makes it to the summit. Some magma penetrates through the layers to form sills or dikes and this can help to build a framework that can support the accumulation of deposits to a greater height (Fisher *et al.*, 1998). These materials are commonly overprinted by zones of variable hydrothermal alteration.

Cone-Building Facies Association

The lithofacies that are found in this area are those that build up the main volcanic edifice (Davidson, 2000). They include many different generations of lava flows, many brecciated, and a number of pyroclastic and reworked epiclastic rocks. The percentage of clastic deposits increases as distance from the vent increases (Schmincke, 2004). Most lava flows are distributed radially from the main vent and can be further reworked and removed from the upper slopes and deposited further down the slope or on the ring plain (Davidson, 2000).

Ring Plain Facies Association

The ring plain is the area directly surrounding the flanks of the cone. It is dominated by fall-tephra and reworked tephra from the cone (Davidson, 2000). The tephra layers can be interbedded with lahar deposits and debris avalanche deposits, which become more common with distance due their high mobility (Schmincke, 2004). The deposits tend to be more continuous and widely dispersed than on the edifice, with wind strongly influencing distribution of tephra (Davidson, 2000). Evidence for youthful debris avalanches can be distinguished in the ring plain by a hummocky topography, for example, at Mt. Ruapehu around the intersection of SH 47 and SH 48, and in the vicinity of Mt. Taranaki at Opunake.

Composite cones are made up typically of more than 90 percent by volume of volcaniclastic materials, which are highly porous (Schmincke, 2004). This means that huge volumes of groundwater can be stored within cone structures, and this, coupled with the high viscosity of andesitic to dacitic magma, is the reason for the common explosivity and the high fragmentation of lava on these volcanoes (Schmincke, 2004).

2.3 Vulcanian Volcanism

Between August 3rd, 1888 and May 17th, 1889 a series of volcanic eruptions took place on the island of Vulcano at a time when volcanologists were recording and classifying different eruption types. As a result these eruptions became among the best documented anywhere in the world during the 19th century and the island gave its name to a style of volcanic activity, vulcanian (Morrissey & Mastin, 2000). This definition was later incorporated into a classification scheme by Lacroix that ranked eruption types in order of increasing explosivity: hawaiian, strombolian, vulcanian and plinian (Morrissey & Mastin, 2000). More recent examples of eruptions that have been described as vulcanian include Ngauruhoe, New Zealand (1975), Irazu, Costa Rica (1963-1966), and Sakarujima, Japan (since 1955).

Vulcanian eruptions are small to moderate-sized (less than 1 km^3) but have eruption columns that have heights greater than those of strombolian eruptions, reaching between 10 and 20 km. They are violently explosive and vary in their noisiness and duration from minutes to hours (Francis, 1993). They are possibly the most common style of eruption displayed by andesitic volcanoes, especially described from summit craters of composite cones. They are characterised by violent, short, discrete explosions (Walker, 1982), ballistic ejection of blocks and bombs, atmospheric shock waves, emission of tephra and by deposits that have a wide range in the percentage of juvenile versus nonjuvenile components (Morrissey & Mastin, 2000). The juveniles are comprised of fragmented intermediate magma, ranging from basaltic andesite to dacite. The eruptions can occur as a single discrete event or as a closely-spaced series of pulsatory explosive events. They can occur as precursors to much larger eruptions, during the late stages of a large eruption or as an eruption on its own with no increase in magnitude (Morrissey & Mastin, 2000).

2.3.1 Eruption Processes

Ballistic Ejection

Vulcanian eruptions typically produce high ejection velocities of 200-400 m/s and eject blocks and bombs to distances of up to 5 km from the vent. The trajectories and velocities of vulcanian erupted blocks were among the first features to be studied (Morrissey & Mastin, 2000). Estimates of velocities made before 1990 assumed ejection into still air and produced speeds significantly greater than more recent calculations that take decreased air drag near the vent into account. This resulted in velocities of ~600 m/s for the 1968 eruption at Arenal volcano and 400 m/s for the 1975 Ngauruhoe eruption (Fudali & Melson, 1972 and Self *et al.,* 1979) being revised to 300-400 m/s and 220-260 m/s respectively (Fagents & Wilson, 1993). However, it is thought that gas jets following a vulcanian outburst could produce much higher velocities, but these have not been measured with any degree of success. The most reliable measurements have been obtained from photographs and videos of eruptions on a smaller scale than those of Arenal and Ngauruhoe (Morrissey & Mastin, 2000), such as eruptions from Sakurajima

Volcano in Kyushu, Japan. The maximum ejection velocity of volcanic blocks, which was obtained from the analysis of photo-trajectories, was 112–157 m/s (Ishihara, 1985).

Deposits

All the deposits produced by vulcanian eruptions are characteristic of brief, violent episodes and include, ballistic blocks and bombs, pyroclastic avalanches and flows and fine grained fall deposits (Morrissey & Mastin, 2000). Block fields at some of the larger volcanoes cover areas up to several square kilometres and contain blocks of up to several metres in diameter. A high proportion of the ejecta from vulcanian explosions is solid or near solid at the time of eruption. Near solid bombs often form a distinctive "breadcrust" texture (Fig. 2.5), where the clast exterior has fractured during flight due to continued expansion of the hot vesiculating clast interior (Walker, 1982).

Figure 2.5: Bomb showing "breadcrust" texture. Found by Lower Te Maari Crater. "Chapstick" measures 3.5 cm long.

On steeper slopes, as these masses of ejected blocks and ash fall to the ground, they can evolve into pyroclastic avalanches or flows, producing poorly-sorted and poorly vesiculated deposits (Morrissey & Mastin, 2000).

Dark, ash-charged, cauliflower-shaped plumes that develop ascend rapidly to heights of 5-20 km above the vent where they are widely dispersed. Beyond a few kilometres from the vent fall deposits are fine-grained and thin, due to the small total volume (Walker, 1982). These fall deposits are characterised by a high proportion of nonjuvenile clasts, presumed to have resulted from the clearing of the vent, consisting of lava dome material or country rock from the vent or conduit walls. The lack of juveniles also indicates that the upper conduit had mostly gas or groundwater instead of magma. Juvenile components are vitric to crystalline, poorly to moderately vesicular, angular and block to ash sized (Morrissey & Mastin, 2000).

Seismic and Air Waves Characteristics

Long-period and tremor events commonly precede vulcanian eruptions. These events are thought to be manifestations of pressure disturbances in fluids flowing through the volcanic structure. This type of seismic activity has provided important information about the role of gases in the eruption process. In several cases, explosive earthquakes have occurred several seconds before vulcanian eruptions. These events are thought to result from rapid pressurisation 2-3 km beneath the volcanic crater (Morrissey & Mastin, 2000).

Another characteristic that is commonly observed during vulcanian eruptions is atmospheric shock waves (Morrissey & Mastin, 2000). This indicates that the erupting fluid at the vent is overpressurised with respect to the atmosphere (Fig. 2.6) (Schmincke, 2004). This air shock propagates ahead of the fluid, exceeding the atmospheric sound speed and is made visible by condensation of water vapour (Cole, 1982). This interesting phenomenon was observed by a TV camera on Sakurajima Volcano in Kyushu, Japan. The shock waves were visible passing through the atmosphere above the crater and the instant disappearance of thin clouds and the condensation of dense clouds were induced

by their passage. The atmospheric shock waves were generated in the crater 1.1–1.5 seconds later than the occurrence of explosion-quakes and propagated with the velocity of Mach 1.3–1.5 in a height range from 300 m to 600 m above the crater (Ishihara, 1985).

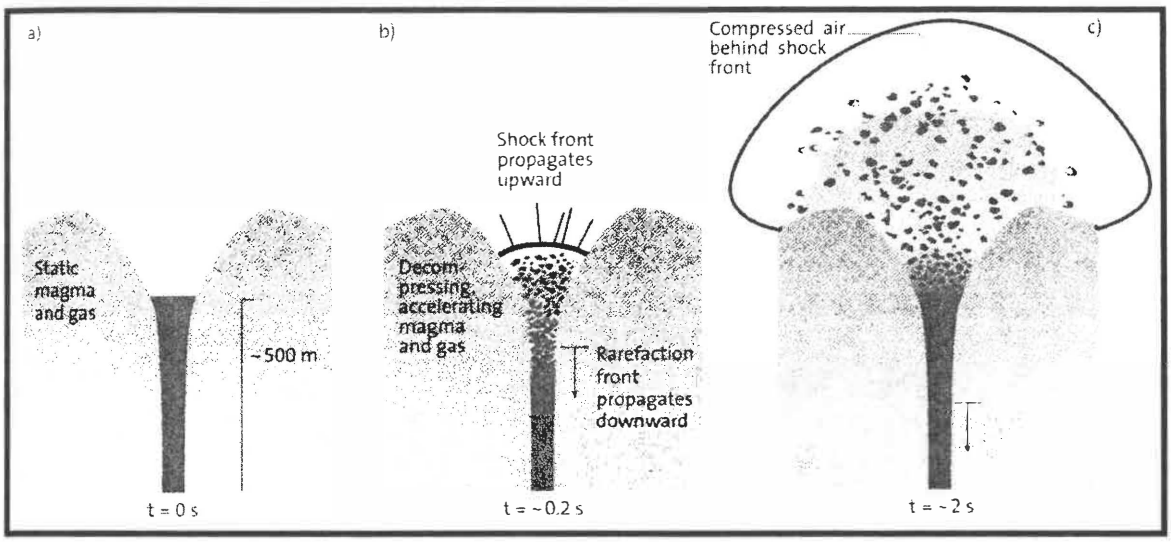

Figure 2.6: Propagation of a shockwave during a vulcanian eruption. After Schmincke (2004).

2.3.2 Eruption Sources

Discrete, intermittent explosions are the result of the sudden release of gas pressure within a magmatic system (Self *et al.,* 1979). There have been a number of models proposed for the source of gases that drive vulcanian eruptions, all relating to either exsolution of magmatic volatiles or superheating of groundwater. A few eruptions have been documented where in the initial stages water was involved and so were classified as phreatomagmatic. As they progressed however, it became apparent that they were displaying characteristics of vulcanian eruptions. The eruptive products of vulcanian explosions also have many similarities with those of obvious phreatomagmatic eruptions (Schmincke, 2004), which has led to an assertion that vulcanian eruptions that involve water may be considered a subclassification of phreatomagmatic eruptions (Morrissey & Mastin, 2000).

2.4 Andesitic Lavas

Andesite is the second most abundant volcanic rock type on earth. It has a 53-63% silica content with a viscosity typically intermediate to that of basalt and rhyolite (Carrigan, 2000). Andesite lava flows are usually of aa or blocky type, are a few metres to tens of metres thick, have a hummocky surface and are emplaced slowly. They can develop flow laminations due to shear failure of the lava often producing joints that roughly parallel flow boundaries and gives the rock a platy appearance (Fig. 2.7) (Gill, 1981).

Figure 2.7: Andesite lava with platy jointing. Outcrop east of Lower Te Maari Crater, Tongariro. Outcrop measures 2 m thick.

There is a range of surface morphologies that identify the various lava flow types, from the smooth, undulating surface of pahoehoe lavas, to the irregular jumble of blocks forming blocky lavas. These morphologies establish a continuous spectrum with three broad categories, aa between the two extremes of pahoehoe and blocky (Kilburn, 2004). The transition from pahoehoe to aa occurs due to two main factors. Viscosity of the lava

as pahoehoe cools is one factor, but strain rate is also important (Fig. 2.8). Pahoehoe can be preserved if the flow stops before a critical viscosity or yield value is reached (Schmincke, 2004). Andesite lavas on Tongariro are all of aa or blocky type.

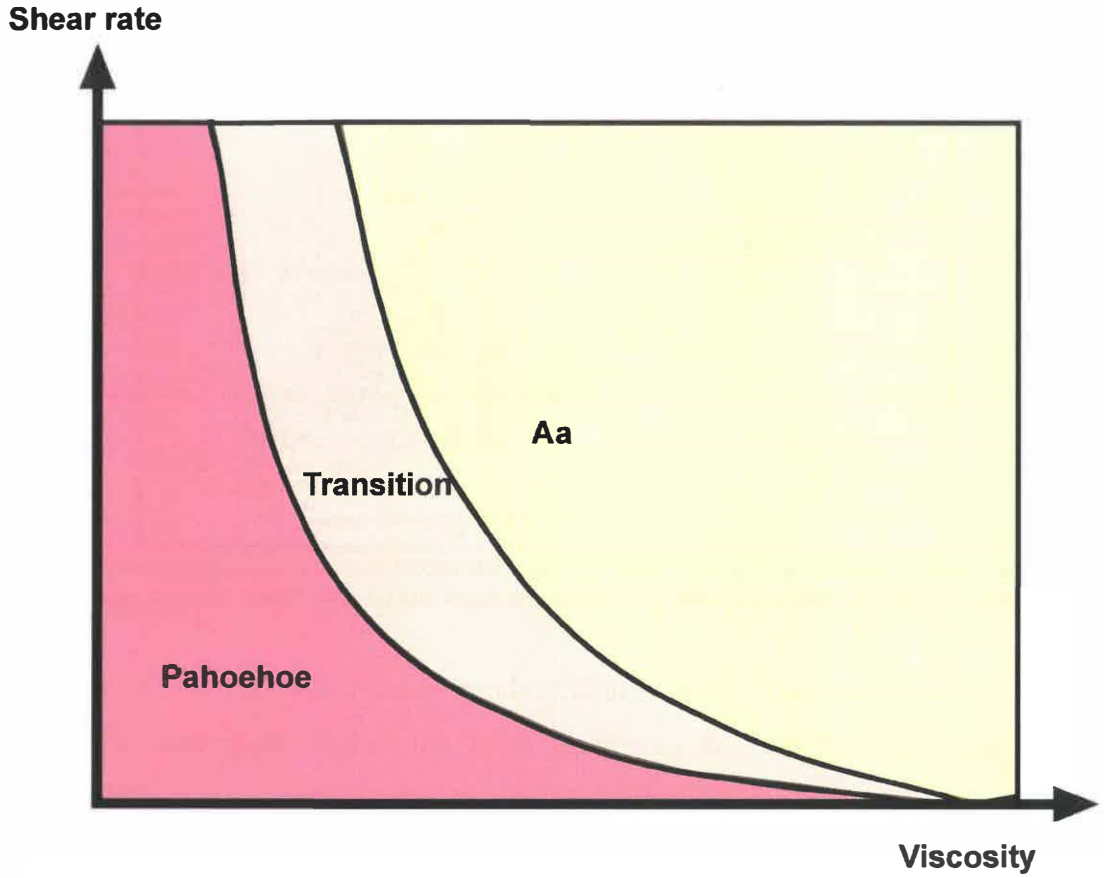

Figure 2.8: Fields of pahoehoe and aa and blocky lavas depending on factors of viscosity and shear rate. Adapted from Schmincke (2004).

2.4.1 Aa and Blocky Flows

Blocky lava flows show a fractured surface covered in blocks up to metres across with smooth, planar and angular surfaces, while the flow centres are dense and coherent (Fig. 2.9). They have high aspect ratios and are characterised by thick flows with high viscosity (Kilburn, 2000). Aa lavas show a fractured, extremely irregular surface with a covering of rough, contorted "cauliflower" or rubbly fragments, ranging in size from

decimetres to metres, also with a dense, coherent centre. The clasts are smaller and more irregular than on blocky flows.

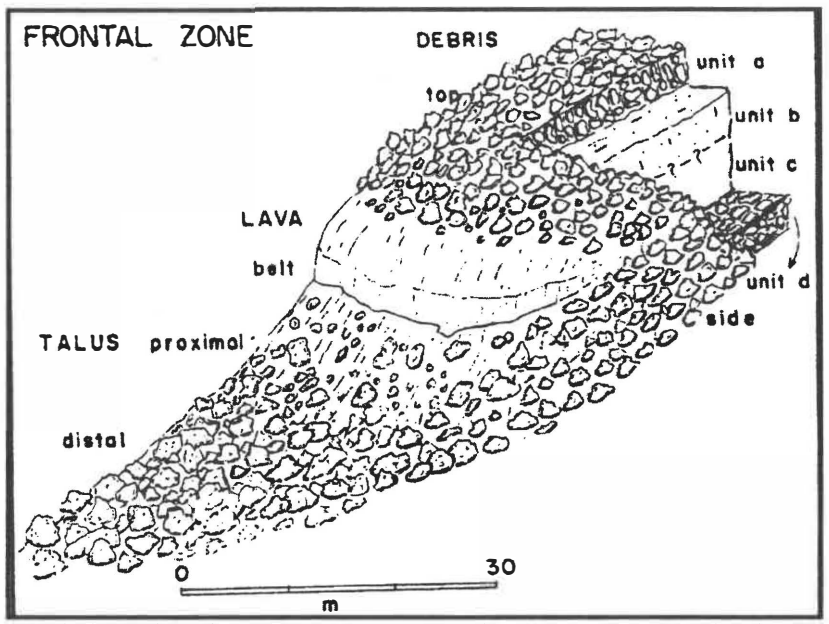

Figure 2.9: Typical blocky lava frontal zone showing top debris (unit A), vesiculated crust of central unit (unit B), dense, coherent centre (unit C) and basal debris (unit D). After Linneman & Borgia (1993).

Both flows show simple evolutionary trends (Kilburn, 2000). They are slow moving with the fronts advancing as single units, often starting as fluid sheets then forming fluid interiors with cooling crusts that are continually broken by movement of the flow (Kilburn, 2004). The fronts thicken as they progress, with rates of advance slowing over time and they finish as near solid masses that have been fragmented throughout their thickness (Kilburn, 2000). It is due to this fracturing that flow fronts can advance as a single unit without forming small lava tongues. However, because their interiors solidify during their advance they eventually reach a stage when they must autobrecciate in order to continue (Kilburn, 2004).

2.4.2 Andesite Lava Flow Emplacement

There are two general trends that a flow normally follows: 1) a constant rate of lengthening throughout emplacement; and 2) an initial stage where the final length is almost reached, followed by a period of much slower advancement for the last few

percent of its final length (Kilburn, 2004). All trends include flow thickening, with the flow front often growing to more than 10 times the initial thickness. Final thickness is typically 20m or less for aa fronts and maximum lengths are measured in tens of kilometres (Kilburn, 2000). While the emplacement of flows may take from hours to days, most of the length is emplaced within days, the flow fronts stopping either when the supply is removed, or they become too resistant to move (Kilburn, 2004). Major flows can achieve volumes of 1-100 million m^3 (Kilburn, 2000).

A lava flow consisting of a single stream extending directly from the vent to the flow front is classified as a simple flow. Compound flows consist of a few lobes or numerous smaller branches formed from the main flow (Blake & Bruno, 2000). This development of flow fields is more common than the formation of a single lava flow (Fig. 2.10) (Calvari *et al.*, 2002).

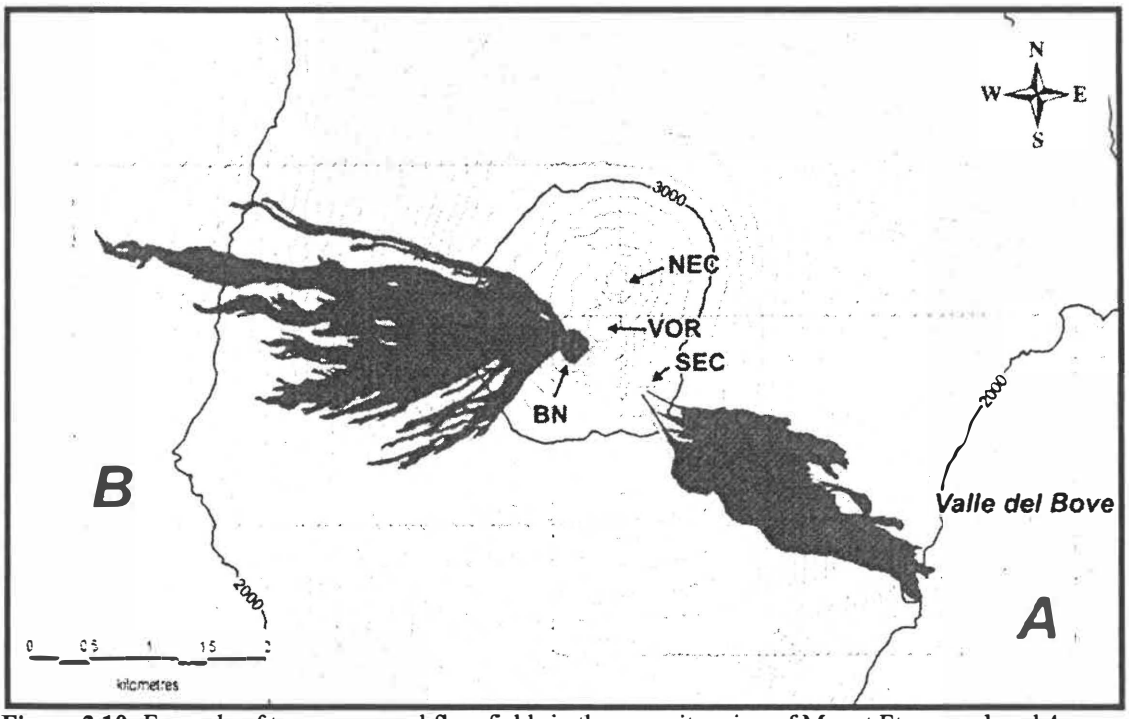

Figure 2.10: Example of two compound flow fields in the summit region of Mount Etna, emplaced 4 February, 1999. After Calvari *et al.*, (2002).

Aa-blocky flows initially develop channels that feed lava to the front. They begin to form following a phase of rapid widening close to the source vent, after which widening

ceases along much of the flow length and lateral motion is concentrated largely at the flow front (Kilburn & Guest, 1993). This concentrates movement downhill as flow becomes confined between static margins or levées (Kilburn, 2000). Within the channel the lava flows downhill with parallel streamlines (Fig. 2.11). The levées can be covered by debris, creating uniform slopes, while the inner channel has a slightly convex upward shape and is always covered with debris (Linneman & Borgia, 1993). These channels disappear at the toe of the flow where the fronts grow as they solidify and decelerate, allowing faster lava from upstream to accumulate (Kilburn, 2004). This build-up in the lava channel exerts increasing pressure on its margins that may eventually lead to a breach, forming an outlet where lava can escape. A small breach may be healed through cooling or by being plugged with crystal debris. Otherwise, a permanent outflow may develop into a major new flow (Kilburn, 2000).

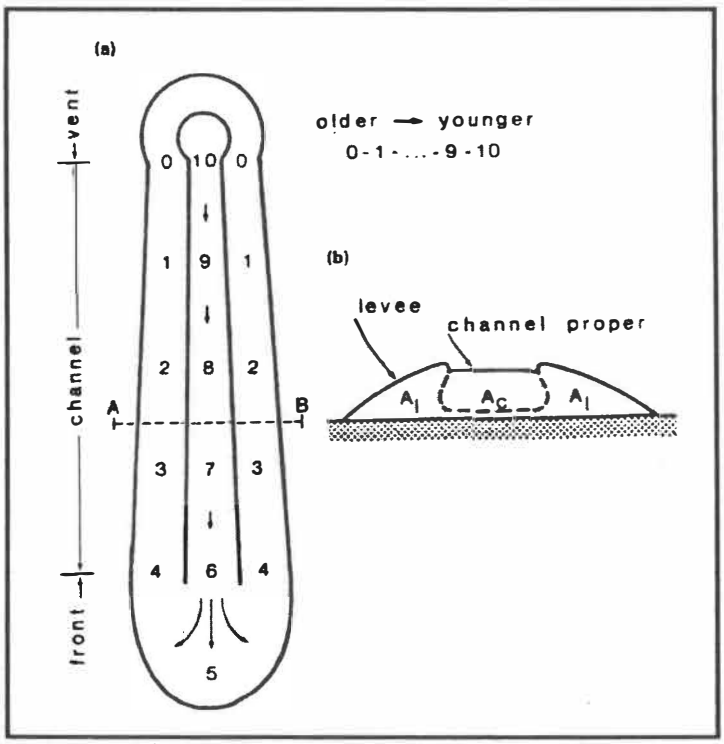

Figure 2.11: a) Map view and b) cross section of a unit flow showing inner channel and outer levées. Numbers decrease with increasing age of lava. After Linneman & Borgia (1993).

In this way, a flow field may evolve from a single flow to a series of interconnected flows (Fig. 2.12), although newly propagated flows rarely increase the length of a lava flow more than half the length of the initial flow. This process is more common in aa than

blocky lavas as the formation of new flows requires channel lava that is much more fluid than its lateral margins in order for it to easily escape through a breach (Kilburn, 2000). This can also occur when there is a fluctuating supply of lava rather than a sustained eruption, causing channel overflows, channel breaching and new flow formation. These conditions generally inhibit the development of lava tubes and results in the widening of lava flow fields (Calvari *et al.,* 2002).

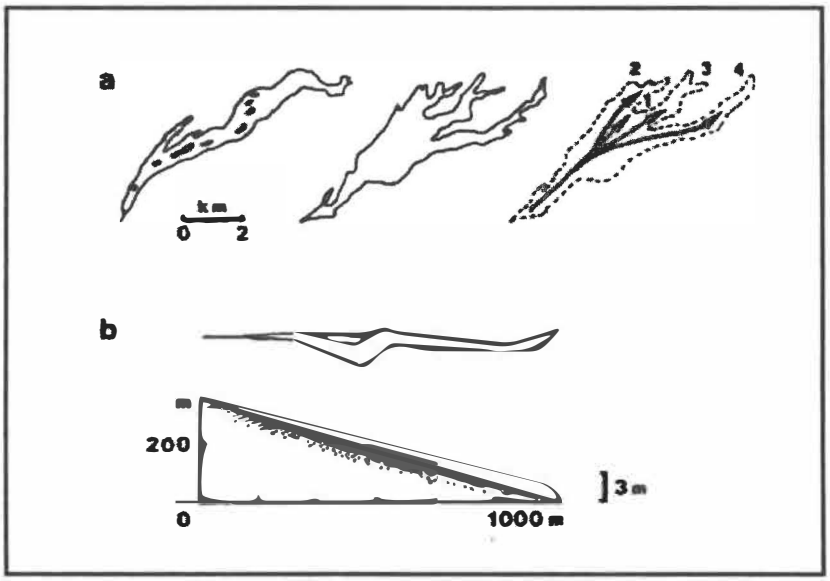

Figure 2.12: Emplacement of a lava flow field. a) Growth of a flow field through the propagation of arterial flows. Numbers show order of emplacement. b) Plan and profile of a simple aa flow. After Kilburn & Guest (1993).

The large, recent lava flow erupted from the Upper Te Maari Crater is a thick andesitic aa to blocky flow (Fig. 2.13). It is approximately 4 km long with multiple overlapping lobes running down-slope to the northwest and has a volume of around 29 x 10^6 m^3. Assessments of the mechanisms and timescale of emplacement of this flow are given in chapter 5.

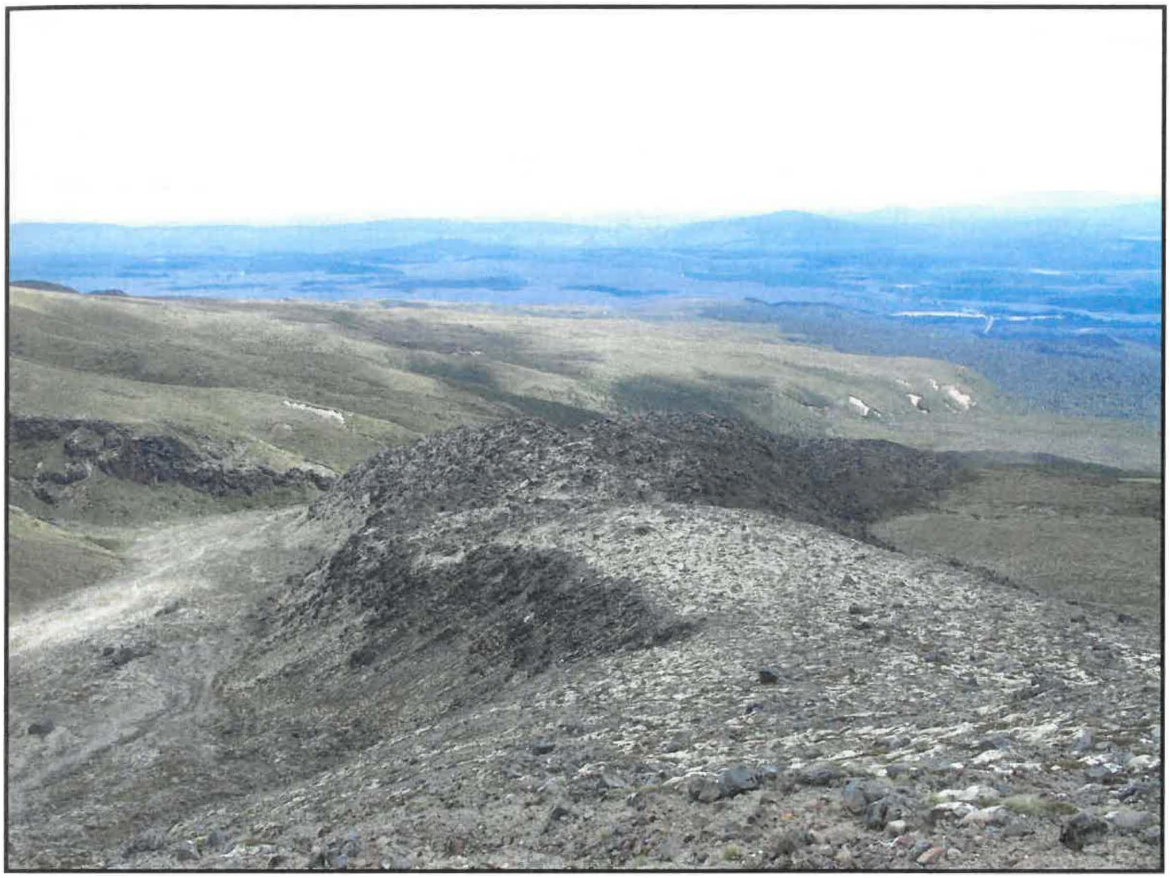

Figure 2.13: 1500 AD andesitic lava flow from Upper Crater. View looking northwest.

2.5 *Volcanic Breccias*

Volcanic breccias are commonly viewed as any volcaniclastic rock that is composed of angular fragments greater than 2 mm across (Smith *et al.,* 1999). Many composite cones consist of a large volume of this coarse-grained, fragmented, angular, lithic material that may be of pyroclastic, autoclastic, epiclastic or mixed origin (Grubensky *et al.,* 1998).

Breccias of volcanic origin can be recognised by their relationship to volcanic units, for example, the lateral continuity of autobreccias with lava flows and lithic-lag breccias with ignimbrites. However, it is possible for autoclastic breccias to exist without intimate association with coherent lava flows in single outcrops, and for the fine matrix to be of autoclastic rather than pyroclastic origin (Smith *et al.,* 1999). Volcanic breccia classification on composite cones is dependent on identifying autoclasts from pyroclasts in all deposits and determining whether the unit is primary or reworked. In most cases

deposits composed of entirely either scoria or lithic fragments can be interpreted as pyroclastic or autoclastic layers, respectively (Grubensky *et al.,* 1998). However, field-based classifications of breccia-clast origin are difficult, due to the fact that andesitic pyroclasts, common in vulcanian eruptions, are characteristically nonvesicular, making them difficult to distinguish from autoclasts (Smith *et al.*, 1999). Rock-magnetic studies, specifically the natural remnant magnetisation (NRM), have been investigated recently as an additional perspective for explaining the origins of breccias through estimating the emplacement temperatures of component fragments (Grubensky *et al.,* 1998).

A primary volcanic breccia is one produced by moving lava flows (autobreccias) or pyroclastic falls and flows emplaced over a range of temperatures (Fig. 2.14). Secondary breccias are formed when primary deposits are remobilised by fluvial or dry mass-movement processes (Grubensky *et al.,* 1998). These deposits are thought to be insignificant components in most proximal cone-forming sequences (Smith *et al.,* 1999).

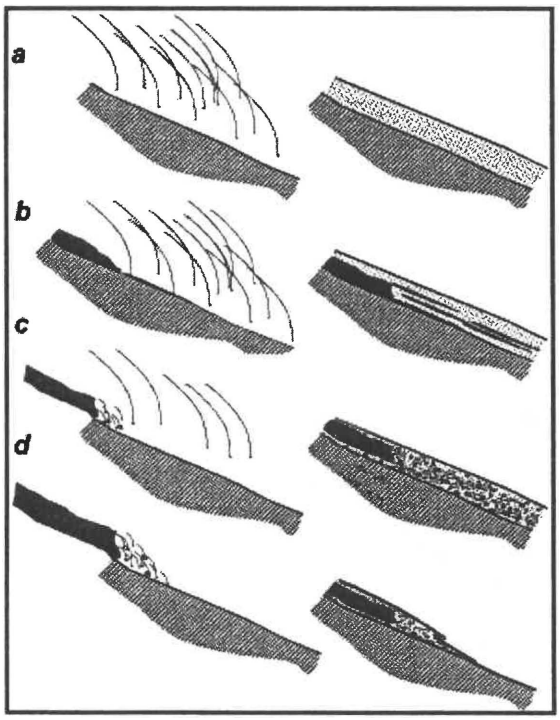

Figure 2.14: Schematic sketches of emplacement mechanisms and fragment sources for four types of volcanic breccias. (a) Fallout and resulting deposit that mantles substrate (slanted-line pattern); (b) Fallout and subsequent emplacement of core-rich lava flow (solid black); (c) Autoclast-rich lava flow (core and associated autobreccia in solid black for simplicity) emplacement accompanied by fallout in advance of and on top of a flow; (d) Autoclast-rich lava flow with core and autobreccia emplaced without consequent fallout. After Grubensky *et al.,* (1998).

Autobreccias (Fig. 2.14 (d), 2.15) are composed of fragments produced by the disruption of flowing lava, and include those generated and transported along the base, upper surface and front of a lava flow, or as dome associated talus breccias (Smith *et al.*, 1999). The formation of autoclastic breccia that is not interlayered with lava-flow cores can arise from the cooling of the front and top of a slow moving flow, causing the entire flow front to brecciate while it continues to be pushed downslope by lava entering at the rear of the flow. The flow would become a mass of advancing breccia, eventually forming a downslope-tapering apron (Smith *et al.,*1999), similar to the breccia found at Upper Te Maari Crater (See chapter 3).

Figure 2.15: Bedded volcanic breccia, Upper Te Maari Crater. Tool handle measures 30 cm long.

Explosion-related breccias are formed through laminar pyroclastic flows, pyroclastic surges, direct fall or from near-vent transport regimes, all resulting from explosive eruptions (Fig. 2.14 (a,b,c)). Deposits resulting from this type of activity display characteristic structures and textures and overlapping grain-size distributions (Grubensky *et al.,* 1998).

CHAPTER THREE

FIELD CHARACTERISTICS

3.1 Introduction

This chapter details the field characteristics of the Te Maari Crater eruptives, including the morphology and stratigraphy of the Upper and Lower Te Maari Craters, lava flows associated with these craters and the cluster of small craters located directly north of the lower crater. Proximal tephra stratigraphy is also described. These data have been compiled using field logging, and site descriptions at various proximal locations around the craters. Figure 3.1 is a map showing the field area, with the Upper and Lower Te Maari Craters, associated lava flows, small northern crater cluster and the locations of the proximal tephra samples.

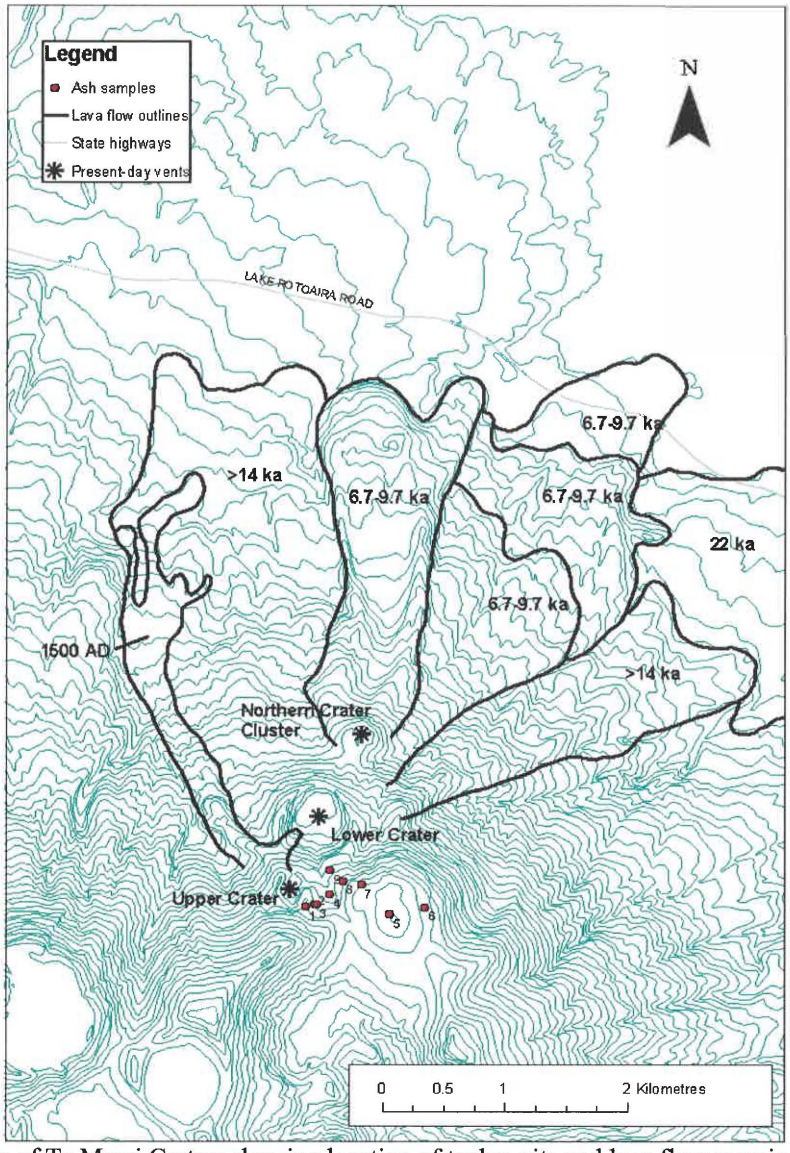

Figure 3.1: Map of Te Maari Craters showing location of tephra pits and lava flow margins.

3.2 Geomorphology

The Te Maari vent system consists of three main craters of contrasting form. The upper crater is a narrow, funnel-shaped structure, the lower crater is a deep, wide, flat-floored structure and there is a cluster of small craters north of the lower crater. The craters and vents associated with Te Maari form a NNE-trending alignment, which is consistent with the structural pattern of the other vents for the young (post-glacial) eruptives in the Tongariro Volcanic Zone. The geomorphology of the Te Maari vents and their alignment is shown in Fig 3.2.

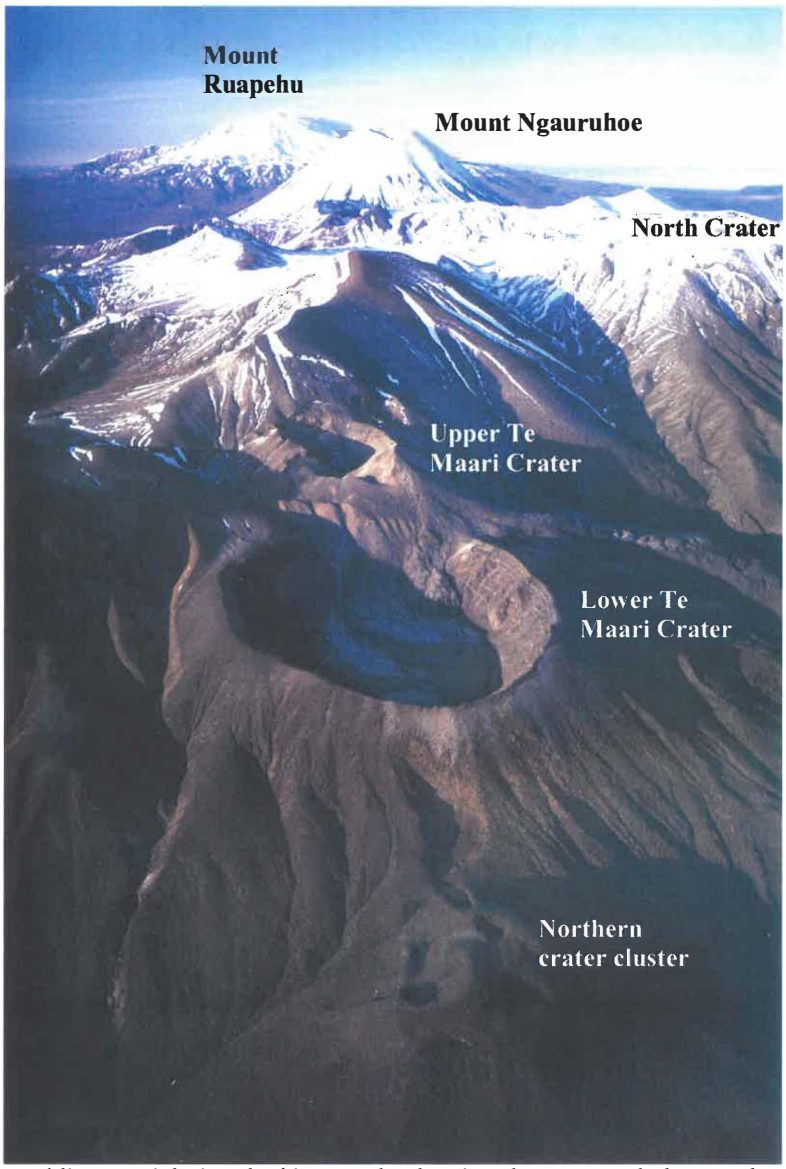

Figure 3.2: Low oblique aerial view looking south, showing the geomorphology and position of the Te Maari Craters and associated vents in the Tongariro Volcanic Centre. After Potton (1995).

3.2.1 Upper Te Maari Crater

The Upper Te Maari Crater is the most recently active of the crater system. It is thought to have been largely formed during the 1869 eruption of Lower Te Maari Crater (Gregg, 1960). It is a 200 m wide, 50 m deep, narrow, funnel-shaped structure with slope angles of about 35° (Fig. 3.2, 3.3). The most recent lava flow (c.1500 AD) and explosive ash eruptions (e.g. 1892, 1896) have been sourced from here. The lithologies exposed within the walls and outer slopes consist of an upper bedded breccia, a lower massive breccia and a central hydrothermally altered vent structure on the crater floor. These lithologies are described in more detail in section 3.3. The inner and outer walls are predominantly covered in talus derived from collapse of this unstable material.

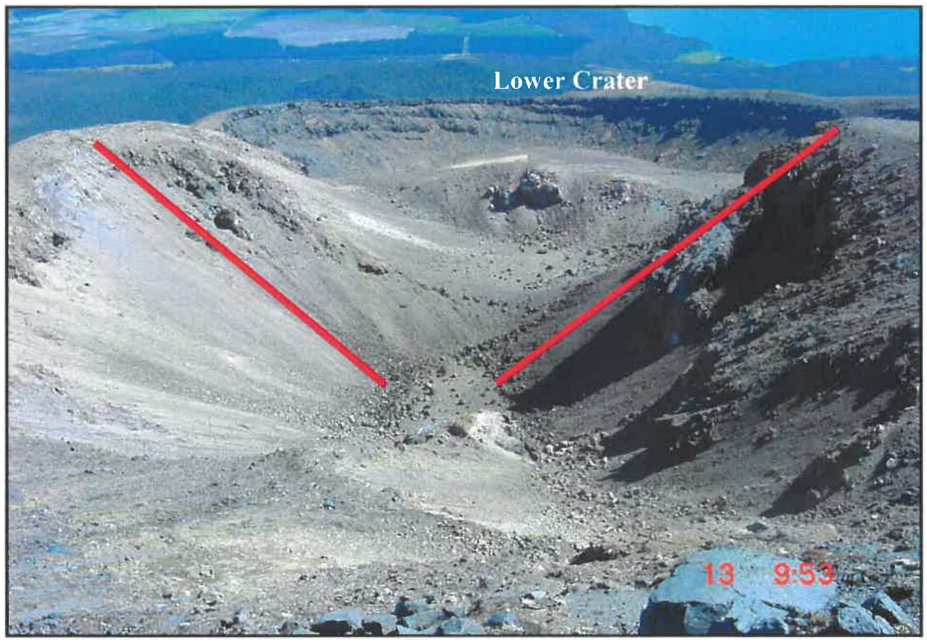

Figure 3.3: Morphology of Upper Te Maari Crater. View looking northeast towards lower crater. Red lines show the dip of the inner crater walls at 35°.

3.2.2 Lower Te Maari Crater

The Lower Te Maari Crater is older and is a 60 m deep, 500 m wide, inclined, flat-floored structure (Fig. 3.2, 3.4). This morphology implies that some shallow collapse has occurred. The crater exposes a series of 5-6 lava flows of massive, jointed Andesite averaging 2-4 m thick. No proximal pyroclastic facies (e.g. agglutinate), have been identified within the inner wall stratigraphy or around the crater rim. A thin tephra bed

mantles the rim of the crater and dense andesite blocks (0.1 – 1 m) litter the outer slopes of the crater.

Figure 3.4: Morphology of Lower Te Maari Crater. View looking northeast.

The Lower Te Maari Crater was named Sulphur Lagoon last century as it was partially covered by a shallow, brown-coloured lake. An ephemeral small pool remains on the floor of the crater and there are areas of suphurous steaming ground on the southwestern wall

3.2.3 Lava Flows

The recent lava flow erupted from Upper Te Maari Crater is a thick andesitic aa to blocky flow. It runs downslope to the northwest and is approximately 4 km long with multiple overlapping lobes, one of which runs into the Lower Te Maari Crater. At the proximal end of the flow the thickness is approximately 80 m. The thickness varies throughout the flow as it runs into steps downslope, but it decreases to approximately 20 m at the flow front. Weighted averages of width and thickness were used to calculate a volume of approximately $33x10^6$ m^3. Towards the middle and lower reaches of the flow there is some levée development as the flow starts to widen about 1 km from the vent. This flow was tree-ring dated to around 1500 AD by Topping (1974).

Using geomorphology and ages, other large flows between 3-4 km long, can be identified north of the craters as having source vents in this vicinity (Fig. 3.1). Especially prominent is a large, <90 m thick, levéed flow directly north of the Lower Te Maari Crater. Topping (1974) used the position of Papakai Tephra above the lava to estimate an age for this flow of between 9.7 and 6 ka. Nairn *et al.,* (1998) found two deposits associated with the ~10 ka eruption sequence beneath and intercalated with proximal

breccias sourced from the Te Maari Craters. This, along with Topping's age estimate led to the conclusion that the large, levéed flow may have been emplaced at the end of the ~10 ka sequence.

3.2.4 Northern Crater Cluster

Directly north of the Lower Te Maari Crater, lying on the outer slope of the crater, is a small cluster of craters on a small dome with 4-5 obvious pits (Fig. 3.5). The largest pit is 100 m wide and approximately 20 m deep. There are a few outcrops exposed within the pits themselves and an outcrop on the eastern slope of the dome of massive, jointed andesite. There is a shallow pool infilling a depression, possibly also a pit, that, unlike the "sulphur lagoon" in Lower Te Maari Crater, appears to be more permanent (Fig. 3.5). There are a few ballistic blocks scattered around the rims of the pits, however, the vegetation cover and the location of the pits downslope from other block fields, makes it difficult to ascertain a block field in this area. No proximal pyroclastic facies were identified.

The dispersal pattern of the older lava flows to the north and northeast of these pits (Fig. 3.1) indicates the possibility that the origin of the flows is from vent(s) in this area.

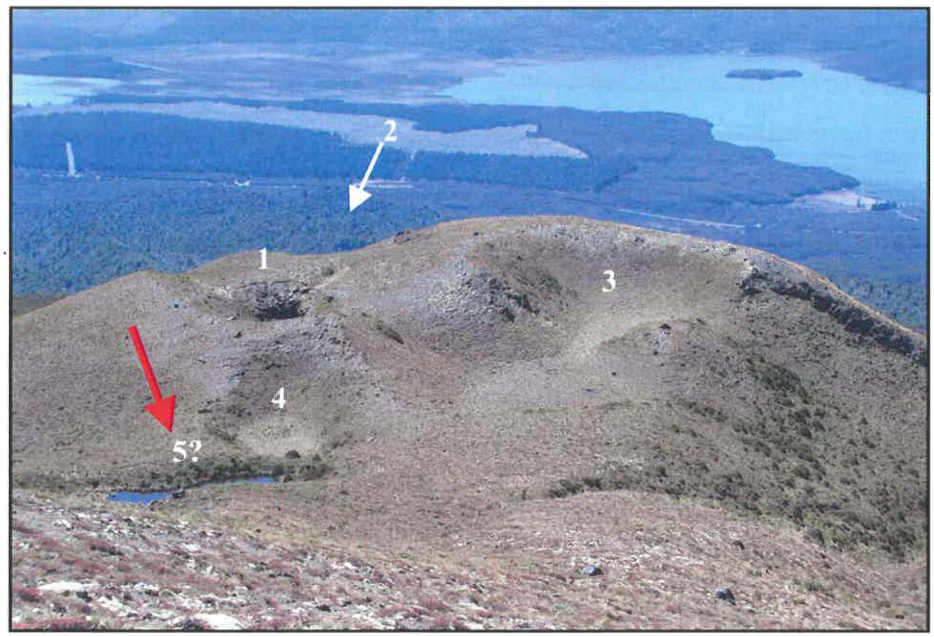

Figure 3.5: Crater cluster north of Lower Te Maari Crater. Pits numbered 1 – 5. Red arrow shows location of pool. White arrow shows location of pit not in view.

3.3 Upper Te Maari Crater Lithofacies and Stratigraphy

The Upper Te Maari Crater has three main units exposed in the inner crater walls and floor (Fig. 3.6)

3.3.1 Upper Bedded Breccia Unit (Fig. 3.7)

The top unit consists of red/orange-brown, bedded, very coarse, two-pyroxene andesite breccia. It is mostly formed of coarse-grained beds 0.3-0.7 m thick and of subordinate, finer grained layers 0.1–0.3 m thick. The coarse layers are made up of abundant lapilli and blocks up to 0.5 m in a matrix of weakly consolidated coarse ash. All the clasts are angular to sub-angular and appear compositionally similar, although they vary in colour and degree of hydrothermal alteration. They are all dense and non to poorly vesicular.

The thin, finer-grained layers intercalated within the coarse-grained beds are comprised of weakly consolidated coarse ash, some lapilli and rare blocks. Like the coarse layers these beds are variable in their thickness, sometimes developing or disappearing within a coarse bed.

3.3.2 Lower Massive Breccia Unit (Fig. 3.7, 3.8)

This thick unit consists of red/orange-grey, massive, very coarse, two-pyroxene andesite breccia. The unit ranges from weakly matrix-supported to clast supported. The clast sizes in this unit range from lapilli to very large blocks <2.5 m. They are angular to sub-angular and again all appear to be compositionally similar with some differences in the degree of hydrothermal alteration. The matrix is weakly consolidated and is comprised of coarse ash with some lapilli.

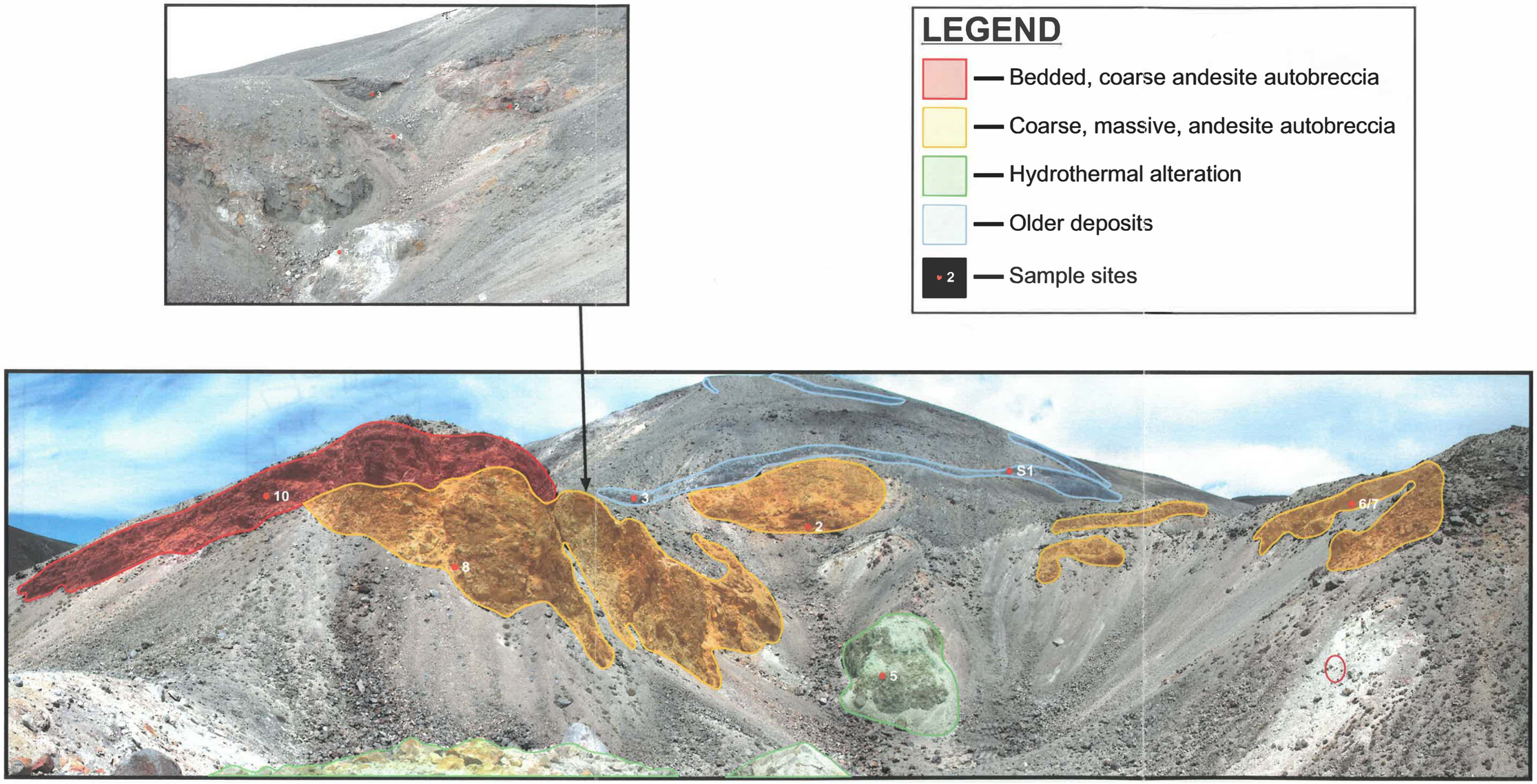

Figure 3.6: Upper Te Maari Crater lithofacies, stratigraphy and sample sites. Note red circle - person for scale.

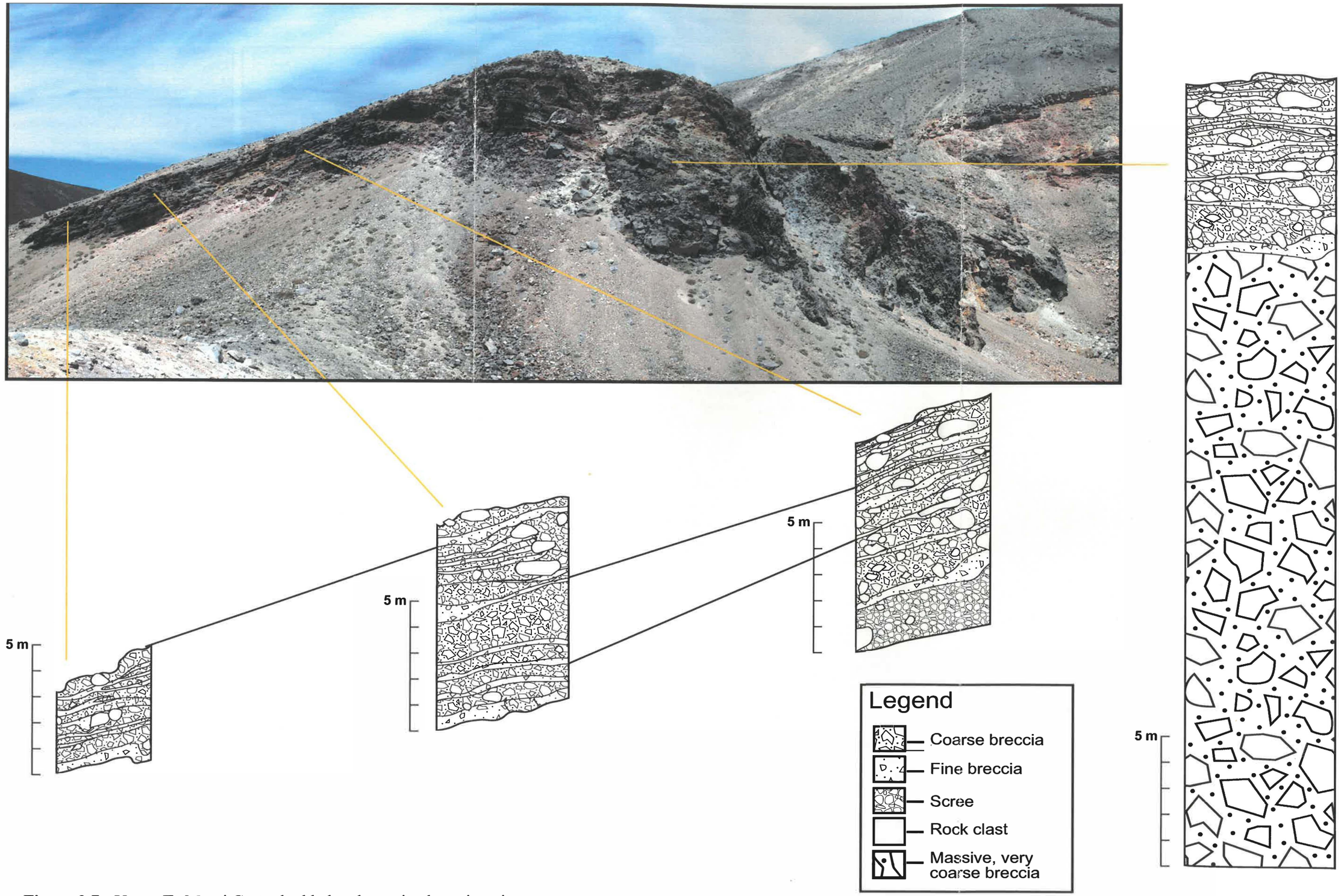

Figure 3.7 : Upper Te Maari Crater bedded and massive breccia units.

Figure 3.8: Lower massive, very coarse breccia unit in Upper Te Maari Crater. Tool handle measures 30 cm long.

3.3.3 Central Hydrothermally Altered Unit (Fig. 3.9)

The final unit exposed in the Upper Te Maari Crater is a central vent structure of white/orange, hydrothermally altered, blocky breccia. Apart from the degree of alteration, this unit displays much the same characteristics as the lower massive breccia unit discussed previously.

This hydrothermal alteration can also be seen in the northern inner crater wall, which includes some sulphur deposits.

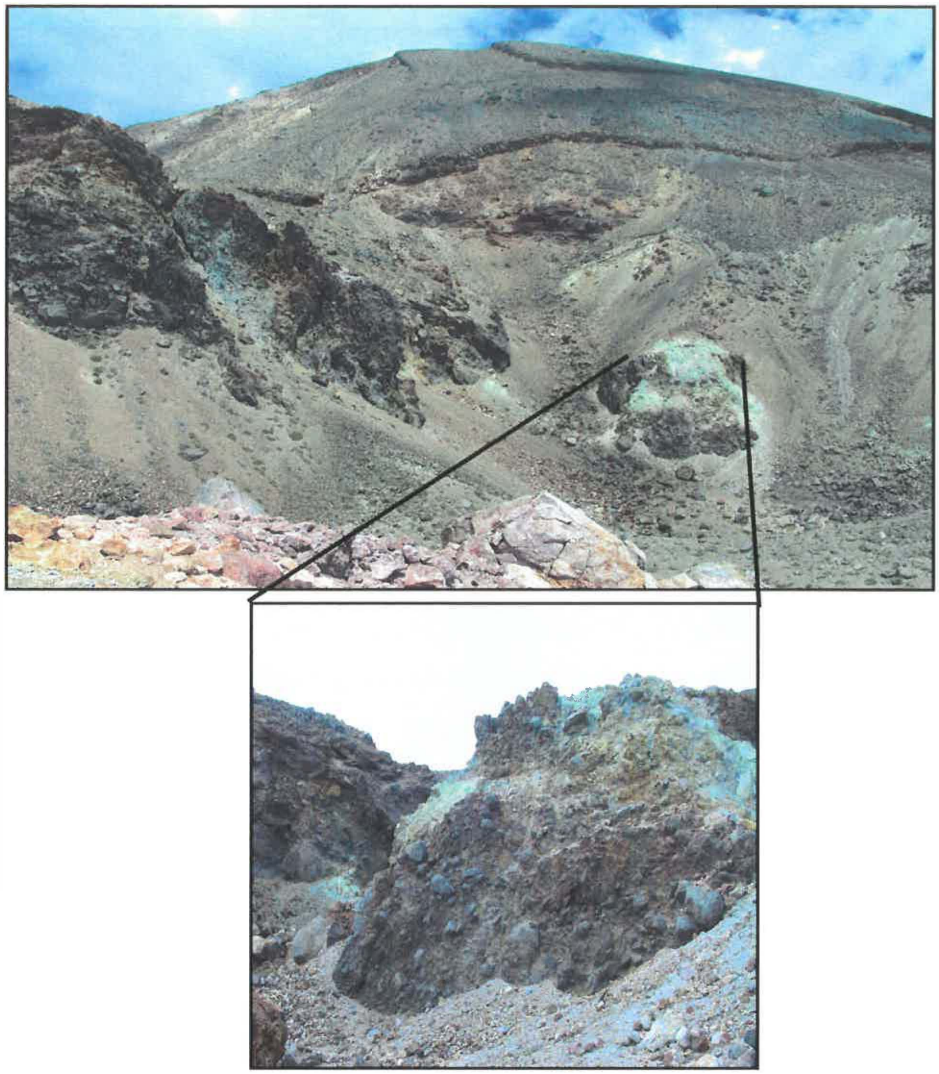

Figure 3.9: Central hydrothermally altered unit in Upper Te Maari Crater. Structure approx. 6 m high.

3.4 Lower Te Maari Lithology and Stratigraphy

3.4.1 Lava Flows

The stratigraphy of the Lower Te Maari Crater is comprised of multiple layers of grey, jointed, two-pyroxene andesite lava. The layers are approximately 2-4 m thick with the top layer thickening to 15 m in the south wall (Fig. 3.10a). The andesite is non- to poorly vesicular and is massive with brecciation and slabby fracturing at base (Fig. 3.10b).

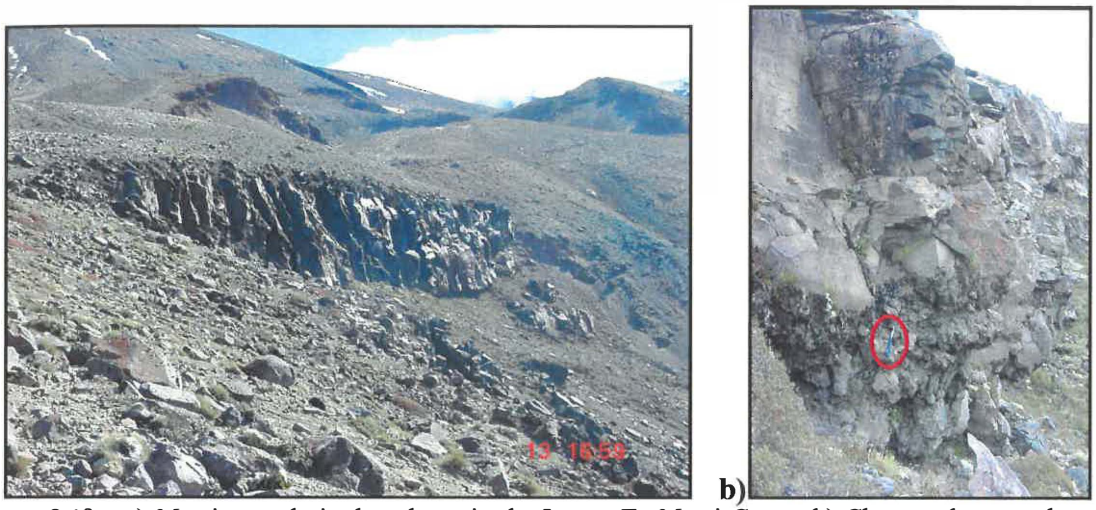

Figure 3.10: a) Massive, andesite lava layer in the Lower Te Maari Crater. b) Close up between lava flows showing brecciated nature of contact. Tool handle measures 30 cm long.

In the western wall of the crater there is a large massive lava body with columnar and platy jointing (Fig. 3.11). The uppermost layers of lava drape this mass, while the lower layers are truncated by it, suggesting it is an intrusion or tube-type structure.

Figure 3.11: Large, massive lava body in the western wall of the Lower Te Maari Crater. Person standing at base for scale.

Also on the western wall of the lower crater is an area of hydrothermal activity, with hydrothermally altered rock, steamy ground and minor sulphur deposits (Fig. 3.12).

Figure 3.12: Hydrothermal area on western wall (hatched line), Lower Te Maari Crater.

3.4.2 Ballistic Block Field

Evidence for explosive eruptions from the craters can also be seen with angular to subrounded ballistic blocks scattered around rim of the crater. These blocks range in size from centremetres to metres in diameter, with some displaying impact fractures and a few with "breadcrust" textures (Fig. 3.13). They appear to be characteristically similar to the andesite exposed in the lower crater walls apart from the "breadcrusted" blocks, which are lighter and more vesicular.

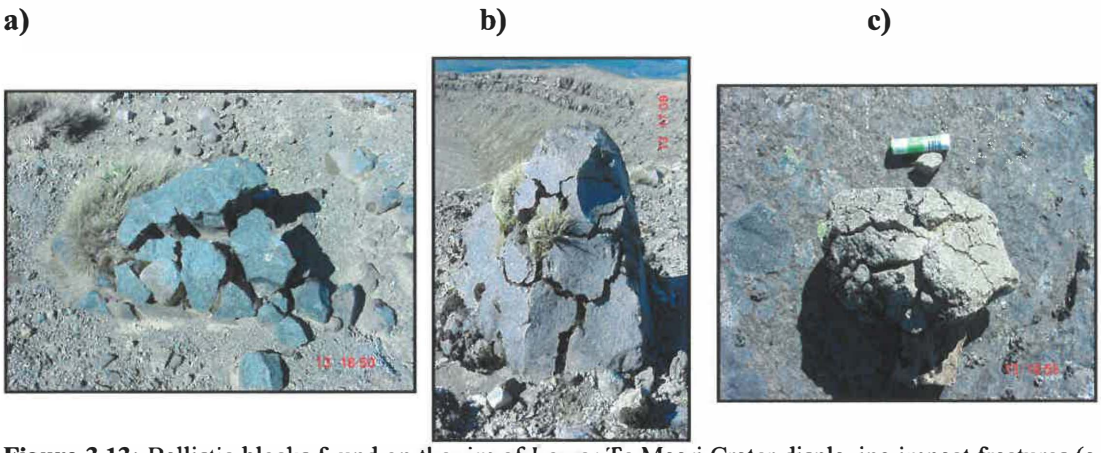

Figure 3.13: Ballistic blocks found on the rim of Lower Te Maari Crater displaying impact fractures (a, b) and "breadcrust" textures (c). Chapstick measures 6.5 cm long.

There is only evidence for minor explosive activity from the lower crater, with ballistic blocks and minor tephra deposits. There is an abscence of any proximal facies that would indicate sub-plinian activity.

3.5 *Hydrothermal Activity*

Apart from the hydrothermal area on the lower crater wall, there are a few other small areas of steaming ground on the outer slopes of Upper Te Maari Crater and between the upper and lower crater. They are generally small cracks or fissures in the rock, between 40 and 70 cm long and are non-sulphurous (Fig. 3.14a, b). They are surrounded by plants not found anywhere else in this proximal area (Fig. 3.14c). The locations for these areas are found in appendix V.

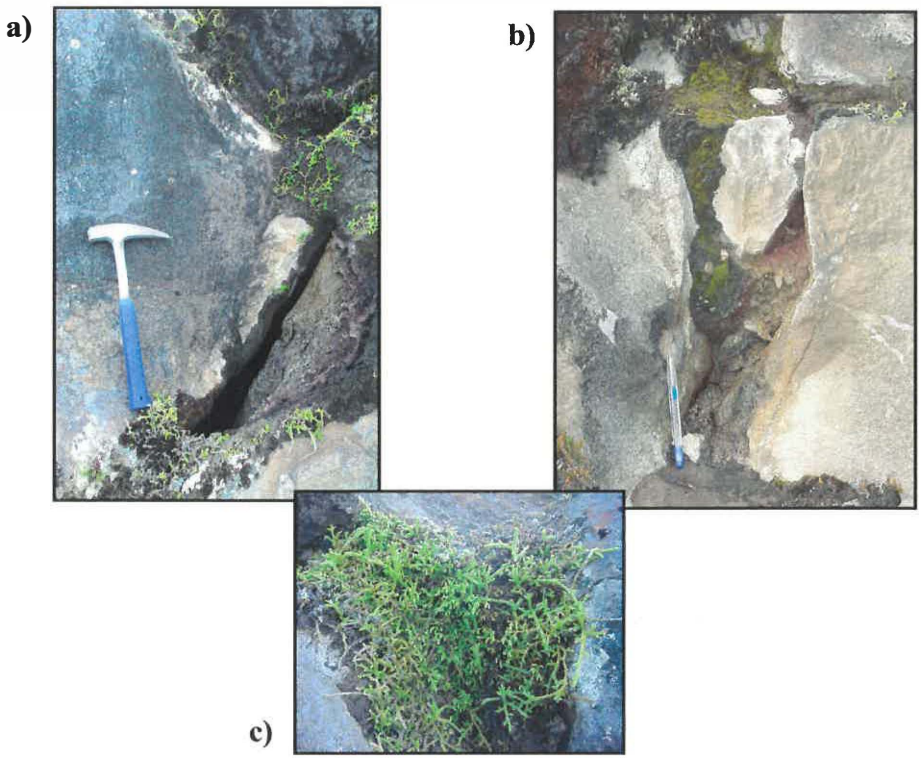

Figure 3.14: Examples of steamy cracks on Upper Te Maari slopes (a, b). c shows close up of plants found in steamy areas. Tool handle measures 30 cm, mechanical pencil measures 15 cm.

3.6 Upper Crater Young Lava Flow

The most recent c.1500 AD lava flow is a thick, andesitic aa to blocky flow erupted from the upper crater. The upper margins of this flow were mapped using GPS while samples were being taken. The overall surface texture is rubbly and vesicular, with angular to sub-angular blocks and a massive, less vesicular core. At the proximal end of the flow the blocks are grey with some hydrothermal alteration to creamy orange/red. The vesicularity or blocks increases further down the flow with more scoriacious surfaces and there are colour changes to red-brown as some rocks are oxidised. At the base of the lava flow front the flow is very blocky with grey angular, andesite blocks, typically <0.5 m, but up to 2-5 m. On top of the flow at the distal end there are fewer large blocks and more scoriacious material (Fig. 3.15).

Figure 3.15: a) 1500 AD lava flow front surface. b) Block texture. Tool handle measures 30cm long.

GPS readings and contours were used to create a transect along the length of the lava flow (L-L') and four transects across the width (a-a', b-b', c-c', d-d') the locations of which are shown in Fig. 3.15. The transects are shown in Fig. 3.16. L-L' shows the thickening of the flow proximal to the vent and places where it has "stepped" downslope.

Figure 3.16: Location of transects and GPS points from the 1500 AD lava flow. Numbers indicate samples taken.

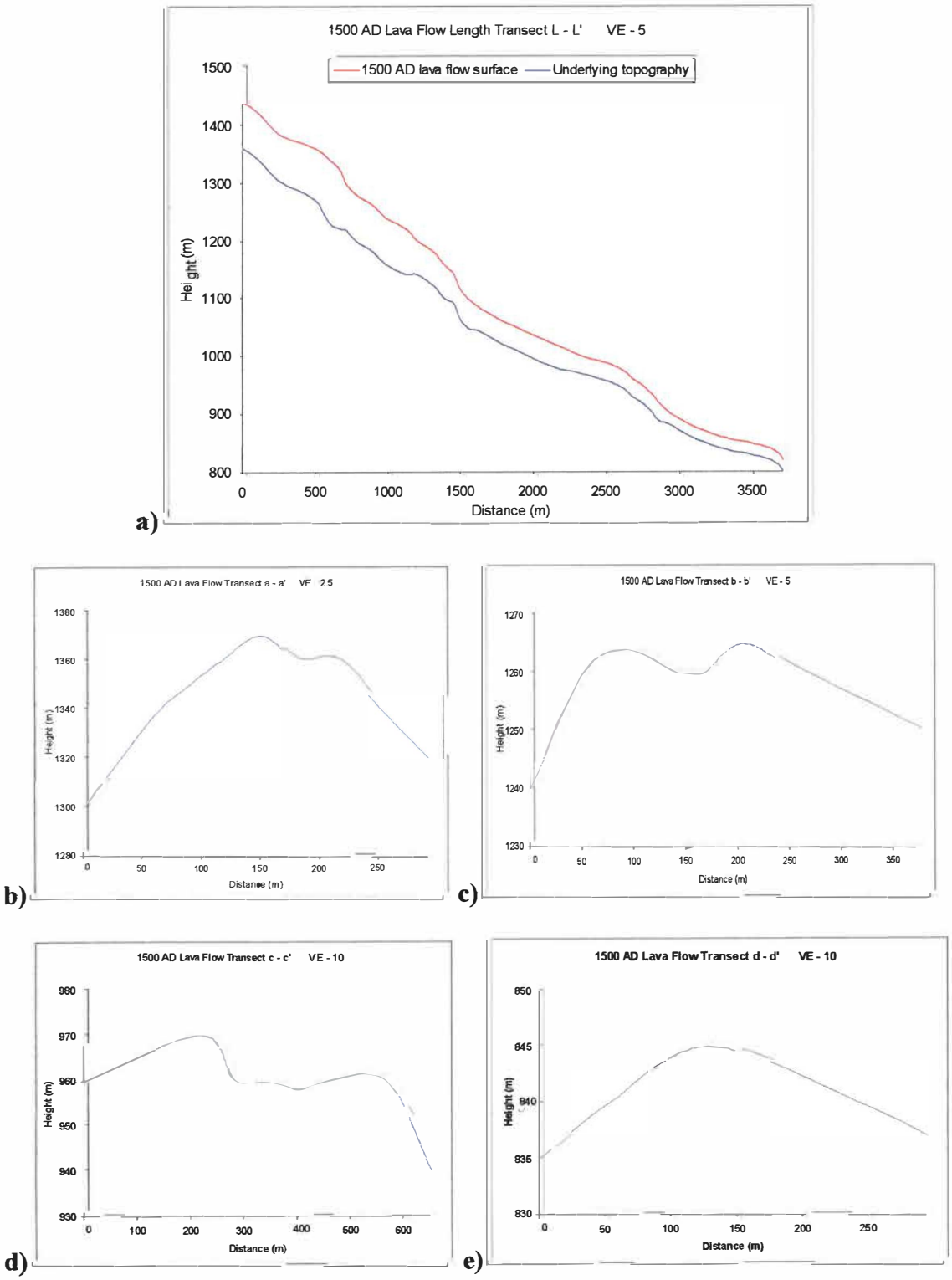

Figure 3.17: a) Transect along the length of the 1500 AD lava flow. b), c), d), e) Transects across the 1500 AD lava flow, from proximal (b) to distal (e). Note VE increases further from the vent.

a-a' is a transect proximal to the vent and shows the flow at its thickest. b-b' is further downslope and displays some levée development where the flow has become channelled between static margins. c-c' is a transect where the flow has widened, thinned and split into multiple lobes and finally, d-d' is a distal transect of the flow front. Each of these morphologies can be seen in a set of evolutionary sequences for aa to blocky flows (Fig. 3.18).

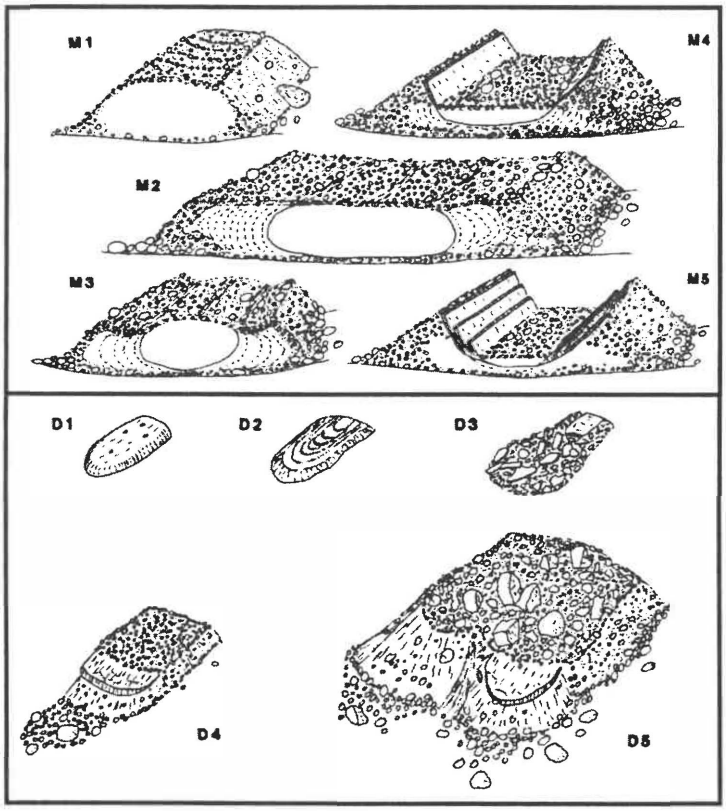

Figure 3.18: Examples of facies changes in medial (M1-M5) and distal (D1-D5) regions of aa lava flows. Morphologies described for 1500 AD lava flow are most similar to M1, M3 and D5 (proximal to distal). After Kilburn & Guest (1993).

There are a range of structural and textural changes that take place during the emplacement of an aa flow due to the effects of temperature on lava rheology (the transition of less viscous aa to blocky). The final form of a flow depends on what stage of evolution it is at when the eruption ceases and lava supply is terminated (Kilburn & Guest, 1993).

3.7 Northern Crater Cluster

Most of the northern crater cluster outcrops are located within the pits. They consist of grey, massive, jointed andesite, 4-6 m thick with slabby fracturing at the base (Fig.3.19). An outcrop on eastern slope of the dome (Fig 3.20) displays the same characteristics as that found within the pits with massive, jointed andesite, 2.5-3 m thick.

Figure 3.19: Andesite unit in crater 1 (Fig.3.5)

Figure 3.20: Outcrop on eastern slope of northern craters. Measures 2.5 m.

3.8 Tephra Stratigraphy

As stated in chapter two, the Te Maari Craters were often observed steaming or in weak eruption during the 19th century, with numerous descriptions of ash clouds, mud and boulders being some of the products produced. With the majority of these eruptions being relatively small compared with others from Tongariro, and the location of the Te Maari Craters on the northern slopes, there has not been any substantial preservation of these deposits. Pits dug in close proximity to the craters revealed a few coherent layers of ash deposits intercalated with light brown soil or reworked deposits. Those forming thick, discrete layers were sampled as being more likely primary deposits.

The majority of the deposits are grey, 2-4 cm thick, well to variably sorted, coarse to fine ash with some fine lapilli (Fig 3.21). An overall increase in thickness of layers toward Te Maari suggests a local origin.

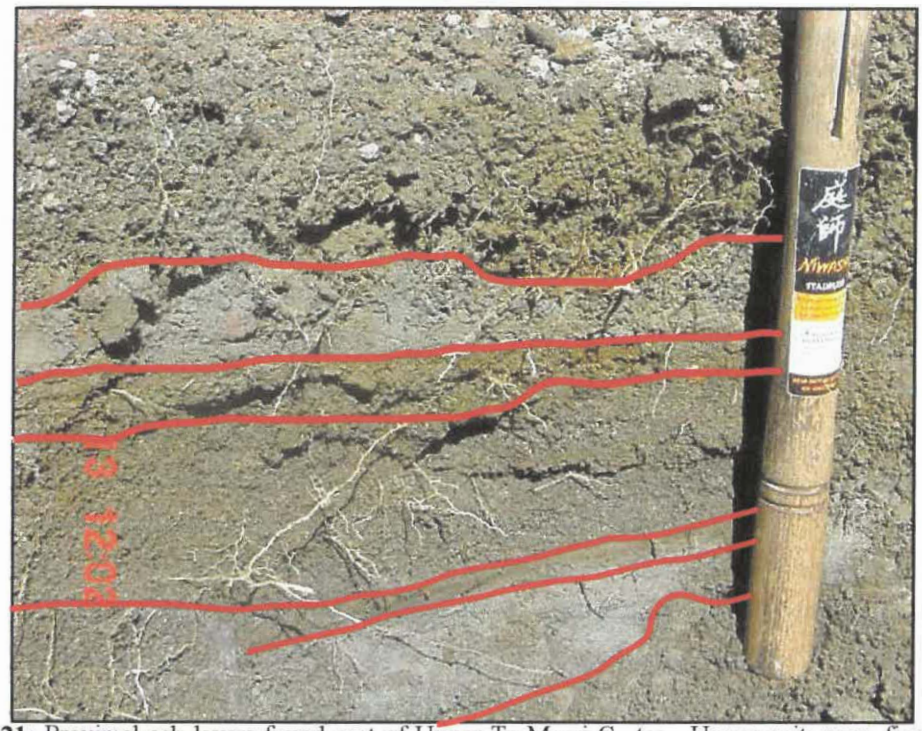

Figure 3.21: Proximal ash layers found east of Upper Te Maari Crater. Upper unit: grey, fine ash with some gravel; Middle unit: grey/brown, coarse ash; Lower unit: grey, fine ash. Tool handle measures 30 cm long.

The composition for most of the deposits coarse material is dominated by andesite lithics with some hydrothermally altered fragments and some white sinter fragments (see chapter four for descriptions).

3.9 Conclusions

The Upper Te Maari Crater is the younger of the two larger craters and the most recently active, with the most recent ash eruptions (1892, 1896) and the c.1500 AD lava flow being sourced from here. It has a narrow, funnel-shaped structure. Three units can be distinguished in the upper crater: an upper unit of weakly consolidated, bedded, coarse andesite breccia; a lower unit of weakly consolidated, massive, very coarse breccia; and a central structure of hydrothermally altered breccia. The origin of these breccias will be discussed in chapter five.

The Lower Te Maari Crater is the older of the two craters. It is a 500 m wide, 60 m deep flat-floored structure, which implies that some shallow collapse has occurred. The stratigraphy of the lower crater is comprised of multiple layers of jointed, massive andesite that has been exposed on the crater wall. There is an intrusion in the western wall with columnar and platy jointing and an area of sulphurous hydrothermal activity. There is also an ephemeral pool on the crater floor where the name "sulphur lagoon" is derived from. Ballistic blocks scattered around the rim of the crater, with a few displaying "breadcrust" textures and impact fractures are the only proximal pyroclastic facies associated with this crater and record minor magmatic explosivity.

Apart from the hydrothermal area on the lower crater wall, there are a few other small areas of steaming ground on the outer slopes of Upper Te Maari Crater and between the upper and lower crater. They are generally small cracks or fissures in the rock and are non-sulphurous.

The lava flows associated with these craters are thick, andesitic, aa to blocky flows. The most recent lava flow has been dated at c.1500 AD by Topping (1974), and was erupted from the Upper Te Maari Crater. It is approximately 4 km long running downslope to the northwest and is comprised of multiple, overlapping lobes. The thickness varies greatly from 80 m near the vent, to 20 m at the flow front. The overall surface texture is rubbly and vesicular, with angular to sub-angular blocks and a massive, less vesicular core. There is some levée development as the flow starts to widen about 1 km from the vent. There are 3-4 older flows, 3-4 km long, north of the craters that can be identified as originating from this area.

A small cluster of craters are found directly north of Lower Te Maari Crater, lying on the outer slope of the crater wall. There are 4-5 pits with a shallow pool possibly infilling one. There are a few outcrops of massive, grey, jointed andesite with slabby fracturing at the base within the pits and one outcrop on the eastern slopes. This area may be the source of the large post-glacial flows on the northern slopes below Te Maari.

There has not been substantial preservation of tephra deposits from any Te Maari Crater eruption. Pits dug proximal to the vent have revealed some coherent ash layers intercalated with soil and reworked deposits. The majority of the deposits are 2-4 cm thick, grey, well to poorly sorted, coarse to fine ash, with some fine-medium lapilli. The composition for most of the coarse material is dominated by andesite lithics with hydrothermally altered fragments and minor white sinter fragments.

CHAPTER FOUR

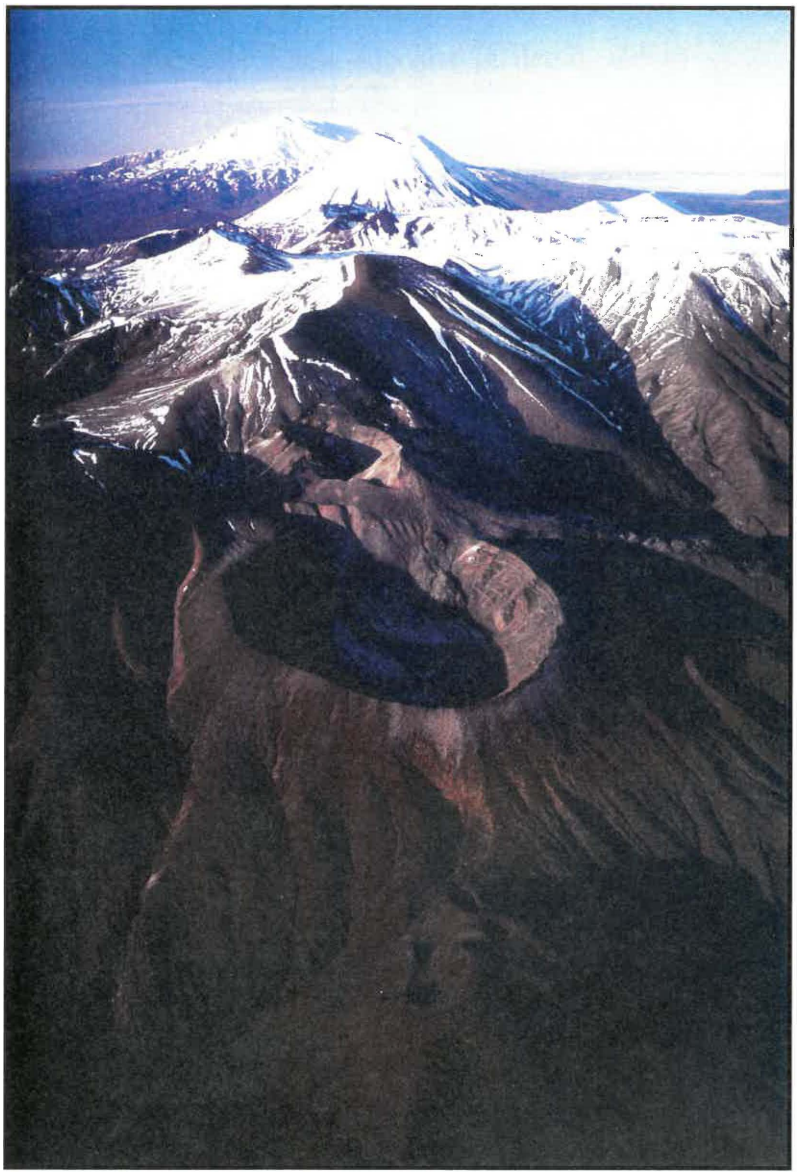

LABORATORY CHARACTERISTICS

4.1 Introduction

Laboratory analyses were conducted on a number of rock and tephra samples from the Te Maari Crater eruptives, including the c.1500 AD lava flow and tephras from various proximal locations. Grainsize, componentry, petrographic and SEM analyses were carried out in order to describe these deposits in detail and to ascertain spatial and temporal differences. Fig. 4.1 shows the locations of the samples taken for analysis, grid references for all sample sites are given in appendix I and lower crater sample labels are shown in appendix IV.

Figure 4.1: Locations of sample sites, Te Maari Craters

4.2 Methods

4.2.1 Thin Sections

Each rock sample was cut into small blocks (~3.5 x 2.4 x 2.4 cm) and then dried at 70° for >3 hours. Vesicular samples were impregnated with araldite K142. One side of the sample was then ground with #600 polish powder, dried once again and then mounted on a frosted glass slide with Hillquist. This was then cured on a hotplate at 60° for >2 hours. The sample was trimmed ~1 mm and then ground to ~30 μm using first a Struers Discoplan-TS and then #600 polish powder on a glass plate.

4.2.2 Sieving

Ash samples were collected from various proximal sites around the Upper and Lower Te Maari Craters (Fig. 4.1). In the laboratory samples containing a mixture of Lapilli and ash were oven dried at 50°C for 48 hours prior to dry-sieving. Sieving was carried out using Endecott sieves, ranging from -4.0 phi up to 4.0 phi at 0.5 phi intervals with a mechanical shaker. Samples were shaken at moderate amplitude for 5 minutes. Each size fraction was weighed and separately retained for later componentry analysis.

Fine ash samples and those ash samples that contained significant quantities of silt and clay sized particles were wet sieved by hand through 2.0 phi and 4.0 phi sieves. The coarser particles were oven dried and dry sieved as above. The grainsize of material <4.0 phi was then analysed using a Malvern Mastersizer-S, laser diffraction particle size analyser.

4.3 Petrography

4.3.1 Upper Te Maari Crater

In hand specimen the breccia associated with the Upper Te Maari Crater is brown/grey where fresh and weathers to red (Fig. 4.2a). The rock has also been altered to purple,

white and yellow where there has been hydrothermal alteration (Fig. 4.2b). It contains coarse ash to block sized, angular to subrounded clasts. It is unconsolidated and poorly sorted with an ash-sized matrix. The clasts within the breccia appear to be monolithologic. They are medium grey, porphyritic, poorly vesicular andesite, with a medium grainsize and a maximum size of 2 mm. The crystals are subhedral and tabular plagioclase and pyroxene.

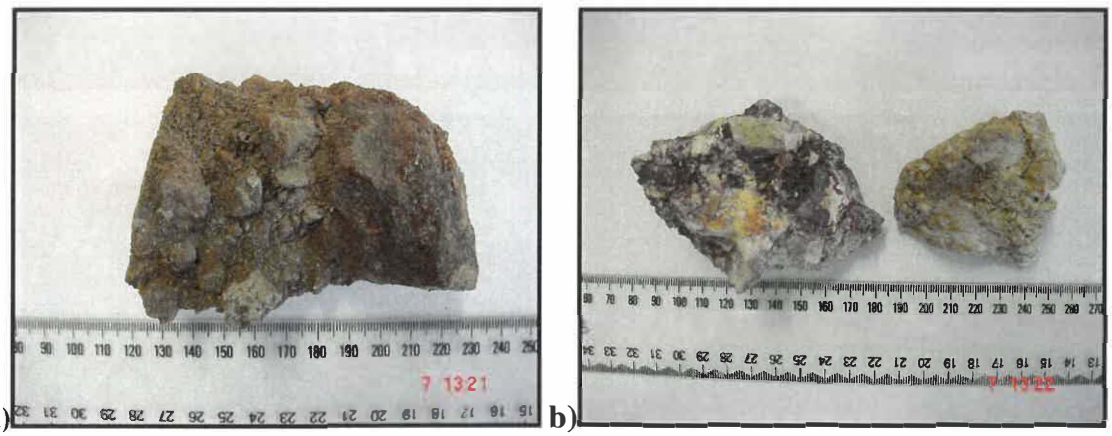

a) b)

Figure 4.2: Hand specimen of A) Upper Te Maari Crater breccia, sample UC9, B) Upper Te Maari Crater hydrothermally altered breccia unit, sample UC5. Ruler units in mm.

In thin section the breccia matrix (material <2 mm) (Fig. 4.3 a, b, e) is porous and weakly consolidated, comprised of crystals ranging in size from 0.2 to 0.5 mm, dense andesite lava and glass. The andesite lava clasts (Fig. 4.3 a, b, c, d) are porphyritic, vesicular and hypocrystalline. They are medium-grained andesite with maximum crystal grainsizes of 4-5 mm. The main phenocrysts are plagioclase, pyroxenes and opaques. The dominant plagioclase crystals display subhedral, tabular forms and show twinning, oscillatory, patchy and reverse zoning. This is often associated with partial resorbtion of plagioclase back into the melt, which occurs with magma mixing (Hobden, 1997). There are also rare sieve and poikilitic textures within the plagioclase crystals. The pyroxenes are in the form of subhedral to euhedral augite and hypersthene. The crystals often form glomeroporphyritic clots. There are also rare xenoliths of greywacke. The groundmass is intergranular and hyalopilitic with black glass often weathered to red-brown.

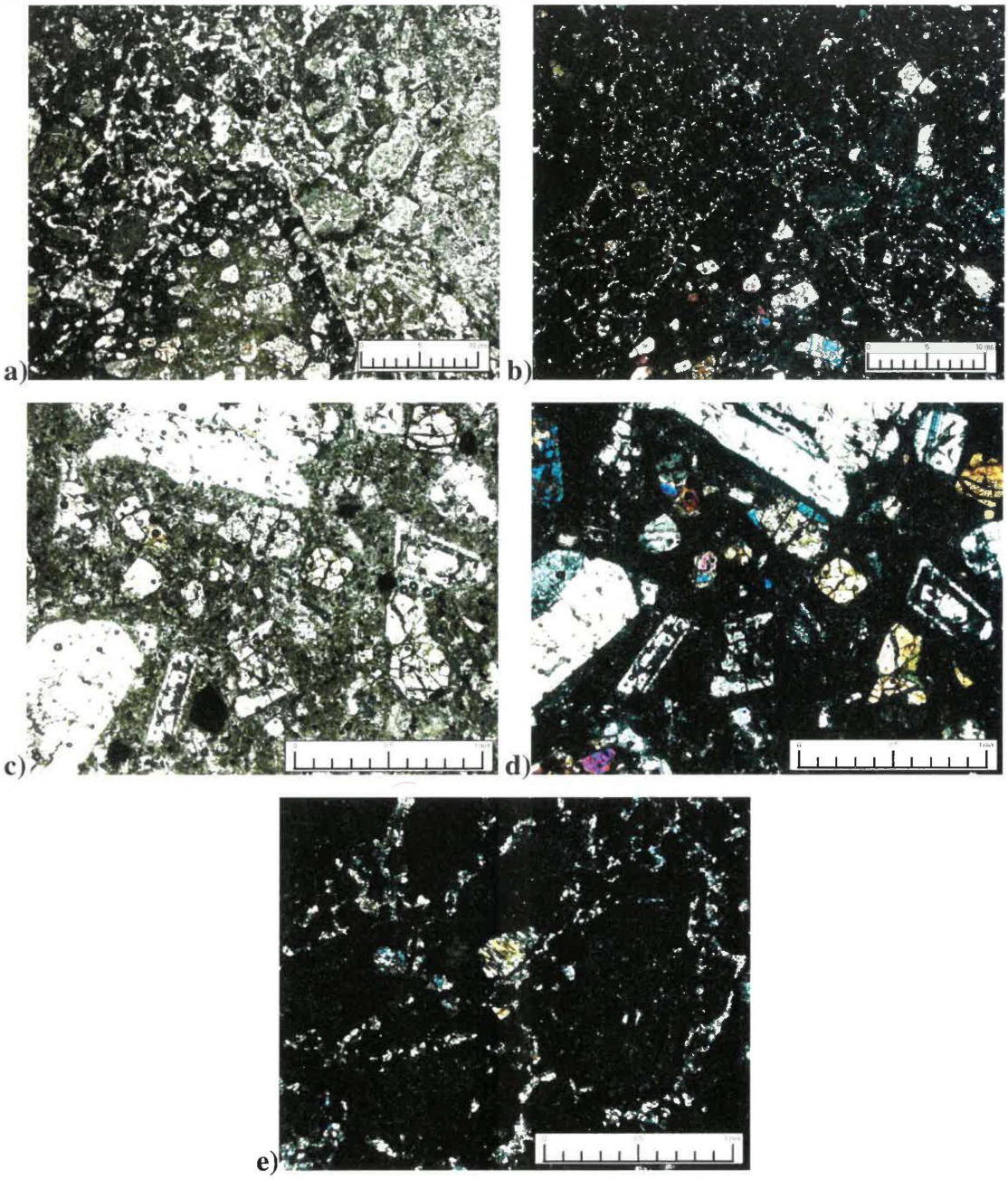

Figure 4.3: Photomicrographs of andesite from Upper Te Maari Crater. A) Breccia under plane polarised light at 1.25x magnification, B) Breccia under cross-polarised light at 1.25x magnification, C) Breccia lava clast under plane polarised light at 4x magnification, D) Breccia lava clast under cross-polarised light at 4x magnification, E) Breccia matrix under cross-polarised light at 4x magnification.

The hydrothermally altered breccia clasts within the Upper Te Maari Crater displays much the same thin section characteristics with plagioclase showing signs of alteration (Fig 4.4).

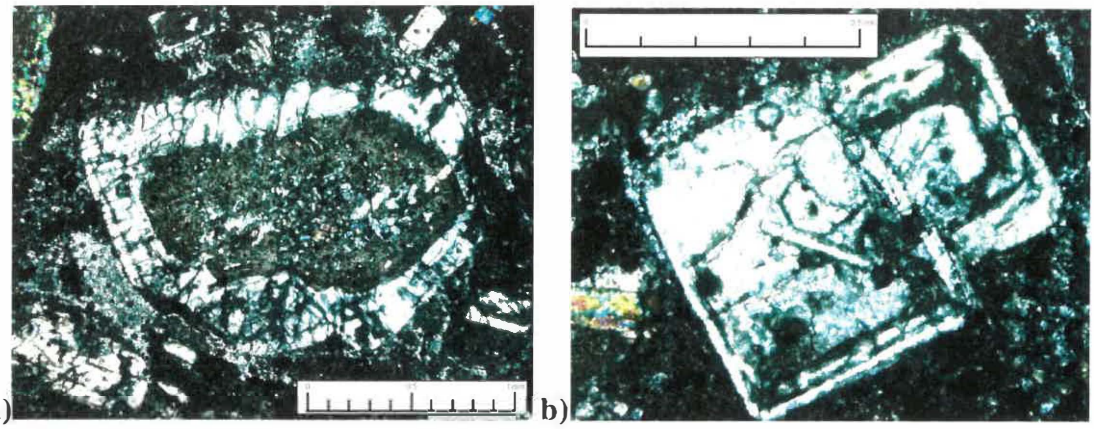

Figure 4.4: Photomicrographs of hydrothermally altered plagioclase in the Upper Te Maari Craters. UC5 – from hydrothermally altered central unit. Photo A) at 4x magnification, B) at 10x magnification.

The upper crater samples were point counted giving a range of crystallinity between 36-50%. The sample mineralogies were very similar (Fig. 4.5) so an average modal mineralogy was calculated (Fig 4.6). This estimated an average crystallinity of 44 % and an average vesicularity of 5-6%.

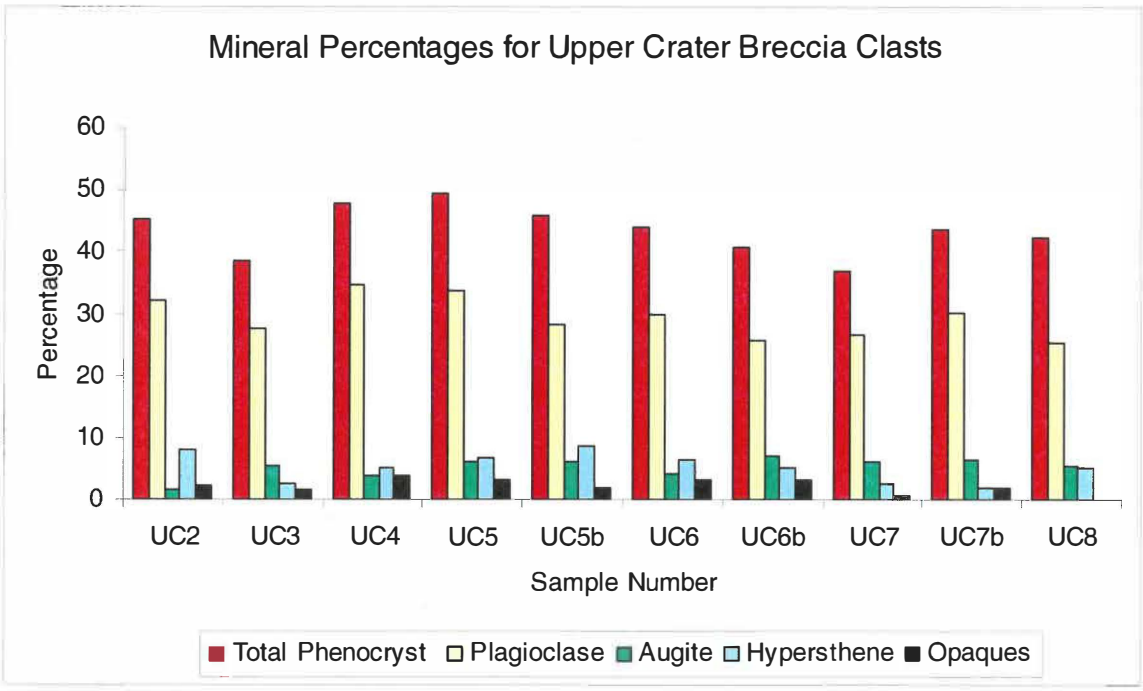

Figure 4.5: Mineral percentages for Upper Te Maari Crater samples.

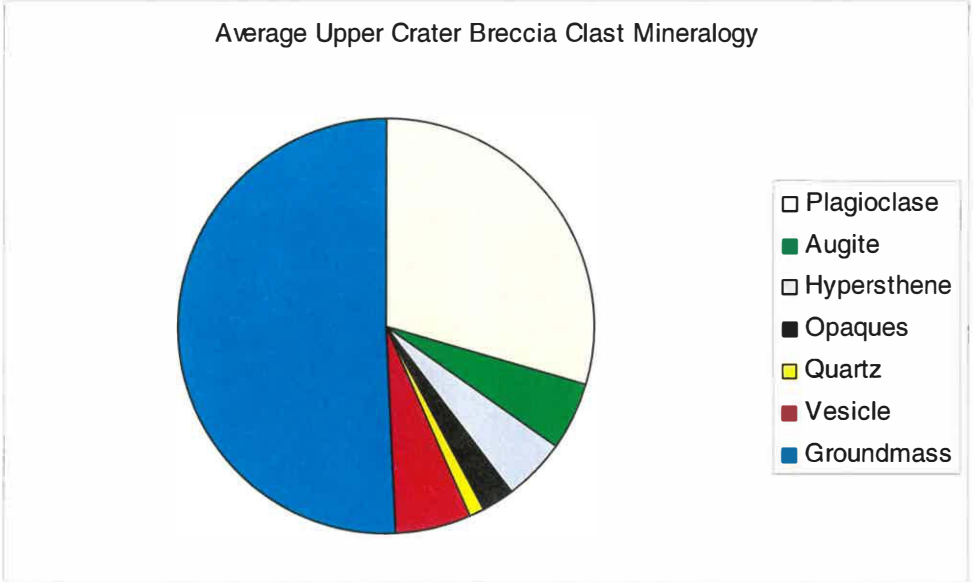

Figure 4.6: Average modal mineralogy for Upper Te Maari Crater breccia clasts.

4.3.2 Lower Te Maari Crater Lavas

In hand specimen there is two andesite rock types that display different characteristics in the Lower Te Maari Crater (Fig. 4.7). The most abundant type is a medium grey, porphyritic andesite. It is medium-grained with a maximum grainsize of 3 mm and crystals of subhedral plagioclase and pyroxene. Samples from the outer margins of the unit have moderate vesicularity, while samples from the middle of the unit are poorly vesicular.

Figure 4.7: Two andesite rock types present in Lower Te Maari Crater. Light grey andesite on left, sample LC8, medium grey andesite on right, sample 26S12. Ruler units in mm.

The second andesite is light grey, moderately vesicular, fine medium-grained with a maximum grainsize of 2 mm and is porphyritic (Fig. 4.8b). The crystals are subhedral, prismatic pyroxene and subhedral, tabular plagioclase.

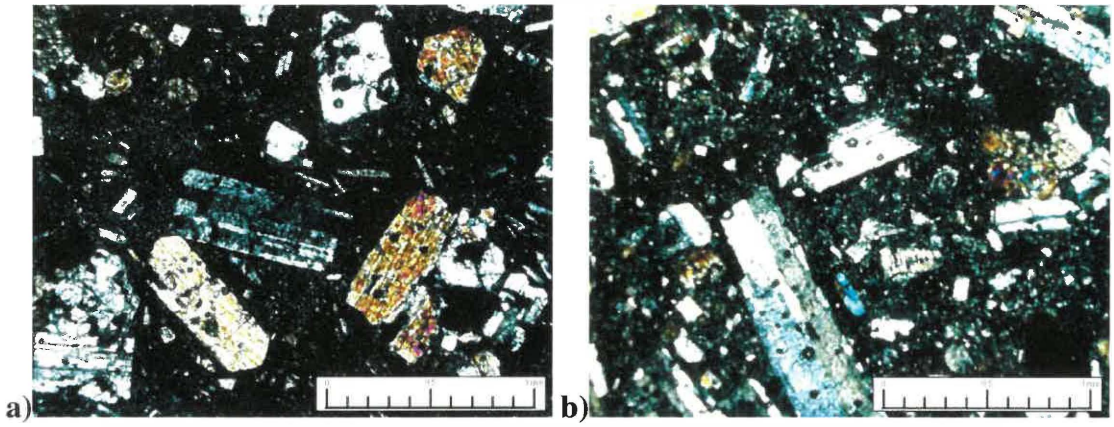

Figure 4.8: Photomicrographs of andesite from Lower Te Maari Crater lavas. A) medium grey andesite under cross-polarised light, B) light grey andesite under cross-polarised light. Photos at 4x magnification.

In thin section the medium grey andesite is hypocrystalline, porphyritic, vesicular and fine to medium-grained with a maximum grainsize of 4.5 mm (Fig. 4.8a). The main phenocrysts are plagioclase, pyroxene and opaques, with glomeroporphyro clasts present. The dominant plagioclase is subhedral and tabular and displays twinning, oscillatory zoning and rare sieve textures. Augite and hypersthene are tabular subhedral to euhedral. There are also crystal xenoliths of predominantly quartz and opaques present in some of the samples (Fig. 4.9). The groundmass is felted, intergranular and hyalopilitic with black glass weathering to red-brown.

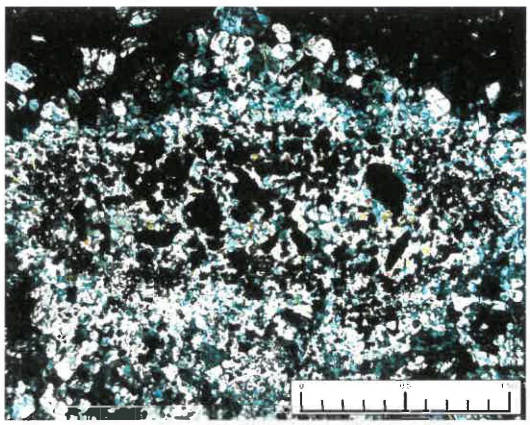

Figure 4.9: Photomicrograph of xenolith in Lower Te Maari Crater andesite. Photo at 4x magnification.

The light grey andesite displays much the same characteristics as the medium grey andesite, but the colour appears lighter and is fine-grained with a maximum grainsize of 2.5 mm (Fig. 4.8b). The groundmass also contains numerous very fine, granular opaques.

The lower crater samples were point counted giving a range of crystallinity between 35-45%. The sample mineralogies were very similar (Fig. 4.10) so an average modal mineralogy was calculated (Fig 4.11). This estimated an average crystallinity of 40% and an average vesicularity of 6-7%.

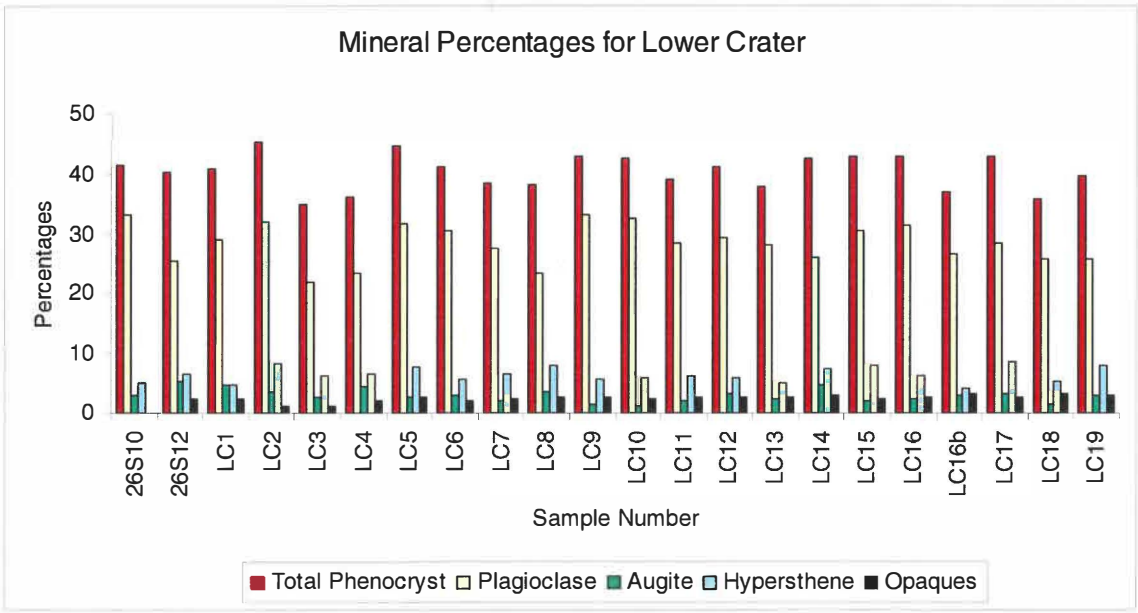

Figure 4.10: Mineral percentages for Lower Te Maari Crater samples.

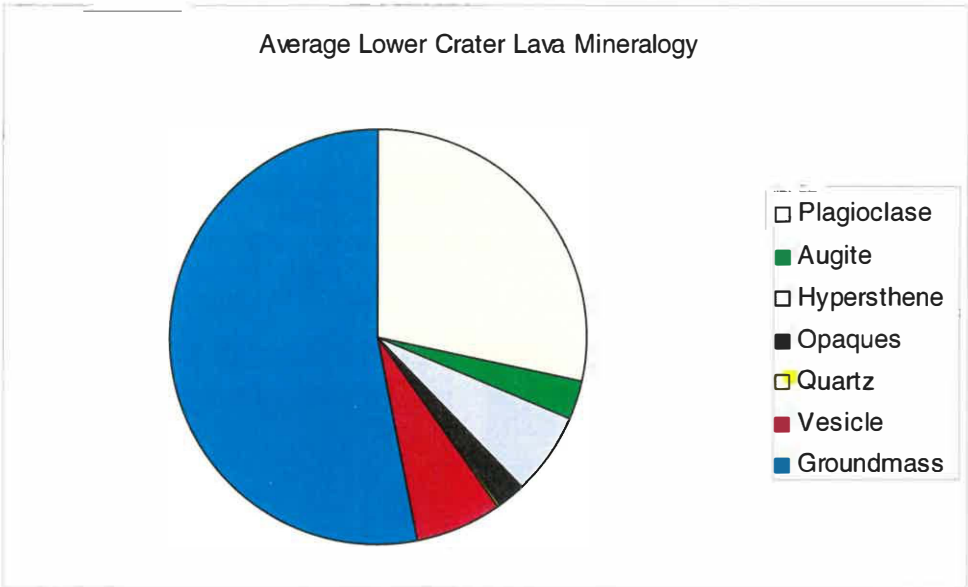

Figure 4.11: Average modal mineralogy for Lower Te Maari Crater lavas.

4.3.3 1500 AD Lava Flow

In hand specimen the rock associated with the 1500 AD lava flow is a dark grey, coarse medium grained, porphyritic andesite, with a maximum grainsize of 5 mm (Fig. 4.12). Samples from the outer margins of the flow are very vesicular (19-29%) and have been weathered to red, while samples from the core of the flow are less vesicular (6-15%). Phenocrysts are subhedral, tabular plagioclase and augite. Some of the samples are very glassy and display concoidal fracture.

Figure 4.12: Hand specimen of 1500 AD lava flow, sample LFF2.

In thin section this andesite is hypocrystalline, porphyritic, vesicular and coarse medium-grained with a maximum grainsize of 7-8 mm (Fig. 4.13 a, b). The main phenocrysts are plagioclase, pyroxenes, opaques and olivine. The plagioclase is tabular subhedral to euhedral and displays twinning, oscillatory zoning, sieve textures and is sometimes poikilitic with pyroxene. The pyroxenes of augite and hypersthene are tabular subhedral to euhedral and the olivine is euhedral. These minerals can also form glomeroporphyritic clots (Fig. 4.13 c). The matrix is felted and hyalopilitic with glass weathering to red.

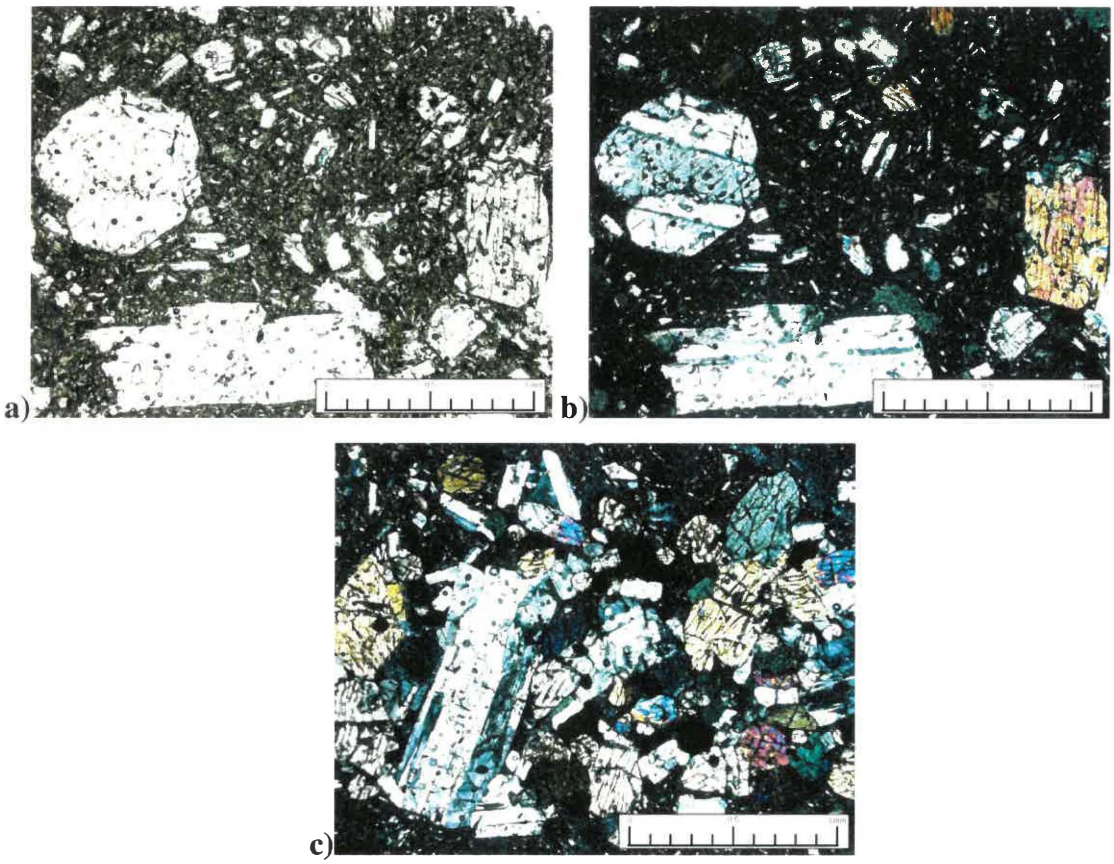

Figure 4.13: Photomicrographs of andesite from 1500 AD lava flow. A) under plane polarised light, B) under cross-polarised light, C) Glomeroporphyritic clast. Photos at 4x magnification.

The 1500 AD lava flow samples were point counted giving a crystallinity range between 35-50%. The sample mineralogies were very similar (Fig. 4.14) so an average modal mineralogy was calculated (Fig 4.15). This estimated an average crystallinity of 41 % and an average vesicularity of 14%. The range of crystallinity within the 1500 AD lava flow samples indicate that the flow was not emplaced as a continuous event, rather as a series of pulses during the eruption. The samples from the 1500 AD lava flow are also

very similar in mineralogy to the upper crater breccia clasts with comparable crystallinities. This implies that the upper crater breccia was probably emplaced during the same eruptive event as the 1500 AD lava flow.

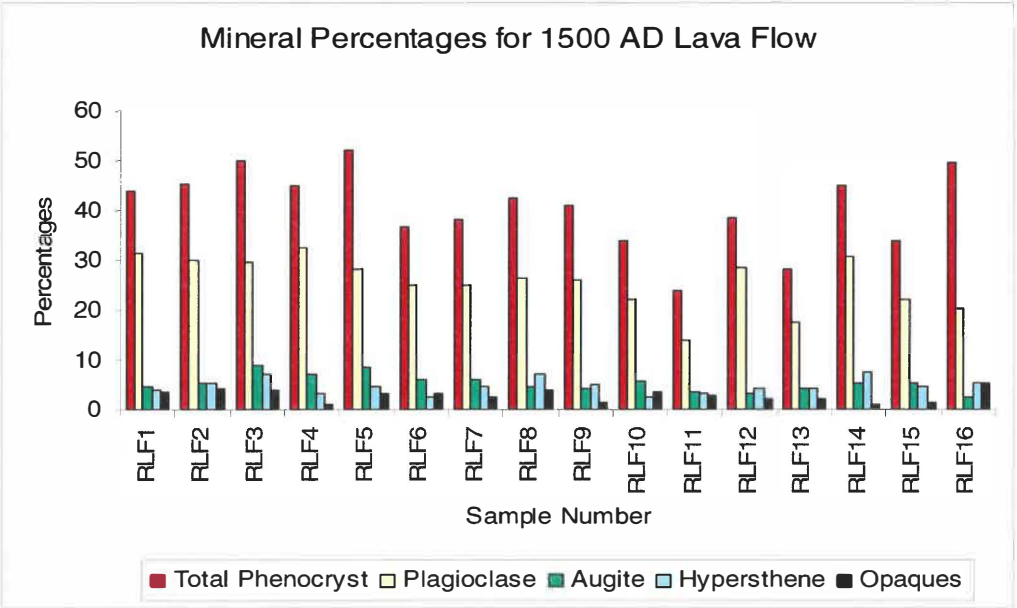

Figure 4.14: Mineral percentages for the 1500 AD lava flow.

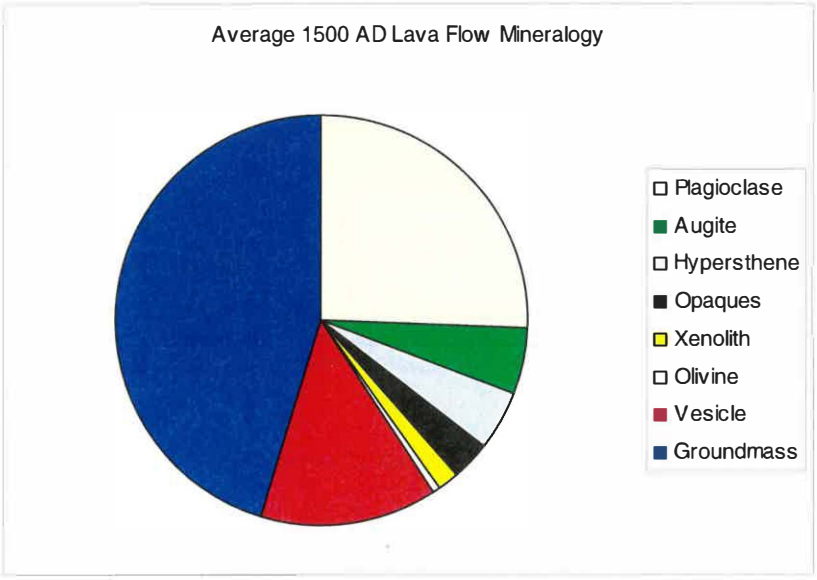

Figure 4.15: Average modal mineralogy for 1500 AD lava flow.

The vesicularity also varies considerably across the samples (Fig. 4.16), although this is probably due to the location of the samples on the flow.

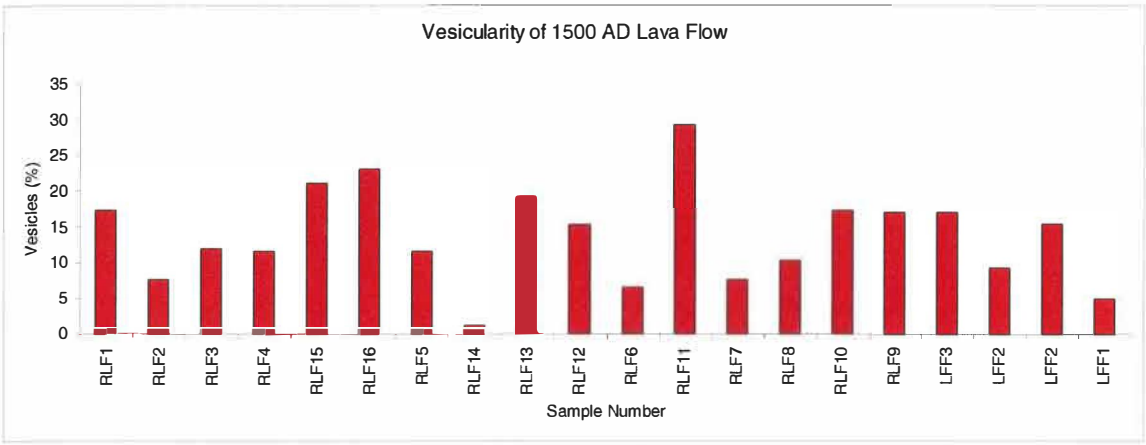

Figure 4.16: Vesicularity of 1500 AD lava samples.

4.3.4 Northern Crater Cluster

In hand specimen the rock sampled in the Northern Crater Cluster is a medium grey, vesicular, porphyritic andesite (Fig. 4.17). It has a medium grainsize with a maximum size of 2 mm. The crystals are subhedral to euhedral plagioclase and pyroxene.

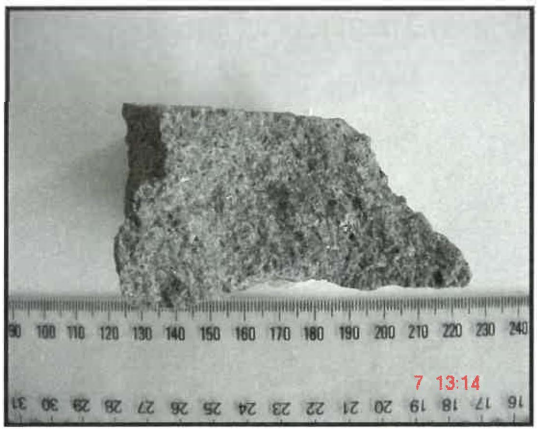

Figure 4.17: Hand specimen of northern crater cluster, sample EC2.

In thin section this andesite is porphyritic, vesicular, hypocrystalline and medium-grained with a maximum phenocryst size of 3 mm (Fig. 4.18). The main phenocrysts are plagioclase, pyroxenes and opaques. The plagioclase is subhedral and tabular and displays twinning and oscillatory zoning. The pyroxenes are augite and hypersthene and are subhedral to euhedral. These minerals can also form glomeroporphyritic clots. The matrix is hyalopilitic and felted with coarser sized plagioclase than any other of the Te Maari eruptives.

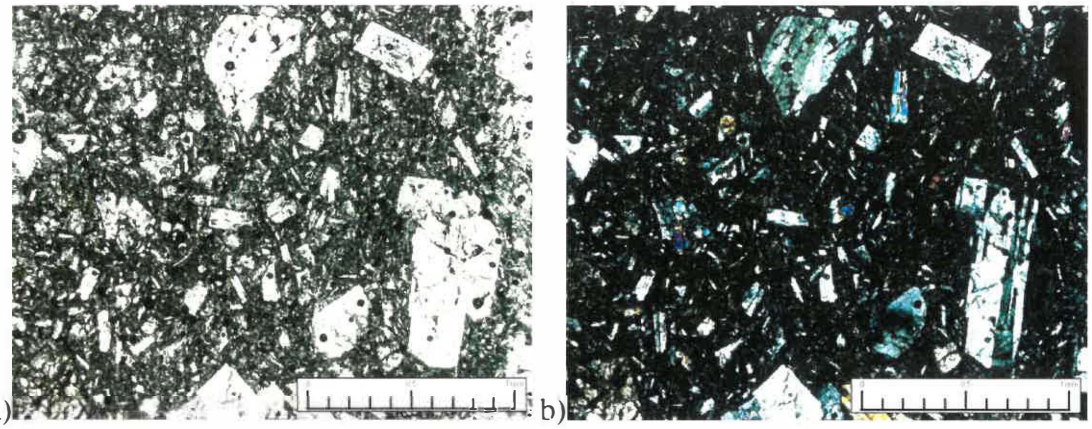

Figure 4.18: Photomicrographs of andesite from Northern Crater Cluster. a) under plane polarised light, b) under cross-polarised light. Photos at 4x magnification.

The northern crater cluster samples were point counted giving a crystallinity range between 33-43%. The sample mineralogies were very similar (Fig. 4.19) so an average modal mineralogy was calculated (Fig 4.20). This estimated an average crystallinity of 40% and an average vesicularity of 11-12%.

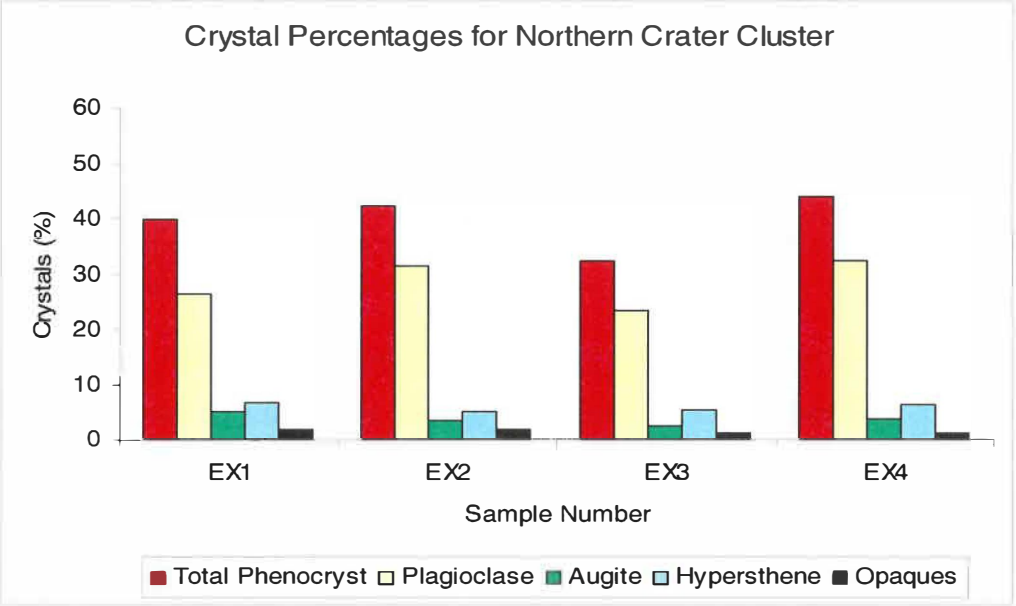

Figure 4.19: Mineral percentages for northern crater cluster.

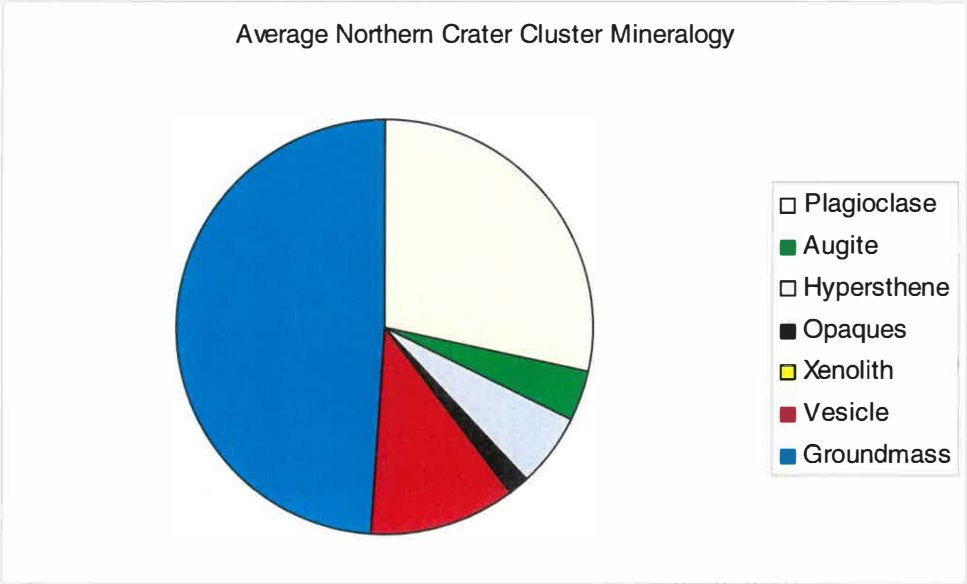

Figure 4.20: Average modal mineralogy for Northern Crater Cluster.

4.4 Scanning Electron Microscope (SEM) Analysis

To analyse the glass in the matrix of the 1500 AD lava flow samples, selected slides were polished further to obtain a flat surface. The SEM was used to produce images of the matrix and microlite crystals within the glass (Fig. 4.20a, b). A quantitative microanalysis was then conducted on the microlites in order to identify the mineral.

Due to problems with the slide preparation the images obtained were not of sufficient quality or contrast to enable an in-depth analysis of the groundmass crystallinity. However, some microanalysis was performed and this resulted in microlites showing peaks of aluminium, silicon and some calcium, indicating pyroxene (Fig. 4.20c), while other results showed peaks of magnesium, silicon and iron, indicating mafic pyroxene microlites (Fig. 4.20d).

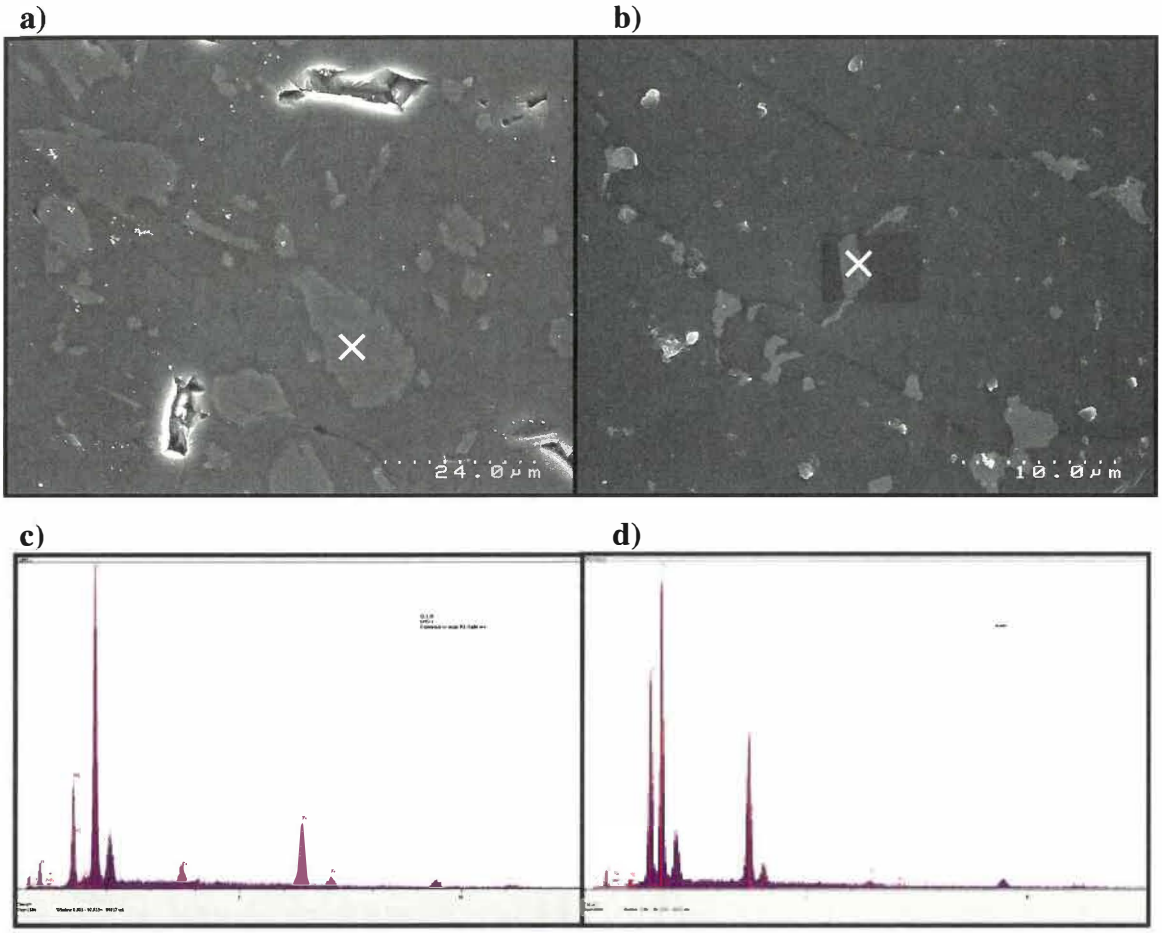

Figure 4.20: A, B) SEM images of glass in the matrix of 1500 AD lava flow samples. White crosses show area microanalysed. C, D) Results of microanalysis for mafic, pyroxene microlite (C) and pyroxene microlite (D).

4.5 Ash Analysis

The componentry of each ash sample was examined and those that were considered to be most likely primary deposits and closely correlated in the field were the focus of detailed component analysis. The remainder of this chapter will be considering just those samples. The full results for all grainsize analyses undertaken in this project are given in appendix II.

4.5.1 Grainsize Analysis

All of the samples generally display a normal distribution with a mean grain size between -1 phi and 1 phi, averaging at 0.39 phi (Fig. 4.21).

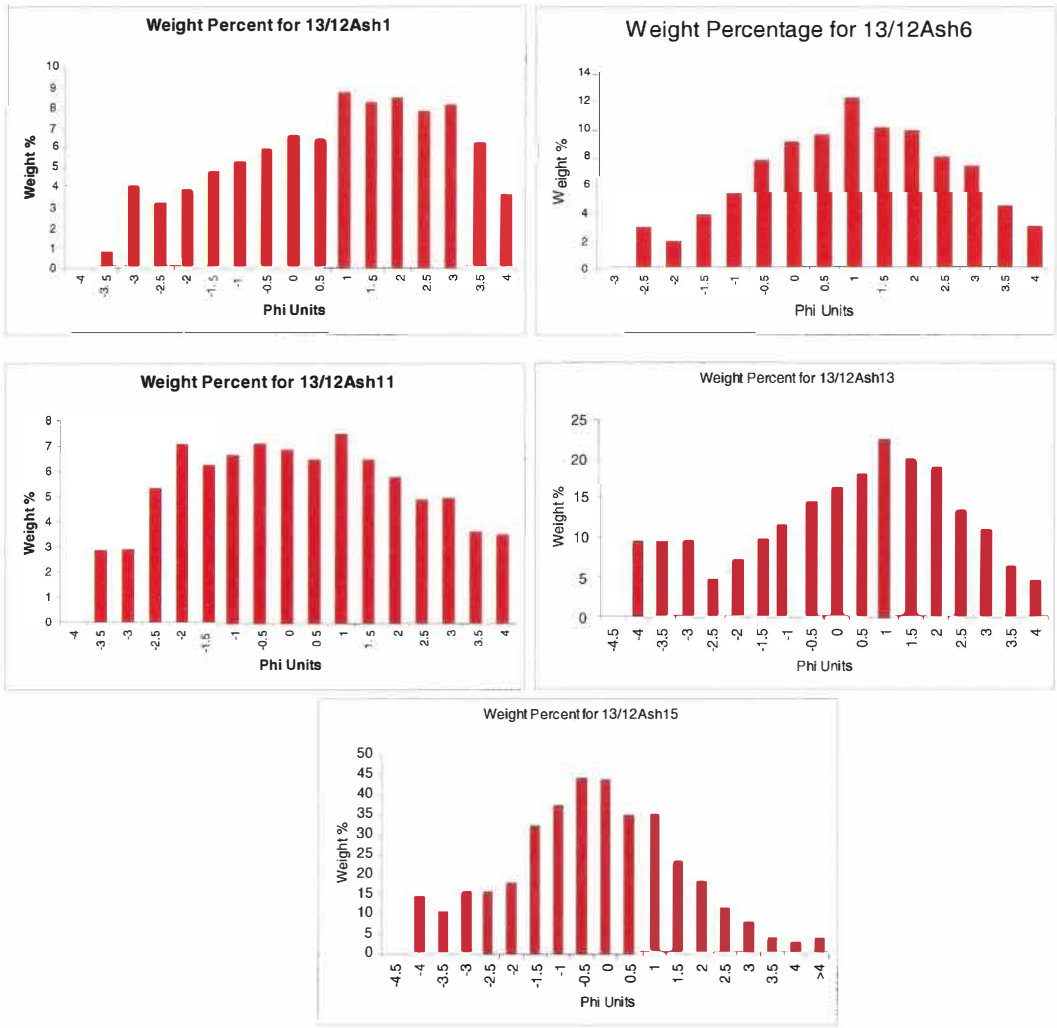

Figure 4.21: Grainsize distributions for proximal Te Maari Crater ash samples.

They are well to poorly sorted with an average sorting of 2.15 phi. Comparisons with ash-fall from Mount Ngauruhoe and Mount Ruapehu (1995-1996) eruptions are shown in figure 4.22.

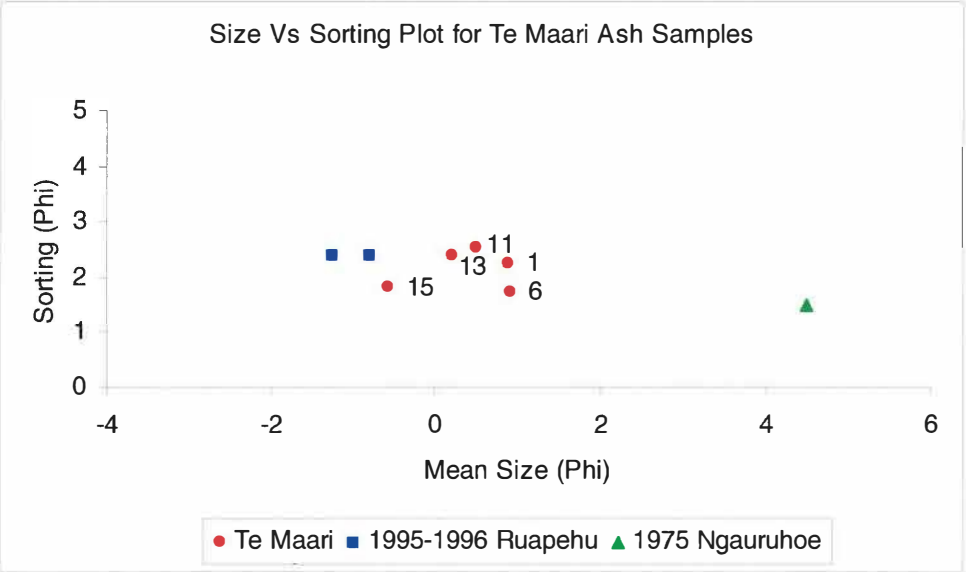

Figure 4.22: Graph of mean grainsizes versus sorting for Te Maari proximal ash samples. Ngauruhoe (1975) ash and Ruapehu (1995-1996) ash samples plotted for comparison.

4.5.2 Componentry

The three coarsest fractions in each sample were used for componentry analysis. There were four main clast types identified in each sample: 1) angular to subrounded, medium grey, non-vesicular, porphyritic andesite clasts up to 10 mm; 2) angular to subangular, dark, coarsely porphyritic, vesicular andesite clasts up to 10 mm; 3) angular to subrounded, red-brown to white, hydrothermally altered lithic clasts up to 8 mm; and 4) angular to subangular, white sinter fragments with clasts up to 10 mm (Fig. 4.23).

Figure 4.23: Lithics found in Te Maari Crater proximal ash samples. A) medium grey andesite, B) dark andesite, C) hydrothermally altered lithics, D) white sinter fragments. Ruler in mm.

Figure 4.24 shows the componentry of each sample averaged over the three coarsest size fractions. Averaging all the samples together gives a composition of 60% medium grey andesite, 33% hydrothermally altered andesite, 5% dark andesite and 2% sinter fragments.

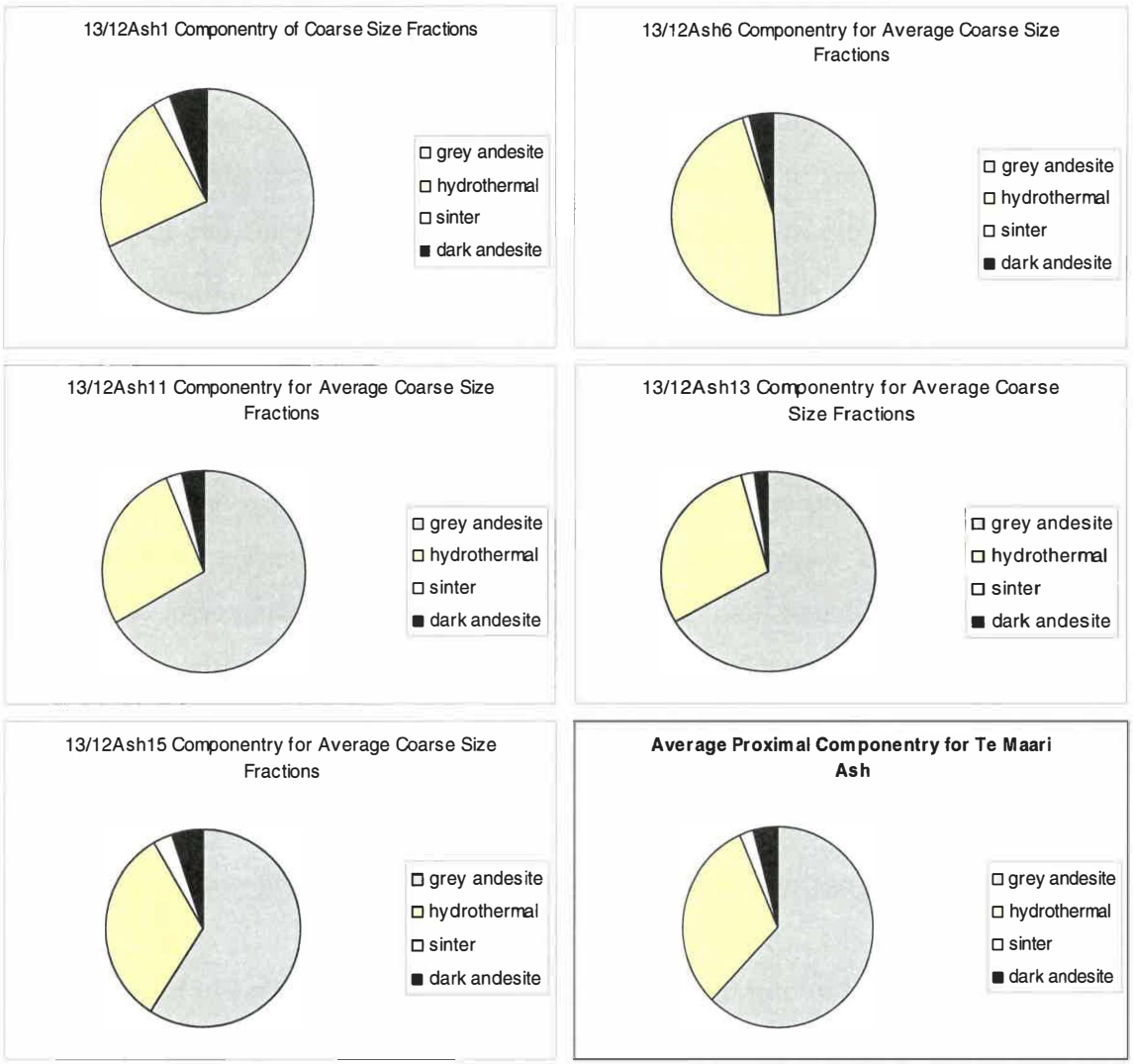

Figure 4.24: Proximal Te Maari ash sample composition, averaged from three coarsest size fractions.

The white sinter clasts found in the samples could be fragments of the white sinter mound in the Lower Te Maari Crater, described by Sir James Hector (chapter 1.4), before the 1869 eruption. For most of the samples there was a coating of dust and mud that was not easy to rinse out of rough surfaces and for a few clasts the coating appeared to be baked on.

4.6 Conclusions

The Upper Te Maari Crater breccia is, in hand specimen, unconsolidated, brown/grey, (weathered to red), containing ash to block sized, angular to subrounded clasts. It is poorly sorted and matrix-supported. The clasts are medium grey, porphyritic, poorly vesicular andesite. They have a medium grainsize with crystals of subhedral and tabular plagioclase, pyroxene and opaques.

In thin section the breccia matrix is very vesicular and granular, comprised of crystals, dense andesite lava and glass. The andesite lava clasts are porphyritic, vesicular and hypocrystalline. They are medium-grained with phenocrysts of subhedral, tabular plagioclase, pyroxenes and euhedral opaques and rare xenoliths. The dominant plagioclase crystals show twinning, oscillatory, patchy and reverse zoning, and rare sieve and poikilitic textures, indicating magma mixing. The groundmass is intergranular and hyalopilitic. The hydrothermally altered breccia within the Upper Te Maari Crater displays much the same characteristics with plagioclase showing signs of alteration. These samples have an average crystallinity of 44% and an average vesicularity of 5-6%.

Lavas exposed in Lower Te Maari Crater can be grouped into two main types according to mineral abundance. The most dominant type is a medium grey, medium-grained, vesicular, porphyritic andesite with phenocrysts of subhedral plagioclase and pyroxene. The second andesite is light grey, moderately vesicular, fine to medium-grained and porphyritic with crystals of subhedral, prismatic pyroxene and subhedral, tabular plagioclase.

In thin section the medium grey andesite is hypocrystalline, porphyritic, vesicular and fine medium-grained with phenocrysts of tabular subhedral plagioclase, tabular subhedral to euhedral pyroxene and euhedral opaques. The dominant plagioclase displays twinning, oscillatory zoning and rare sieve textures. There are also xenoliths present in some of the samples. The groundmass is felted, intergranular and hyalopilitic. These samples have an average crystallinity of 40% and an average vesicularity of 6-7%.

In hand specimen the 1500 AD lava flow from Upper Te Maari Crater is dark grey, coarse medium grained, vesicular and porphyritic with phenocrysts of tabular subhedral plagioclase and pyroxenes. Samples from the outer margins of the flow are vesicular and have been weathered to red, while samples from closer to the core are less vesicular. Some of the samples are very glassy.

In thin section this andesite is hypocrystalline, porphyritic, vesicular and coarse medium-grained with phenocrysts of subhedral to euhedral plagioclase, pyroxenes, euhedral opaques and euhedral olivine. The plagioclase displays twinning, oscillatory zoning, sieve textures and is sometimes poikilitic with pyroxene. The groundmass is felted and hyalopilitic with glass weathering to red. These samples have an average crystallinity of 41% and an average vesicularity of 14%.

In hand specimen the andesite exposed in the Northern Crater Cluster is medium grey, medium grain-sized, moderate to highly vesicular and porphyritic with subhedral to euhedral plagioclase and pyroxene.

In thin section this andesite is porphyritic, vesicular, hypocrystalline and medium-grained with phenocrysts of tabular subhedral plagioclase, pyroxenes and euhedral opaques. The plagioclase displays twinning and oscillatory zoning. The groundmass is hyalopilitic and felted with coarser sized plagioclase than any other of the Te Maari eruptives. These samples have an average crystallinity of 40% and an average vesicularity of 11-12%.

The proximal primary ash samples found at the Te Maari Craters All generally display a normal grainsize distribution with mean grainsizes between -1 phi and 1 phi, averaging at 0.39 phi and are well to poorly sorted.

There were four main clasts found in each sample: 1) angular to subrounded, medium grey, non-vesicular, porphyritic andesite; 2) angular to subangular, dark, coarsely porphyritic, vesicular andesite; 3) angular to subrounded, red-brown to white,

hydrothermally altered lithics; and 4) angular to subangular, white sinter fragments. An average of all the samples together gives a composition of 60% medium grey andesite, 33% hydrothermally altered andesite, 5% dark andesite and 2% sinter fragments.

CHAPTER FIVE

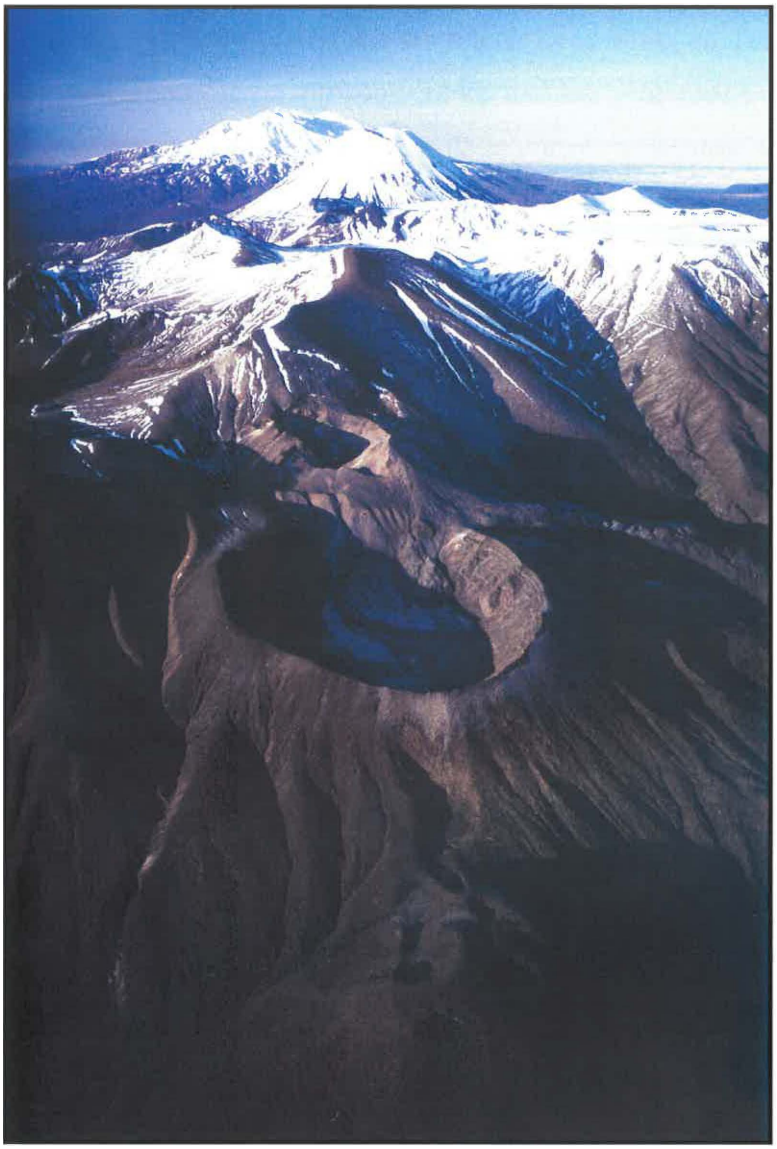

ERUPTIVE PROCESSES AND HISTORY

5.1 Introduction

The Te Maari Craters are perhaps one of the most long-lived vents on Tongariro, being active since the last glacial maximum, probably 14 ka, and has continued through historic times. Historical eruptions have been observed at these craters throughout the 1800's, the most notable being in 1892 and 1896. The funnel-shaped form of Upper Te Maari Crater is thought to be the result of the 1869 and 1896 eruptions. The lava flows associated with these craters have been dated at ~14 ka, 6.7-9.7 ka and with the youngest flow dated at around 1500 AD. From historic observations made of eruptions and analysis of the eruptive products in the field, the typical eruptive style of these craters range from phreatic to vulcanian with associated lava flows.

5.2 Previous Work

Previous work on the eruptives and history of Te Maari Craters has produced varying accounts of the timeline and products that can be attributed to them. Maps of the northern lava flows especially have evolved over time as more information is collected.

5.2.2 Tephrostratigraphic Description

Using the position of tephras in the stratigraphic column, Topping (1974) dated and produced a map of the lava flows from the Te Maari Craters, with the 1500 AD lava flow, the large, levéed, 6.7-9.7 ka, flow north of lower crater and a smaller, 9.7-12 ka flow to the northeast of the lower crater. Through chemical and titanomagnetite analysis, Topping (1974) also attributed the Rotoaira Lapilli to the Lower Te Maari Crater.

Hobden (1997) described the volcanic stratigraphy of the Te Maari Craters, stating that at least 15 lava flows and pyroclastic units could be recognised from the northernmost vents. The flows sampled in this study were all identified as andesitic with SiO_2 ranging from 57.5 to 60.2 wt%. This occupied the highest SiO_2 section of the MgO-SiO_2 diagram, indicating that they were not parental to any other eruptives from Tongariro.

Based on geochemical analysis and the lack of consistent AFC trends, it was concluded that the plumbing systems for Ngauruhoe, Red Crater and Te Maari Craters were not closely inter-connected over the last thousand years or so. This presents the probability that several spatially separate reservoirs coexisted, feeding vents a few kilometres apart (Hobden, 1997).

Nairn *et al.,* (1998) identified two stages in the 10 ka eruption sequence at the Tongariro Volcanic Centre that the Te Maari Craters may have been active in (chapter 1.4). These stages produced the PM 2/Te Rato Lapilli and the PM 6/Poutu Lapilli, a component of which the Te Maari Craters are thought to have contributed. Nairn *et al.,* (1998) also thought the large levéed flow north of the crater cluster may have been emplaced at the end of the 10 ka sequence, based on Topping's date using the Papakai Formation, and the PM2/PM6 deposits found preserved under and intercalated, respectively, with explosion breccias sourced from Te Maari.

Based on this previous work done on the Te Maari Craters and others on the Tongariro Volcanic Centre, including Hobden *et al.,* (1996), Lecointre *et al.,* (2004) produced a map with Topping's lava flow outlines and which also outlined older >14.7 ka flows (Fig. 5.1).

More recently, additional mapping by T. Kobayashi of the 14 ka Rotoaira deposits, has correlated the agglutinates of North Crater with the sub-plinian fall, therefore suggesting that the Rotoaira Lapilli is not from Te Maari, but is sourced from North Crater. Work is continuing on this deposit (T. Kobayashi, pers. comm., 2004). This is supported by the mapping in this study which has identified no proximal pyroclastic facies in the vicinity of the Te Maari Craters which can be correlated with the 14 ka Rotoaira deposits.

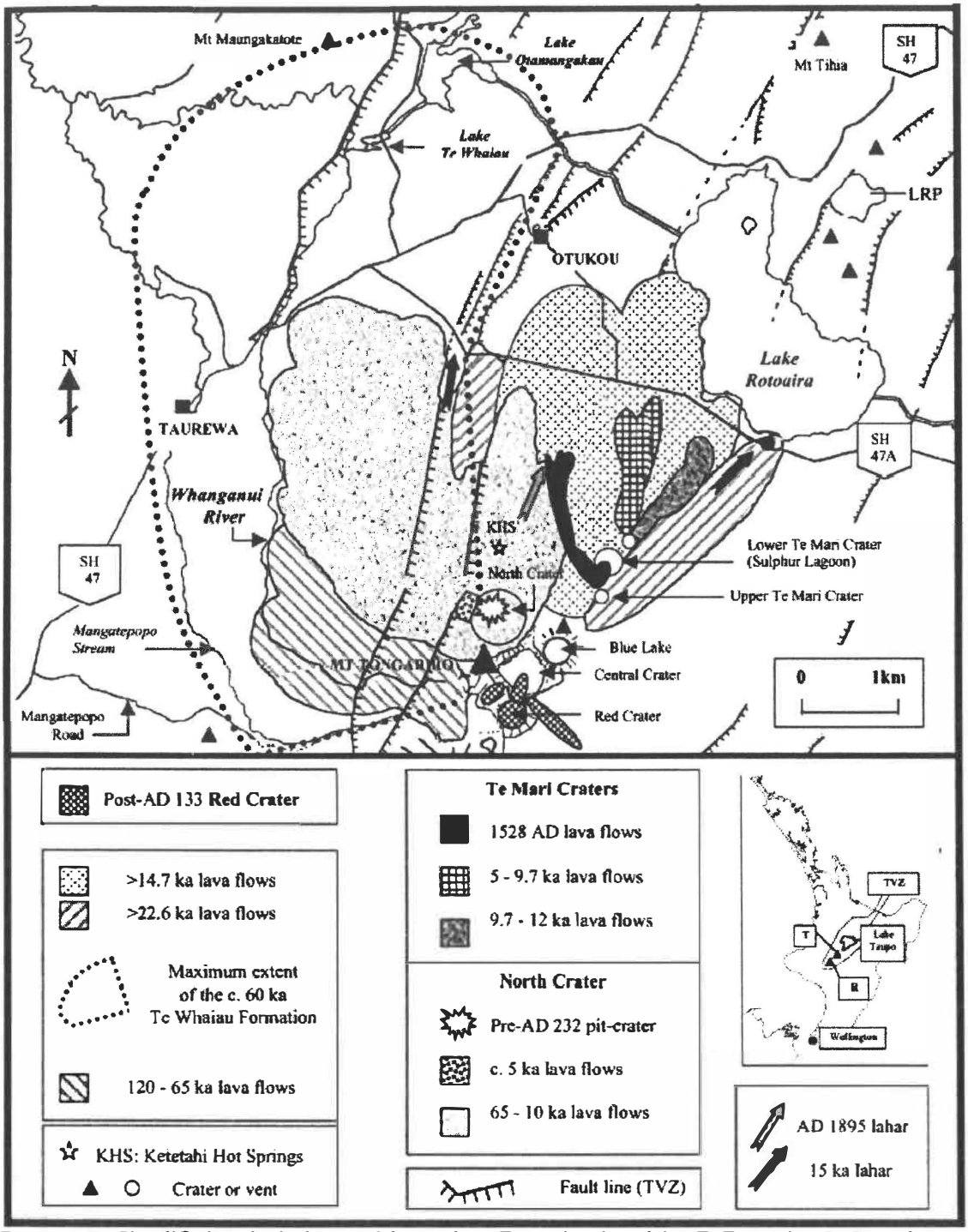

Figure 5.1: Simplified geological map of the northern Tongariro ring plain. T=Tongariro, R=Ruapehu. After Lecointre (2004).

5.3 *Styles of Eruptive Activity*

The eruptive style of the Te Maari Craters ranges from phreatic steam and ash (Fig. 5.2) and vulcanian eruptions to lava producing eruptions.

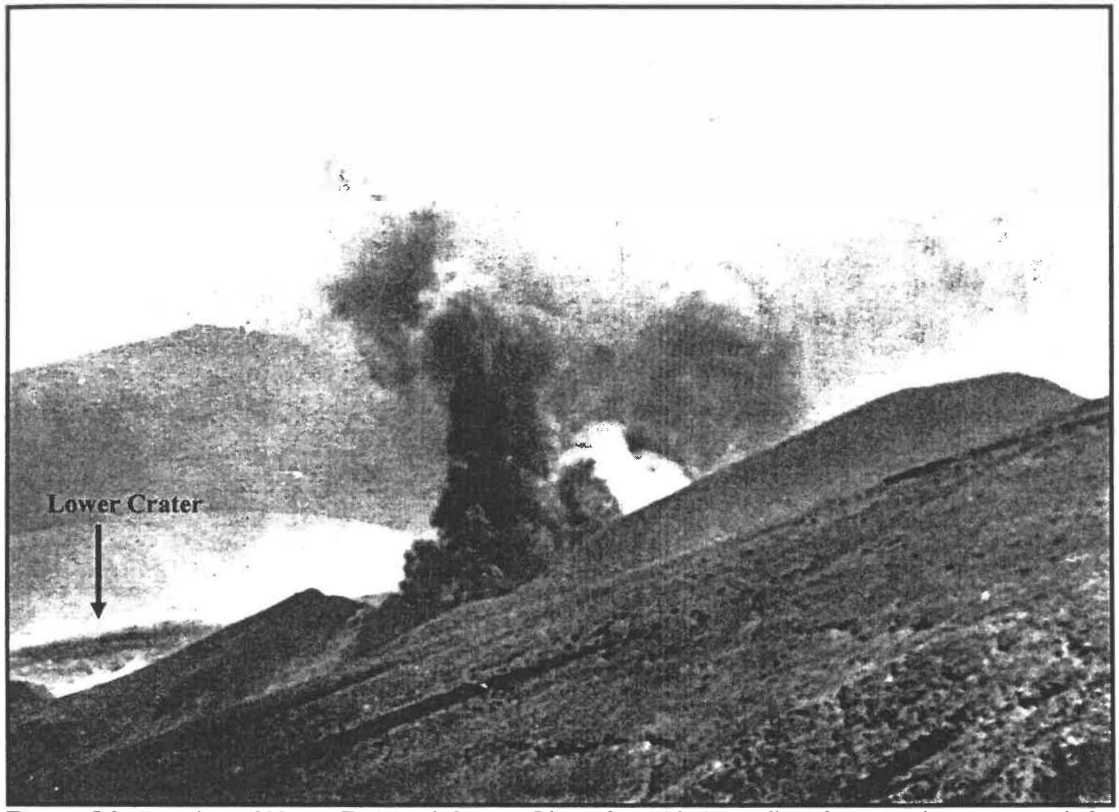

Figure 5.2: Eruption of Upper Te Maari Crater. Photo from 1890's. View from southwest on track from Ketetahi to Central Crater. After Gregg (1960).

The historical observations of the Te Maari Craters provide descriptions of the upper and lower crater (chapter 1.4) and first-hand accounts of eruptions.

5.3.1 Eruption Descriptions

Lower Te Maari 1869

(Maori observations) – "a bright red flame was seen through the smoke, and as it reached the top of the smoke cloud it would burst and fall in little parts like snow falling."
(Greg, 1960)

Ash eruptions from craters 1886

– rumblings heard at Rotoaira

(Greg, 1960)

Upper Te Maari 1892

(NZ Herald) – "After a few preliminary shocks and rumblings, Te Mari…belched forth an immense quantity of steam, mud, and boulders in a terrific manner. The stuff ejected rose 2000 or 3000 feet in the air and fell in the vicinity, thence it came rushing down the mountain-side, scorching up the trees on its way. It was a pretty sight to see the huge mass pouring down from the crater until it was lost sight of in the bush; thence it emerged two miles further down, divided into several small streams, looking in the distance like a number of mobs of sheep. The mass came rolling down the mountain-side and fell on to the dray road near the Rotoaira Lake."

(Greg, 1960)

Upper Crater Nov 1896 – end of year

(Friedlander,1898) – "We were awakened by a thundering noise…Against the starlit and cloudless sky stood a gigantic pillar of ash-bearing steam, broadening towards its summit, and overtopped by a detached roundish mass of the same appearance. Evidently the explosion had begun by a single shot, followed by a rest of some seconds. The pillar of steam…was of an exquisite cumulus character. This and its absolute opaqueness and dark colour gave it a strange appearance, almost like that of a solid body – an enormous stalagmite, as it were. But the most surprising sight was the wonderful display of different kinds of light phenomena. Whereas at no time had I seen the slightest fire-reflection above Te Mari, the lower parts of the steam column were now all aglow with a dark-red glare. A large number of what looked like bright sparks shot high up, and fell down in parabolic lines. There was going on, besides, a continuous play of electric lightening in the clouds, mostly, but not always, in the lower parts. I think there was on the average fully one lightening flash to the second…The thunder blended together and formed a continuous roar, which, however, at our station was not deafening. But the most remarkable and interesting phenomenon had yet to come. The upshooting

sparks...by degrees became rarer, and the lightening also; and then there appeared large flames of a brilliant-blue hue, which mingled with the ascending steam – apparently floating, as it were, free in the air at some distance above the mouth of the crater. I estimated the height of the flames at about 1000 ft."
"The only other specimen of volcanic activity similar to that of Te Mari that I know of by personal observation is the small volcano on the southernmost of the Liparian Islands (north from Sicily) called 'Volcano.'"

Lowe, 1897 – "...the surrounding hills for a couple of miles are covered with sand and ash, and the vegetation has been subjected to boiling water." Topping (1974)

5.3.2 Vulcanian and Phreatic Activity

These historic observations of eruptions from Te Maari closely resemble vulcanian activity (chapter 2.3), with Friedlander (1898) actually comparing it with personal observations made at 'Volcano' (Vulcano, Italy). The "upshooting sparks" seen by Friedlander were later identified by him as red-hot, angular boulders and the "gigantic pillar of ash-bearing steam" are characteristic of vulcanian activity, as well as the short duration and violence of the eruption. These historic observations all describe at times the eruption of incandescent blocks, indicating the involvement of fresh magma and that the events were not exclusively phreatic in nature. The newspaper account in the New Zealand Herald, 1892, also provides evidence for vulcanian-type activity with a description of a pyroclastic avalanche resulting from the accumulation of masses of ejected blocks and ash. This is similar to the sequence of events during the 1975 vulcanian eruption of Ngauruhoe.

Prior to the eruption described by Friedlander (1898), there had been reports of ash eruptions from the craters throughout the month before. Around that time Te Maari was "always steaming furiously, and sometimes emitting dark, dense, brownish-grey clouds." Three days before the eruption a continuous roaring and thundering was heard in the direction of Te Maari (Friedlander, 1898).

Most of the craters in the Tongariro cone complex are underlain by a vapour-dominated geothermal reservoir topped by a condensate layer (chapter 1.4, Hagerty and Benites, 2002). The surface manifestation of which can be seen at Ketetahi Springs and at the steaming areas in and around the Te Maari Craters. The interaction of magma with condensates in this zone could be the triggering mechanism for steam-driven explosions at the Te Maari Craters (M.P. Hochstein pers. comm., as cited in Wood & Topping, 1980).

Case Study of a Vulcanian Eruption: 1974-1975 Ngauruhoe Eruptions

Ngauruhoe has grown rapidly over the last 2,500 years with a variety of eruptive styles, alternating between effusive, strombolian, vulcanian and sub-plinian eruptions of andesitic magma. Any one eruption can display a number of defined styles and eruption rates have varied by one to two orders of magnitude (Hobden *et al.,* 2002). The 1974-1975 eruptions at Ngauruhoe were dominantly vulcanian (Fig. 5.3). Much of the activity that took place during these eruptions can be compared to the documented accounts of the Te Maari Crater eruptions.

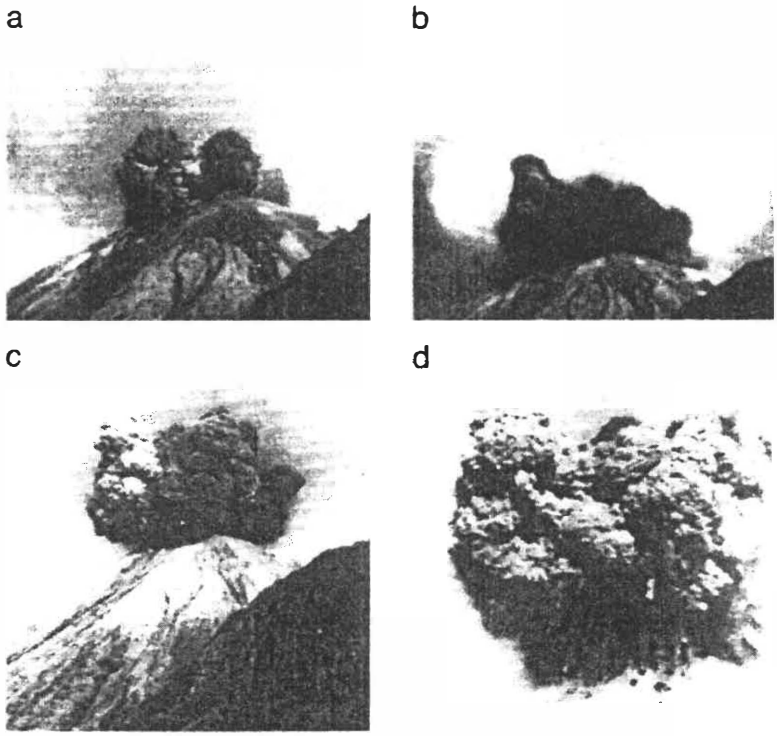

Figure 5.3: Vulcanian eruption at Ngauruhoe, 1975. Photos taken approx. A) 0.5 s, B) 1 s, C) 2 s and D) 11 s after event. D) displays characteristic ballistic blocks and ash cloud of vulcanian eruptions. After Morrissey & Mastin (2000).

17 years before the 1974-1975 eruptions, Ngauruhoe was relatively quiescent, with semi-continuous steaming and sporadic small ash eruptions. The first eruptions containing a fresh magmatic component began in December, 1973 (Hobden *et al.,* 2002). Explosive eruptions ejected ash, incandescent blocks and eruption columns up to 4 000 m high. The partial collapse of these columns produced block-and-ash flows down the flanks of the cone (Nairn & Self, 1978). An eruption on 28th March, 1974 began with a turbulent, grey, ash-laden eruption column reaching 6 km high (Self, 1975). Incandescent blocks were ejected falling on or near the cone but the most voluminous ejecta was fine ash material, which remained in the eruption cloud for a long time with very slow accumulation rates (Self, 1975). The eruption was diminishing by early the next morning and by the morning of 30th March, steam from the summit crater was the only activity remaining. The crater floor and summit area was covered by blocks and debris and sulphur was visible over much of the crater floor (Self, 1975).

An eruption on 19th February, 1975 began with 90 minutes of voluminous gas-streaming, producing a 7 km high eruption column. Large incandescent blocks fell to the ground, accumulating and generating avalanches although these deposits were unlikely to have been preserved as they were characteristically thin (Hobden *et al.,* 2002). After a 40 minute interval there were 4 hours of intermittent, violent, cannon-like explosions ejecting blocks to 2.8 km (Nairn & Self, 1978).

The low proportion of juvenile ejecta from these eruptions indicated vulcanian activity, with the non-juvenile component thought to be mainly pulverised 1954 or 1949 lava (Self, 1975).

5.4 Origin of Craters and Upper Crater Breccia

5.4.1 Origin of Craters

The field characteristics of the craters (chapter 3) indicate minor explosive activity and lava producing eruptions. The ballistic block fields and minor tephra deposits indicate phreatic and phreatomagmatic activity, but the absence of any proximal pyroclastic

deposits, such as agglutinate or thick accumulations of scoria/pumice, implies that this has not been significantly explosive (sub-plinian). This brings into question the origin of the Rotoaira Lapilli, as there doesn't seem to be any proximal evidence that it was produced by the Lower Te Maari Crater. This is supported by Kobayashi's (unpublished) work on the 14 ka Rotoaira deposits mentioned earlier. This also has implications for the formation of the lower crater and the northern crater cluster. The flat-floored structure of the lower crater indicates some degree of collapse, and with no sub-plinian activity sourced from these craters it is likely they were partially formed through minor explosions and from collapse, through the extrusion of magma from a shallow reservoir. This is not the only source of lava however, as the volume of the lower crater is 12×10^6 m^3 while the total volume of the northern lava flows is 315×10^6 m^3.

5.4.2 Upper Crater Breccia

The origin of the breccia found in the Upper Te Maari Crater is problematic. Volcanic breccias can be formed by a number of processes which can be difficult to identify in the field. This includes moving lava flows (autobreccias), pyroclastic falls and flows (explosion breccias) (chapter 2.5). Breccias can also be remobilised by mass movement processes to form secondary deposits. The upper crater breccia is poorly sorted and the clasts are dense and monolithologic. These characteristics, along with the proximity to the source vent, imply that it is a primary deposit. The clast characteristics also indicate this is an autobreccia, produced by the disruption of flowing lava, rather than an explosion breccia, where the clasts would be more pyroclastic in texture and there would be a mixture of vesicular, juvenile clasts and wallrock lithics.

The similar composition and crystallinity of the clasts to the 1500 AD lava flow indicates that the breccia was sourced from the same material. The bedding was probably formed through shearing during the laminar flow or granular cascades of material down the talus slope, separating the coarse and fine grains. Subsequent phreatic and phreatomagmatic explosions, possibly during the 1869 and 1896 eruptions, blasting through this autobreccia talus apron is the most likely cause of the collapse and excavation of the upper crater's general morphology seen today (Fig. 5.4).

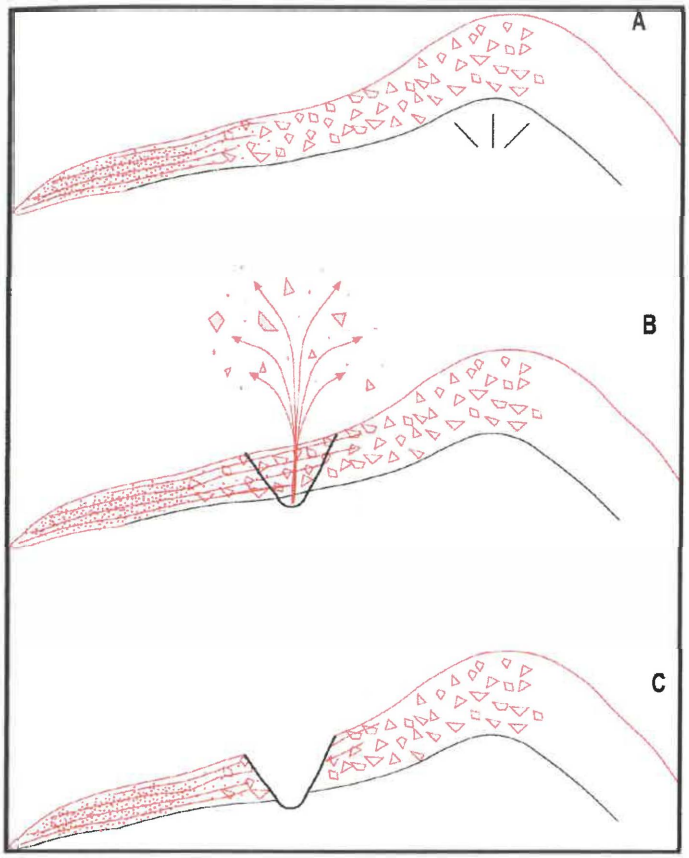

Figure 5.4: Sequence of events for upper crater breccia origin.
A) Emplacement of lava, producing autobreccia in a downslope tapering apron. Beds forming downslope from vent. B) Subsequent explosions cause collapse and excavate through the breccia fan. C) Final morphology of crater with lower, massive breccia and upper, bedded breccia.

5.5 Lava-Producing Eruptions

The map of lava flows produced in chapter 3 was created using data from previous workers and new mapping and analysis of aerial photographs.

Various physical properties were measured in order to constrain aspects of the Te Maari lava-producing eruptions. Weighted averages of width and thickness were used to calculate a volume for the 1500 AD lava flow of approximately 29 x 10^6 m^3. In order to estimate the minimum time required for emplacement of this flow, Jefferys Equation was used to calculate flow velocity.

$$(\rho g t^2/B\eta)\sin\alpha$$

where ρ=density, g=gravity, t-thickness, B=a constant associated with channel confinement, η=viscosity and α=slope angle. The density and viscosity used was average values for andesite lava, 2450 kg/m^3 and 10^7 kg/m/s respectively, and a range of thicknesses and slope angles were calculated using weighted averages (Table 5.2) over the flow length. A range of these values were used (Table 5.1) in order to ascertain a realistic value. Using this data, a minimum emplacement time of 10.10 hours was calculated for the flow. This assumes that it was a single unit emplaced in a single, constant event. As this flow has multiple overlapping lobes and was not emplaced as a single unit, it is more likely the emplacement time took days rather than hours. This agrees with flow emplacement estimates calculated by other techniques (see following section). The 2001 eruption of Mount Etna produced seven flow fields from seven eruptive fissures. The vent that produced the largest volume of lava (16.208 x 10^6 m^3) with a length of 6.9 km, had varying effusion rates and had an emplacement time of 23 days (Behncke & Neri, 2003).

Table 5.1: Range of averaged thicknesses and slope angles used in Jefferys Equation to calculate lava flow velocity.

Thickness (m)	Slope Angle (°)	Velocity (m/s)	Emplacement (hours)
40	9.4	0.209	5.32
40	8.8	0.196	5.67
30	9.4	0.118	9.42
30	8.8	0.11	10.10
20	9.4	0.052	21.37
20	8.8	0.049	22.68

Table 5.2: Example of a weighted average calculation for lava flow thickness

	Proportion of Flow	Thickness (m)
	0.175	80
	0.15	60
	0.15	40
	0.3	30
	0.375	20
Weighted Average		39.6

The lava flows and scoria cone erupted from the 1955 Ngauruhoe eruptions took 116 hours to emplace and had a total volume of around 6.5 x 10^6 m^3 with an overall discharge rate of 0.65 m^{3}s^{-1}. The largest single flow from this eruption was 0.6 x 10^6 m^3 and took 4 hours to emplace with an average discharge rate of 3.5 m^{3}s^{-1}.

The flows erupted from Te Maari are summarised in table 5.2. The total erupted volume of all the flows is 0.4 km^3. This doubles the estimate of Hobden (1997) which only

considered the 1500 AD flow, the ~10 ka levéed flow and a smaller flow to the northeast of the lower crater (Fig. 5.1).

Table 5.3: Volume estimates for lava flows sourced from Te Maari Craters.

Lava Flow	Source Crater	Estimated Area (m^2)	Estimated Thickness (m)	Volume (m^3)
1500 AD flow	Upper Te Maari	960030.1	30	29×10^6
~10 ka levéed flow, north	Crater Cluster	2552756.5	40-60	125×10^6 +/- 25
14-22.5 ka flow, northwest	Lower Crater	5512536.5	20	110×10^6
~10 ka flow, northeast	Crater Cluster	4068214.2	20	80×10^6
>14 ka flow, east	Older vent	2203107.9	30	66×10^6
Total		14336615.1		~400×10^6

The volumes and lengths of the Te Maari flows are plotted on Fig. 5.5 along with other lava flows from Tongariro for comparison.

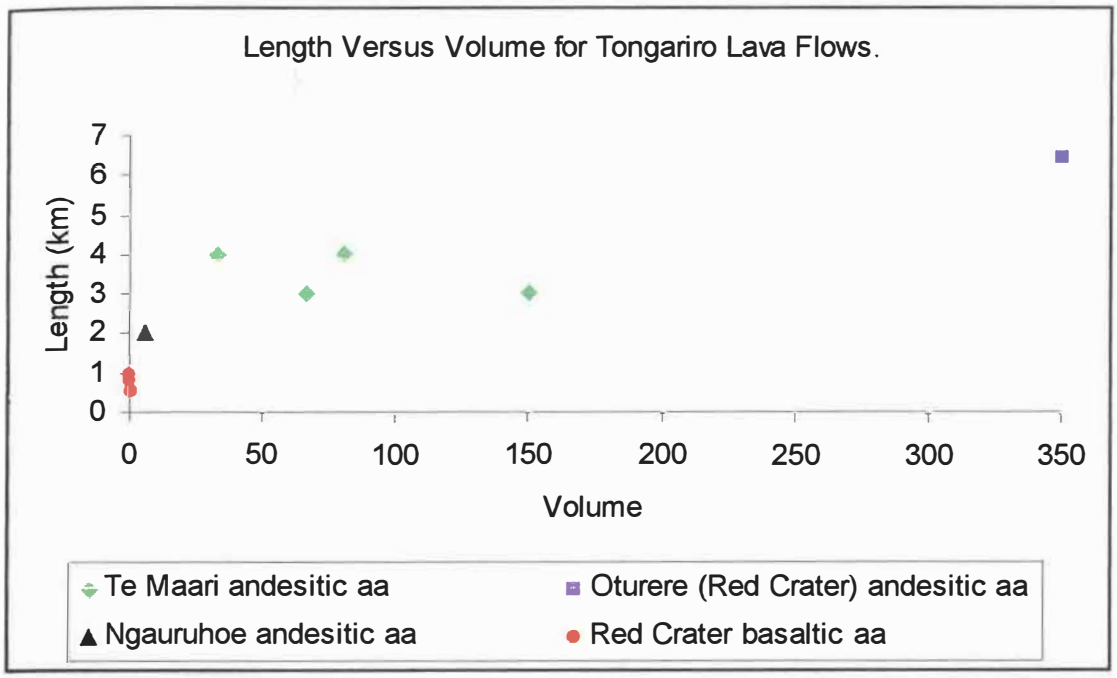

Figure 5.5: Length versus volume graph comparing Te Maari Crater flows with other Tongariro flows.

Aa Flow Behaviour

The characteristics of previous lava flows are useful for the prediction of lava flow behaviour and so can be used in hazard analysis and short-term forecasts during an eruption (Kilburn, 2000). The surface criterion of aa lavas relates to the velocity a flow must travel to keep breaking crust. This, combined with the time a flow can continue to advance before the flow front solidifies, can link the maximum length of a lava flow to other properties (Kilburn, 2000).

Relating flow length to the slope angle results in a trend of increasing length with the decrease in underlying slope. This is becuase in order to keep breaking the surface the flow must maintain a greater thickness on shallower slopes, therefore needing longer times for the front to solidify (Kilburn, 2000). The Te Maari Crater flows agree fairly well with this model and plot on this graph with flows from Kiluea and Etna (Fig. 5.6).

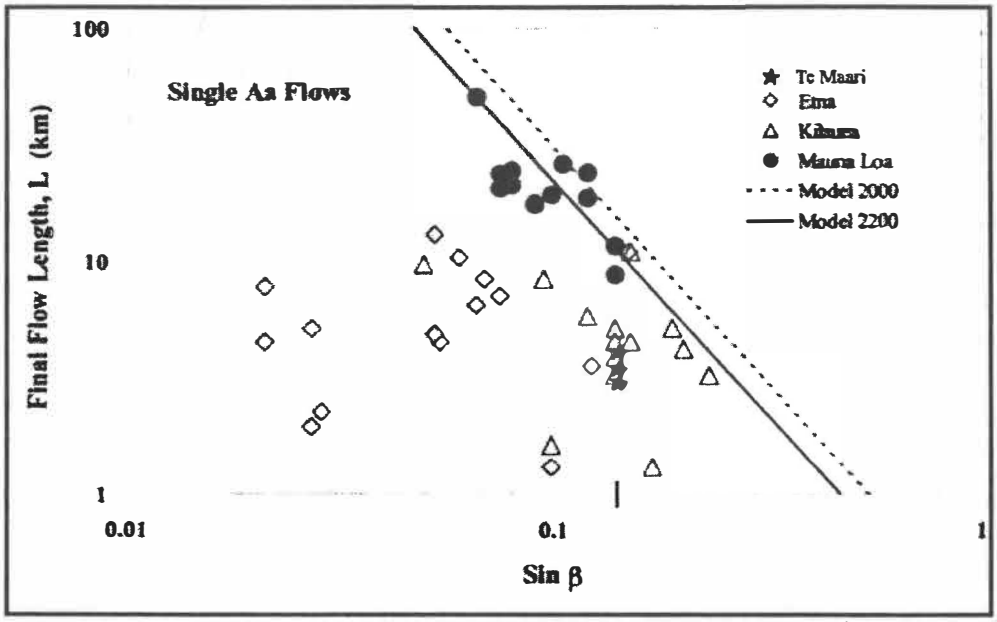

Figure 5.6: Lava flow length versus slope angle with criteria, i) aa surfaces must break before they cool to their maximum strength and ii) flow fronts advance until solidified. Relates the maximum potential length of a single aa flow to slope angle. Solid and dashed lines relate to to respective mean crustal densities of 2200 and 2000 kg m^{-3} within the model equations After Kilburn (2000).

Relating flow length to discharge rate can be useful in predicting flow length during an eruption. With slow-moving aa flows a discharge rate can be estimated that can provide a maximum flow length, as was done at Etna during the 1991-1993 eruptions (Kilburn, 2000). For a realistic emplacement time for the Te Maari Crater flows, the mean discharge rate would be between 10 and 100 m^3 s^{-1}. This again plots the Te Maari flows on the graph with flows from Kiluea and Etna (Fig. 5.7).

These models are for single aa flows and are fairly successful in their predictions, regardless of the fact they use averages, because slope angle and discharge rates can vary considerably. In cases of extreme variation, e.g. flow over a cliff or into ravines, they may need to be evaluated individually (Kilburn, 2000).

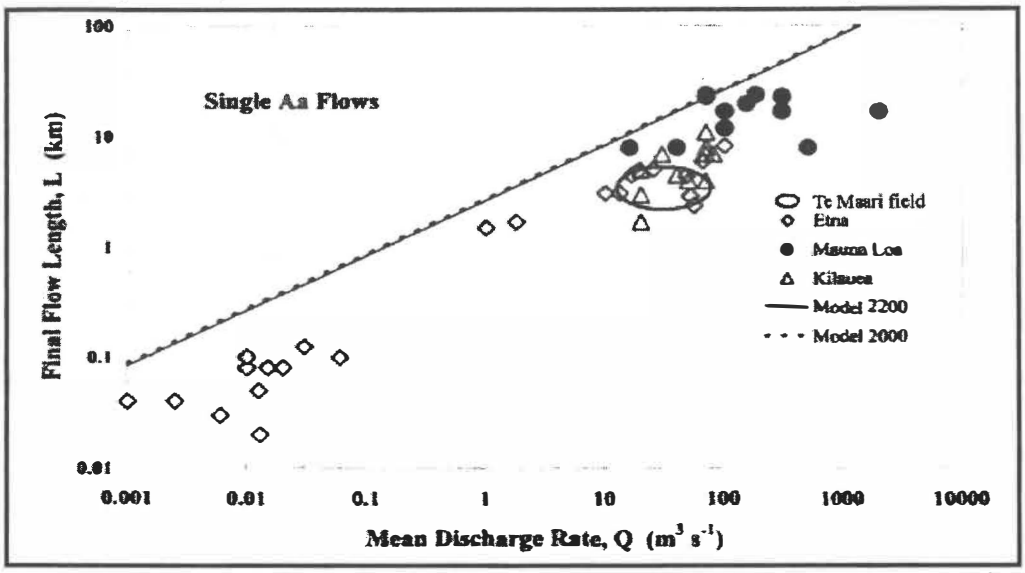

Figure 5.7: Lava flow length versus mean discharge rate with criteria, i) aa surfaces must break before they cool to their maximum strength and ii) flow fronts advance until solidified. Relates the maximum potential length of a single aa flow to mean discharge. Solid and dashed lines relate to to respective mean crustal densities of 2200 and 2000 kg m^{-3} within the model equations After Kilburn (2000).

5.6 Chronology of Eruptive Events

A detailed eruptive history for the Te Maari Craters is difficult to ascertain due to the lack of definite stratigraphy associated with eruptions from the craters. Most information about past eruptive activity at the craters is obtained from historic observations made over the past 150 years, while older events are inferred from mapping lava flows and their stratigraphic position. A summary of events from the Te Maari Craters is shown in Fig. 5.8. The eruptive rate of the craters over 14 ka is approximately 0.028 km^3/ka. This is relatively low compared with Ngauruhoe, which has an eruptive rate of 0.8 km^3/ka over 2.5 ka (Hobden, 1997).

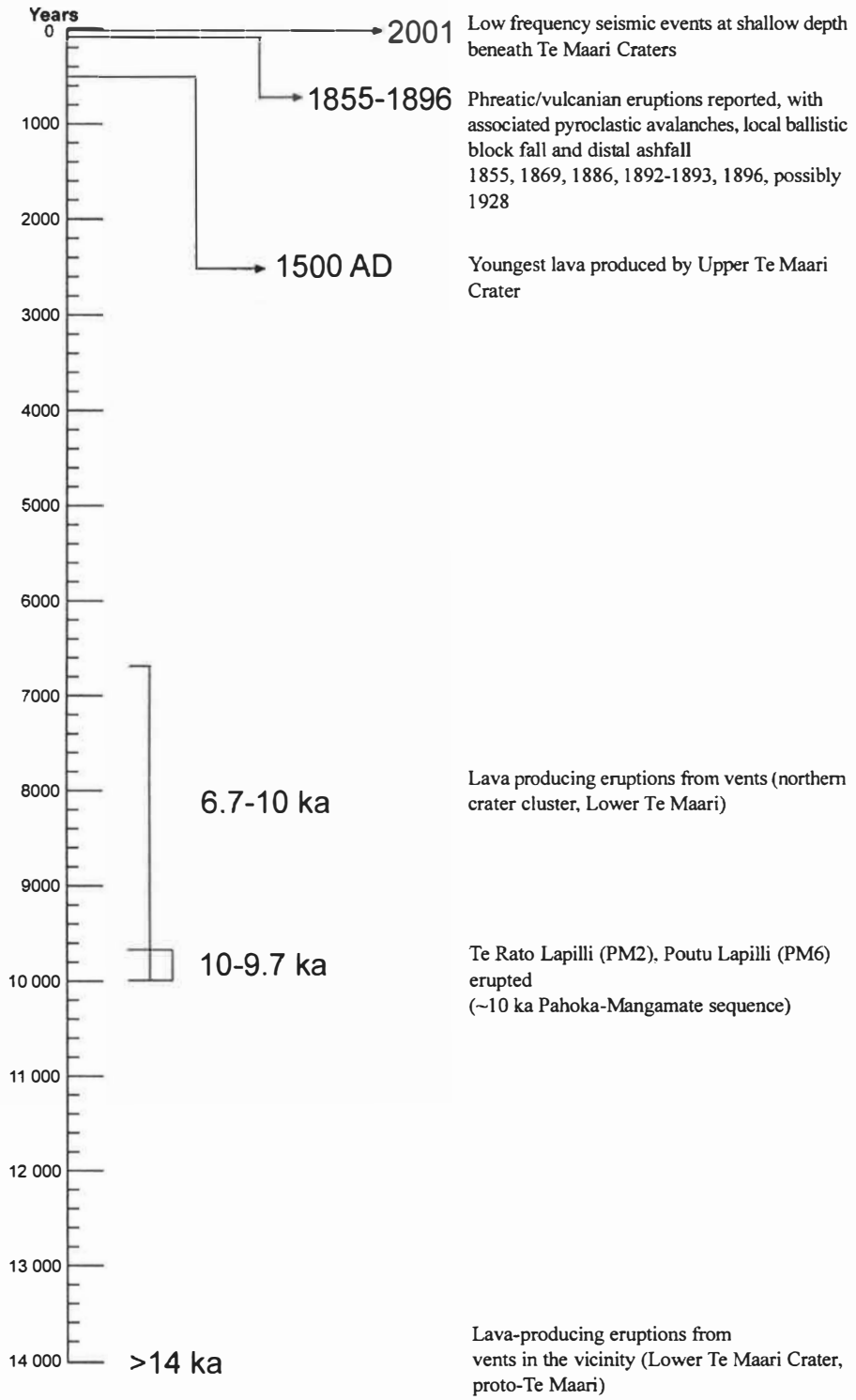

Figure 5.8: Chronology of main eruptive and seismic events for the Te Maari Craters, Tongariro.

5.7 Conclusions

Previous work on the eruptives and history of Te Maari Craters has produced varying accounts of the timeline and products that can be attributed to them. Maps of the northern lava flows especially have evolved over time as more information is collected.

Topping (1974) produced a map of the lava flows from the Te Maari Craters, with the 1500 AD lava flow, the large, levéed, 6.7-9.7 ka, flow north of lower crater and a smaller, 9.7-12 ka flow to the northeast of the lower crater. He also attributed the Rotoaira Lapilli to the Lower Te Maari Crater.

Hobden (1997) described the volcanic stratigraphy of the Te Maari Craters, stating that at least 15 lava flows and pyroclastic units could be recognised from the northernmost vents. The flows were all identified as andesitic with SiO_2 ranging from 57.5 to 60.2 wt%.

Nairn, *et al.,* (1998) identified two stages in the 10 ka eruption sequence at the Tongariro Volcanic Centre that the Te Maari Craters may have been active in, the PM 2/Te Rato Lapilli and the PM 6/Poutu Lapilli. It was also thought the large levéed flow north of the crater cluster may have been emplaced at the end of the 10 ka sequence.

Based on this previous work done on the Te Maari Craters and others on the Tongariro Volcanic Centre, Lecointre *et al.,* (2004) produced a map with Topping's lava flow outlines and which also outlined older >14.7 ka flows.

Tetsuo Kobayashi (Univ. of Kuyoshima) has correlated the agglutinates of North Crater with the sub-plinian fall, therefore suggesting that the Rotoaira Lapilli is not from Te Maari, but is sourced from North Crater.

The eruptive style of the Te Maari Craters ranges from phreatic steam and ash and vulcanian eruptions to lava producing eruptions. The historic accounts of eruptions provide detailed descriptions that can be correlated to vulcanian and steam-driven activity. This is further supported by field evidence of ballistic blocks and minor Tephra deposits.

The absence of any proximal pyroclastic deposits, such as agglutinate or pumice, implies that this has not been significantly explosive (sub-plinian). This implies the Rotoaira Lapilli does not originate from the Te Maari Craters, which is supported by Kobayashi's work. This also has implications for the formation of the lower crater and the northern crater cluster. With no sub-plinian activity sourced from these craters it is likely they were partially formed through minor explosions and from collapse.

The flows erupted from Te Maari have a total erupted volume of 0.4 km^3. The 1500 AD lava flow had a minimum velocity of 0.11 m s^{-1}, with a minimum emplacement time of 10.10 hours, but it is more likely to have taken days to be emplaced.

The breccia found in the Upper Te Maari Crater was emplaced during one of the lava-forming eruptions as a down-slope tapering, autobreccia apron. The similar composition and crystallinity of the clasts to the 1500 AD lava flow indicates that the breccia was probably emplaced around the same time. Subsequent phreatic and phreatomagmatic explosions, possibly during the 1869 eruption, blasted through this autobreccia talus apron causing the collapse and excavation of the upper crater's funnel-shaped morphology seen today.

Timelines of eruptive events at the Te Maari Craters are difficult to determine with any degree of certainty because of the lack of definite stratigraphy. All the information on past eruptions is obtained from historic descriptions in the past 150 years and lava flow mapping. The geochronology of the Te Maari Craters can be summarised as follows:

~14 ka	- lava-producing eruptions
10-9.7 ka	- PM sequence (PM2 and PM6)
6.7-10 ka	- Lava-producing eruptions
1500 AD	- Youngest lava produced by Upper Te Maari Crater
1855-1896	- Phreatic/vulcanian activity (possibly to 1928)
2001	- Low frequency seismic events at shallow depth beneath craters

CHAPTER SIX

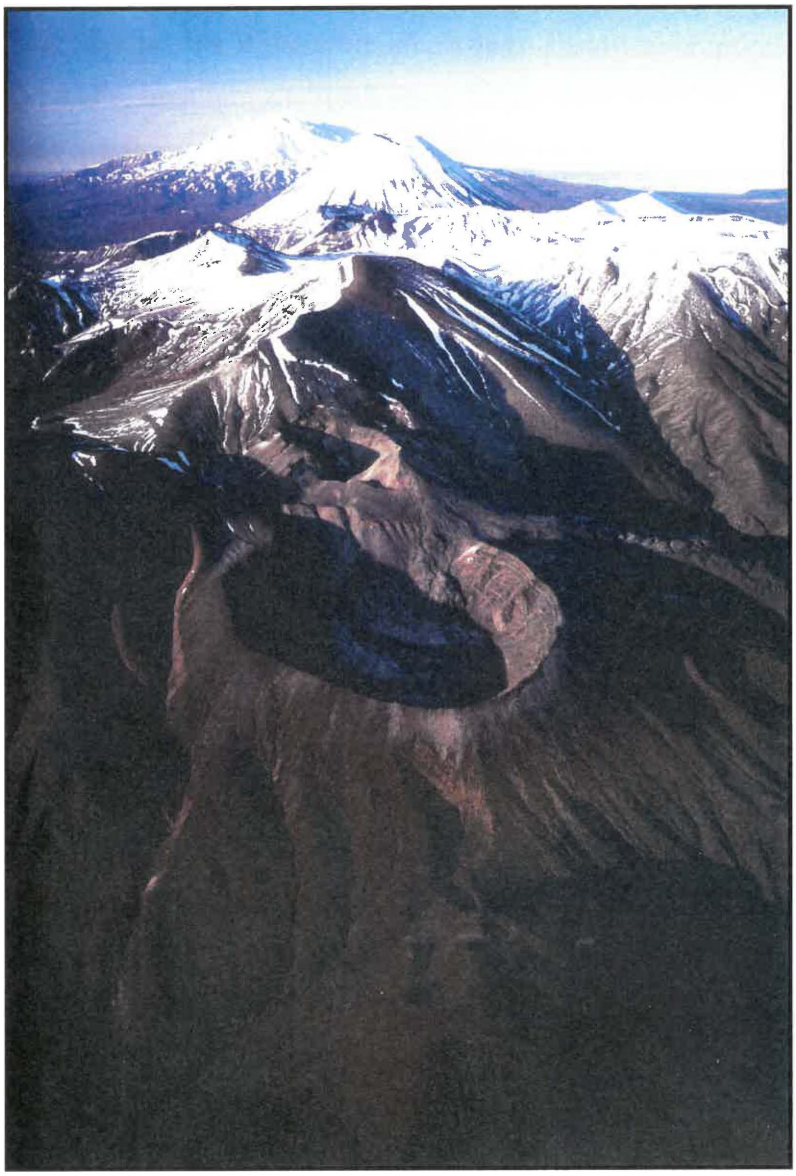

VOLCANIC HAZARDS

6.1 Introduction

Volcanic eruptions have a wide range of impacts, spanning physical, social and economic factors. As the world's population grows it can encroach into areas of high volcanic hazard and global volcanic risk is therefore increasing. Historical eruptions, which have had devastating effects, highlight the need for accurate hazard analysis in those places where populations are threatened. Volcanic hazards can take many forms, but can be thought of as a threatening event defined by a particular type, magnitude and probability of occurrence (Schmincke, 2004). Volcanic risk defines the volcanic hazard in relation to life or property in an area for a specific time (Blong, 1996). The amount of human life lost in an eruption depends on the population density in the vicinity and also the state of preparedness and organisation within the population (Schmincke, 2004). Therefore risk can be defined as, Risk = Hazard x Vulnerability, with vulnerability including consequences for people, buildings, infrastructure and economic activity (Blong, 1996).

The recent eruptive style of the Te Maari craters is dominantly vulcanian with associated thick aa lava flows, which is similar to historic eruptions from Ngauruhoe. The hazards that would have the most impact if this style of eruption were to occur at Te Maari today would be widespread ash fall and lava flows, with volcanic gases affecting local areas. The location of these craters close to the boundary of the national park also presents a unique hazard, as it may prove difficult to prevent members of the curious public from gaining access to the area following an eruption and endangering their lives. Much of the land surrounding the Tongariro National Park is used for primary production, predominantly pastoral livestock farming and forestry. Dairying, horticulture and cropping are prevalent in the Waikato and Bay of Plenty, while sheep, beef and deer farming are common in the rolling hill country of the area (www.insights.co.nz, 2004). There are also a number of lifelines (roads, railways, telecommunication networks, gas and water pipelines and electricity distribution systems) that would be affected, e.g. the Rangipo power station and State highways.

6.2 Eruption Scenario

The sparse historical observations and little remains of physical evidence limit the accuracy of any quantitative assessment of volcanic risk from the Te Maari Crater system. However, although no detailed frequency-magnitude curve is available for the Te Maari Craters, useful and instructive risk assessment is achievable using an "eruption scenario" approach (Johnston *et al.,* 1997).

The new mapping in this study and by Tetsuo Kobayashi (Univ. of Kuyoshima) has found no evidence for sub-plinian eruptions from the Te Maari Craters. For this reason an event such as the Rotoaira eruption is considered an inappropriate scenario for assessing volcanic risk. The eruption scenario for the Te Maari craters uses a 100-1000 year return period event from Ngauruhoe, which is based on a small (10^5 – 10^6 m^3) eruption. The prevailing winds for this area are generally southwesterlies, so three scenarios have been considered with ash plumes to the north, northeast and east of the craters (Fig. 6.1). This scenario represents the largest credible eruption for this return period probable from these craters.

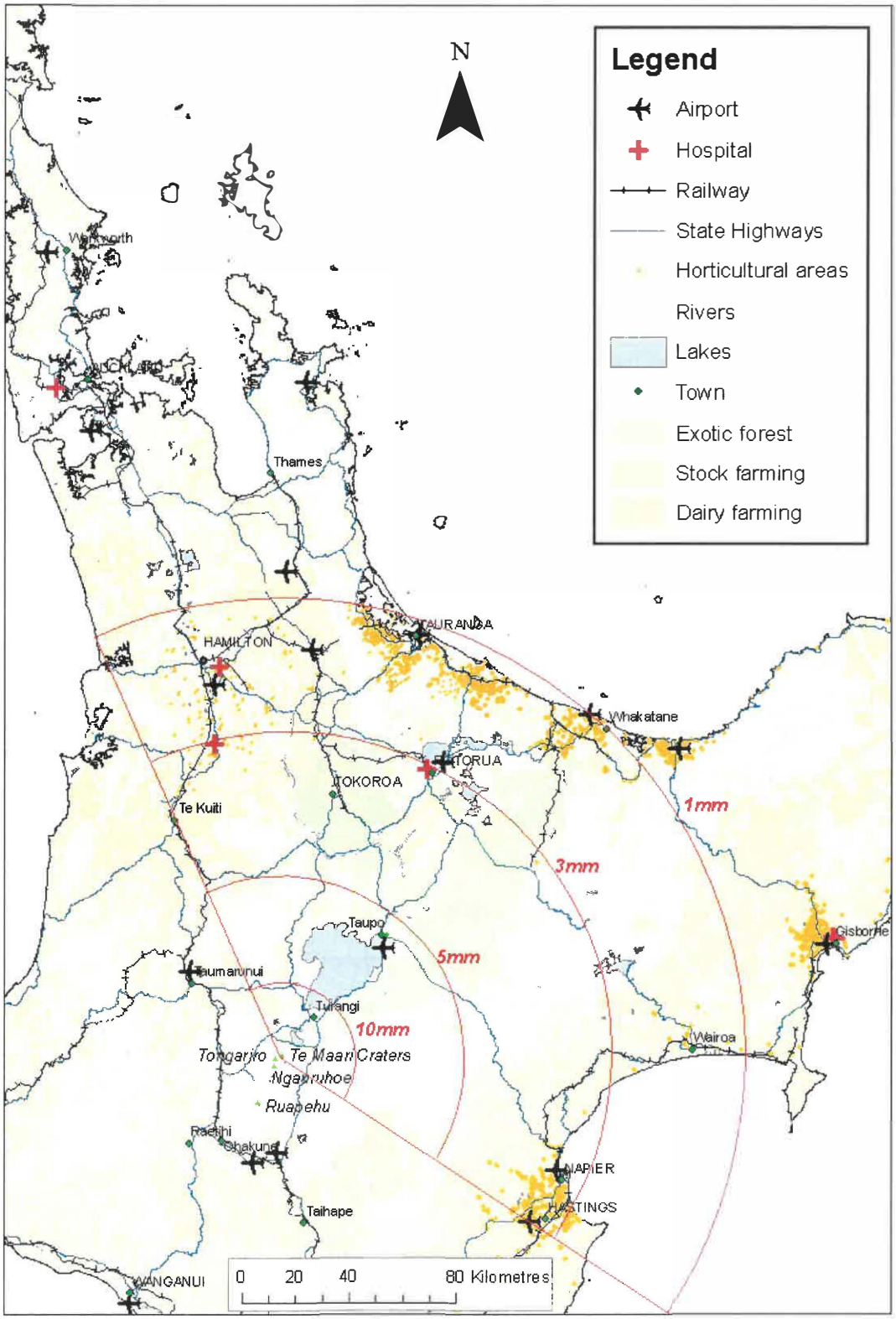

Figure 6.1: Isopach map of an ashfall for Te Maari Craters scenario. Includes main features that would be affected.

6.3 Physical Impacts

6.3.1 Tephra Fall

Ballistic Blocks (Fig. 6.2)

In explosive eruptions blocks, bombs and lapilli can leave the vent with ballistic trajectories (Blong, 1984). Cold blocks are sourced from the vent wall, while clots of magma form bombs as it is ejected, the shape depending on fluidity, length and velocity of flight, rate of cooling and gas escape and deformation on impact (Blong, 1984). Apart from high impact energies, another hazard associated with ballistic blocks/bombs is that some of the larger blocks could have temperatures that are above ignition points for many materials, such as vegetation and wooden buildings (Blong, 1996).

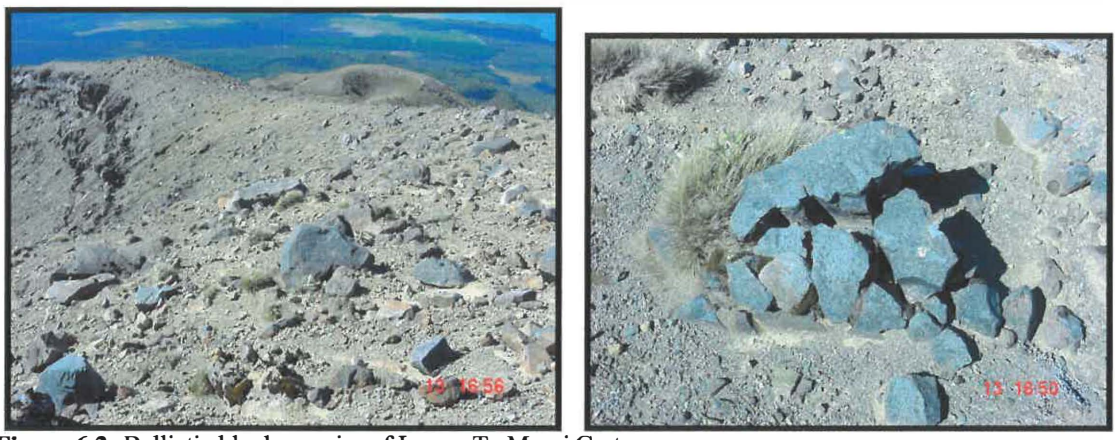

Figure 6.2: Ballistic blocks on rim of Lower Te Maari Crater.

Ballistic blocks would pose a risk within 2-3 km of the source vent (Fig. 6.3). This includes parts of the Tongariro Crossing track, the Ketetahi hut and the lower northern slopes. Large blocks may initiate fires within native and plantation forest downslope of the Te Maari Craters.

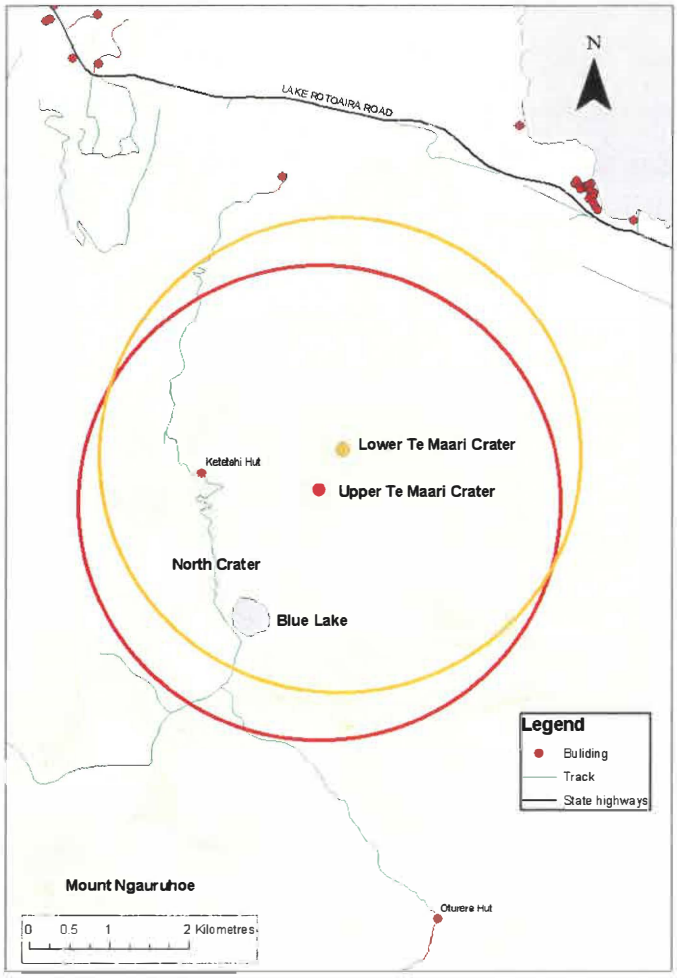

Figure 6.3: Areas at high risk from ballistic blocks in Te Maari Crater eruption scenario. Upper Crater source vent = red circle, Lower Crater source vent = orange circle.

Ash

Fine ash can be transported hundreds of kilometres away from the source, depending on the height of the eruption column and the wind conditions, making this hazard the most widespread and the most likely to affect the greatest number of people (Neild *et al.,* 1998). About 10% of volcanoes that erupt each year have eruption columns that reach into the stratosphere (8-18 km) (Schmincke, 2004).

The physical and economic consequences of ash fall will increase with the thickness of ash that is deposited (see Table 1). The main features affected by the Te Maari eruption scenario are shown in Figure 6.1.

Agriculture

Damage to vegetation and soil depends on the thickness of tephra and the composition of the ash (Neild, *et al.,* 1998). There are generally four causes for the death of vegetation due to ash fall: i) complete burial; ii) partial burial with the result that roots are restricted access to oxygen; iii) the stripping and prolonged absence of leaves; and iv) the layer of tephra covering foliage causes clogging of stomata and blocks sunlight (Blong, 1984). Damage to crops will also depend on what time of year the eruption takes place, with crops being more at risk during certain times e.g. initial growth stages and flowering (Neild *et al.,* 1998). During the 1995 Ruapehu eruption, cauliflower growers reported around a $250,000 loss in Gisborne, nearly 250 km away, which only received a trace amount of ash. The damage was mainly cosmetic, with grey ash discolouring the white vegetable, but this was enough to reduce quality. Market gardens were more fortunate, as there were few crops in the ground at the time (Neild *et al.,* 1998). Damage to soils from ash fall may affect production also, although small amounts may actually improve soil fertility. The composition of the ash is important because even where ash is removed plants can still die where the ash is acidic (Neild *et al.,* 1998). In the 1995 Ruapehu eruption, where there was ash deposits >0.25 mm-0.5 mm there was significant elevation in soil sulphur levels, and the pH was lowered by 0.2-0.3 units (Cronin *et al.,* 1998).

All the variables involved, e.g. wind direction, weather and eruption duration, mean that prediction of ash fall distribution can not be accurately assessed until the time of eruption occurrence. The main horticulture centres that are at risk in this scenario include the Bay of Plenty, Waikato and Hawke's Bay (Neild *et al.,* 1998).

Table 6.1: Impacts of ash fall with increasing thickness (Modified after Blong, 1984, Neild *et al.*, 1998 and EW, 1999).

Ash-fall Thickness	Impacts
<1 mm	Possible areas affected for Te Maari eruption scenario: Bay of Plenty, Hamilton ✦ Irritant to lungs and eyes ✦ Closure of airports due to potential damage ✦ Possible minor damage to vehicles, houses and equipment by abrasion ✦ Possible contamination of water supplies, especially roof-fed tanks ✦ Dust affects road visibility and traction
1-5 mm	Possible areas affected for Te Maari eruption scenario: Rotorua, Tokoroa, Napier/Hastings, Taupo, Taumarunui, Pueora Forest, Kaingaroa Forest and Kaweka Forest ✦ Some livestock affected. May suffer from lack of feed, wear on teeth, contamination of water supply ✦ Minor damage to houses if ash enters buildings, blocking air-conditioning filters etc. ✦ Electricity cuts may occur; ash shorting occurs if ash is wet and conductive ✦ Water supplies may be cut or limited due to pump failure ✦ Irrigation systems may be disrupted ✦ Contamination of water by chemical leachate ✦ Ash fall into the Tongariro River may disrupt and/or damage the Tongariro Power Scheme (Rangipo Power Station) ✦ Roads may need to be cleared to reduce dust and prevent storm-water system blockages ✦ Sewerage systems may be blocked ✦ Damage to electrical equipment and machinery ✦ Possible crop damage, but no burial or breakage ✦ Ash incorporated into soil within a year ✦ Vegetation canopies recover within weeks
5-25 mm	Possible areas affected for Te Maari eruption scenario: Turangi, National Park, Tongariro, Lake Rotoaira, Lake Taupo, Tongariro River, power station canals, State Highways, Kaimanawa Forest and Rotoaira Forest. ✦ Buried macrophytes may survive and recover ✦ Larger grasses damaged ✦ Vegetation canopies recover within next growing season ✦ Tephra layer remains intact on soil surface after one year
25-150 mm	+ Note: Unlikely level of ash accumulation associated with Te Maari eruption scenario, except in cases of wind drifts ✦ Major ash removal operations required in urban areas ✦ Most buildings will support ash load but weaker roof structures may collapse at 100 mm, particularly if ash is wet ✦ Road transport may be halted. Air filters in cars may be clogged ✦ Rail transport may be halted due to signal failure ✦ Burial of pasture and low plants. Foliage may be stripped off trees. ✦ Most pastures killed by over 50 mm of ash ✦ Soil burial is complete and will sterilise soil profile by isolation from oxygen ✦ Several hundred to thousands of years may pass before new equilibrium soil is established

Although ash fall is unlikely to kill livestock, the destruction or burial of pasture results in lack of food, with animals being put off their feed by deposits of around 2-5 mm thickness (Neild *et al.,* 1998). Respiratory and intestinal illnesses may increase in areas of higher ash thickness or with prolonged exposure. Cattle and other large mammals may also suffer from teeth problems with the grinding away of teeth surfaces from eating tephra-coated vegetation (Blong, 1984). Again the scale of impact would depend on the time year. Sheep, beef and dairy farms would be most effected by an eruption in early spring, where lactation would be depressed, affecting both milk yields and calf survival (Neild *et al.,*1998).

The toxic element content of tephra is also a concern for soil, pastures and grazing animals. Fluorine aerosols attached to fine tephra pose a significant threat to livestock. Poisoning occurs where the fluorine content of dry grass exceeds 250 ppm (Cronin *et al.,* 1998). During the 1995 Ruapehu eruption, in the Rangitaiki Plain (Taupo) area, minor sheep deaths were reported where 1-3 mm of ash had accumulated due to chronic fluorosis and starvation. Deaths started to occur 10 days following the fall, amounting to 2-3 % of the flock (Cronin *et al.,* 1998)

Forestry

The central North Island is New Zealand's largest wood-producing region, with a total planted forest area of around 560,000 hectares, 91% of which is radiata pine (www.insights.co.nz, 2004). Although pines have been noted to survive 1240 mm of tephra (Blong, 1984), the damage to trees varies with the basal diameter of the trunk. Pine seedlings and smaller trees are more susceptible to burial and bending from ash, while larger trees experienced more branches breaking from overloading. Trees with diameters between 100 mm-300 mm are able to survive as they are strong enough to resist bending, but they are flexible enough to allow ash to fall off (Blong, 1984).

Infrastructure

The ash fall expected in the Te Maari eruption scenario would have little impact on buildings beyond the lower slopes of the volcano, as the amount is not sufficient enough

to collapse roofs or bury houses. There may be minor abrasion on exteriors but the ash would be more of a nuisance inside buildings, soiling interiors and causing blockages in air-conditioners (Neild *et al.,* 1998). What is of more concern for populated areas is the impact on utilities (especially fresh and wastewater systems) and transport and communication networks.

The Tongariro Power Scheme operates in this area with canals, reservoirs and the Rangipo Power Station. In the 1995 Ruapehu eruption, electricity generation in the Rangipo Power Station was disrupted when two turbines were damaged by the ash-laden Tongariro River (www.gns.cri.nz, 2004). Power lines are also at risk from tephra, especially when wet, as it becomes conductive. In a 1924 eruption from Kilauea, a severe electrical storm began and 21 consecutive power poles were destroyed 8 km from the vent (Blong, 1984).

The effects on the water supply include both water quality, distribution and water usage. Reservoirs and tanks are contaminated by even minor tephra falls, and tephra entering rivers and other waterways increases turbidity and acidity in some cases (Blong, 1984). This contamination of drinking water affects not only humans but also animals. Water supplies may also be cut or limited due to pump failure (Neild *et al.,* 1998). There is also the problem of increased water usage during the clean-up phase. In some cases, even relatively minor tephra falls have generated a 50% increase in user demand (Blong, 1984). This problem would be exacerbated if the eruption were to occur in summer months.

Tephra is easily washed into storm water drains, which could affect waste water and sewerage systems through blockages and abrasion to pumps. Roads would need to be cleared to prevent this (Neild *et al.,* 1998).

Transport would be affected by the burial of roads, poor visibility and the reduction of traction (Blong, 1984). Even in small deposits, traction is reduced by wet and dry ash,

producing surfaces similar to driving on ice (Barnard, 2004). This would be particularly dangerous on the State Highways and would create problems for emergency vehicles.

Air travel across the North Island would cease as tephra plumes have frequently caused problems in the past for aeroplanes, inadvertently flying through ash many kilometres away from the erupting vent (Blong, 1984). The main cause of engine thrust loss is the accumulation and solidification of ash on the turbine nozzle guide vanes (Fig. 6.4) (Schmincke, 2004).

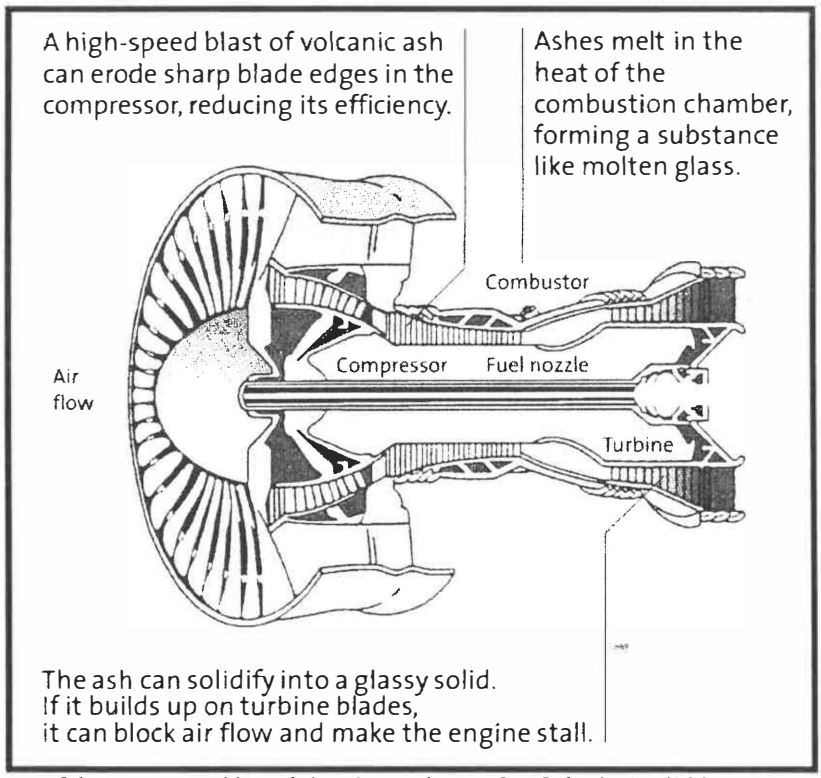

Figure 6.4: Areas of damage caused by ash in a jet engine. After Schmincke (2004).

Machinery and virtually any item of equipment with moving parts can be damaged by tephra (Blong, 1984), through clogging or abrasion. This is of particular concern for agriculture in the area, with impacts on farm machinery, particularly dairy farms, likely to be severe (Neild *et al.,* 1998). Regular washing can help reduce the effect, but some ash and water can create a grinding paste, which can damage surfaces further (Neild *et al.,* 1998).

Health

The main effects on humans for this scenario would be largely of discomfit, with ash getting into eyes and minor respiratory and throat irritations, which would be more serious for asthma sufferers (Neild *et al.,* 1998). A study from the 1995-1996 Ruapehu eruptions suggested a slight increase in acute bronchitis caused by inhaling fine ash particles (Hickling *et al.,* 1999). There were other health problems in the Ruapehu eruptions that were attributed to the ash, which included, skin rashes, coughs, sore throats and nausea (Becker *et al.,* 2001).

6.3.2 Lava Flow

Lava flows move relatively slowly, rarely exceeding a brisk walking pace and affect only a limited area, depending largely on temperature, viscosity, output rate, volume, slope and topography. However, they may cause significant local impacts, and the location of the Te Maari vents high on northern slopes, and the proximity of the park boundary increases the volcanic risk.

The youngest lava flow (1500 AD) from the Upper Crater is a thick andesitic aa flow that runs down slope to the northwest and intersects at several points with the Tongariro Crossing walking track. There is also a large, levéed flow directly north of the lower crater.

Emplacement of similar sized flows during the next Te Maari eruption would probably have the following impacts:

- destruction of native and plantation vegetation on the northern flanks of Tongariro
- initiation of local forest fires in Rotoaira Forest through avalanching of hot blocks
- destruction and inundation of infrastructure, potentially including the lower Tongariro Crossing track and Ketetahi road-end carpark and, for a large event, the Lake Rotoaira Road (SH 47a)

- instability of the steep lava flow fronts may generate small, hot pyroclastic avalanches (Neild, *et al.,* 1998) that would extend the impact zone as far as the state highway, and prove a greater risk to human life
- proximity of these vents to the northern national park boundary may enhance the volcanic risk due to access by the public and sightseers to the area during an eruption. Road access from Rangipo and SH 47a would need to be controlled.

Using the present-day topography potential lava flow paths have been extrapolated in Fig. 6.5 a. Zones of impact have also drawn in Fig. 65.5b showing areas that are moat at risk of fires or pyroclastic avalanches.

Because of the slow moving nature of these flows mitigation strategies can be employed to reduce impact. For example, in Catania, situated at the base of Mount Etna, an attempt to protect a pine forest was made by ground crews from the fire department and the forest corps. Helicopters aided by water bombing lava flows from the air, and in this way fires were stopped from spreading far beyond the edges of the flow. Although over 80 hectares of forest was still destroyed (Barnard, 2004).

a)

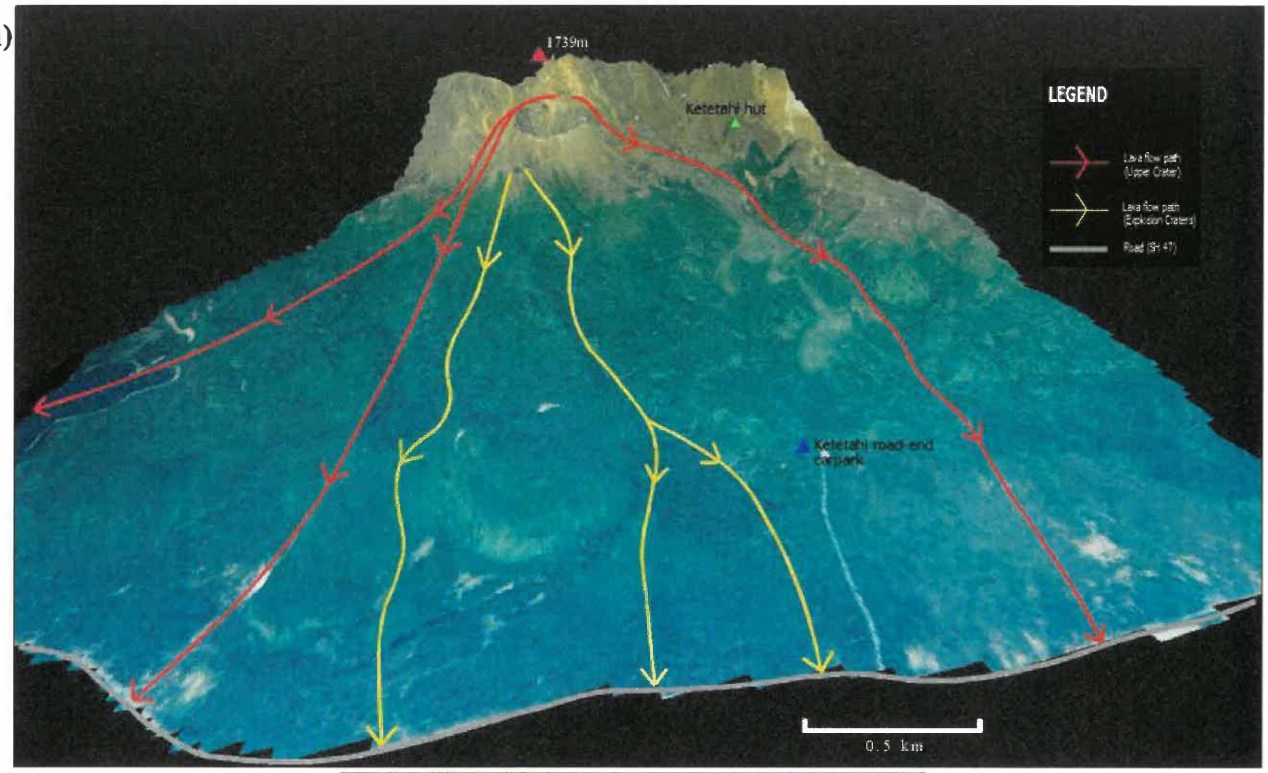

b)

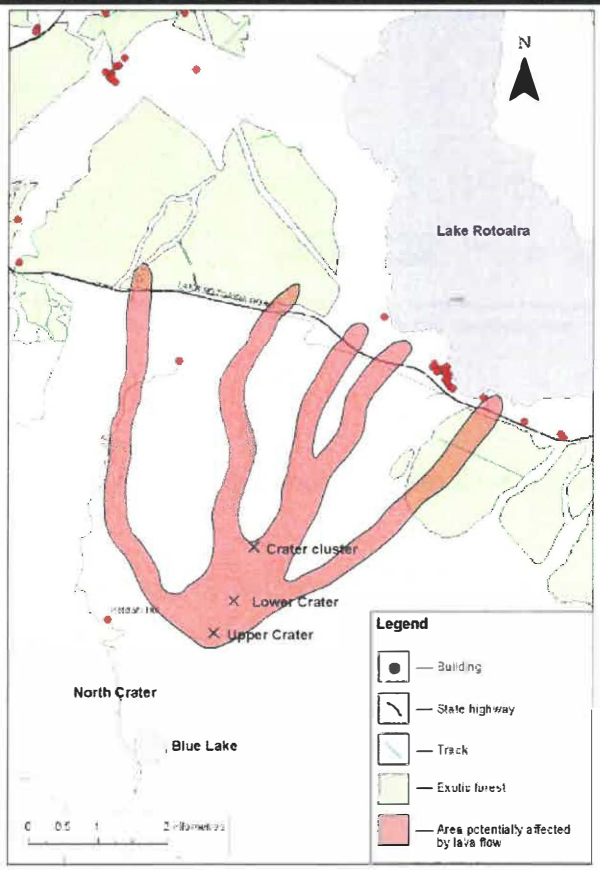

Figure 6.5: a) DEM of Te Maari Craters view towards southwest, with potential lava flow paths from the Upper Crater and Northern Crater Cluster. b) High risk zones of impact from fires and pyroclastic flows.

6.3.3 Volcanic Gas and Acid Rain

The magmatic gas stream typically consists of H_2O, CO^2, SO^2, H_2S, HCl, HF and other minor species. There are three hazards associated with volcanic gases:

1) Direct exposure

- symptoms are restricted to eye and respiratory irritation in humans and animals. Significant exposure is likely to be restricted to zones within about 5-7 km of the vent (Neild *et al.*, 1998).

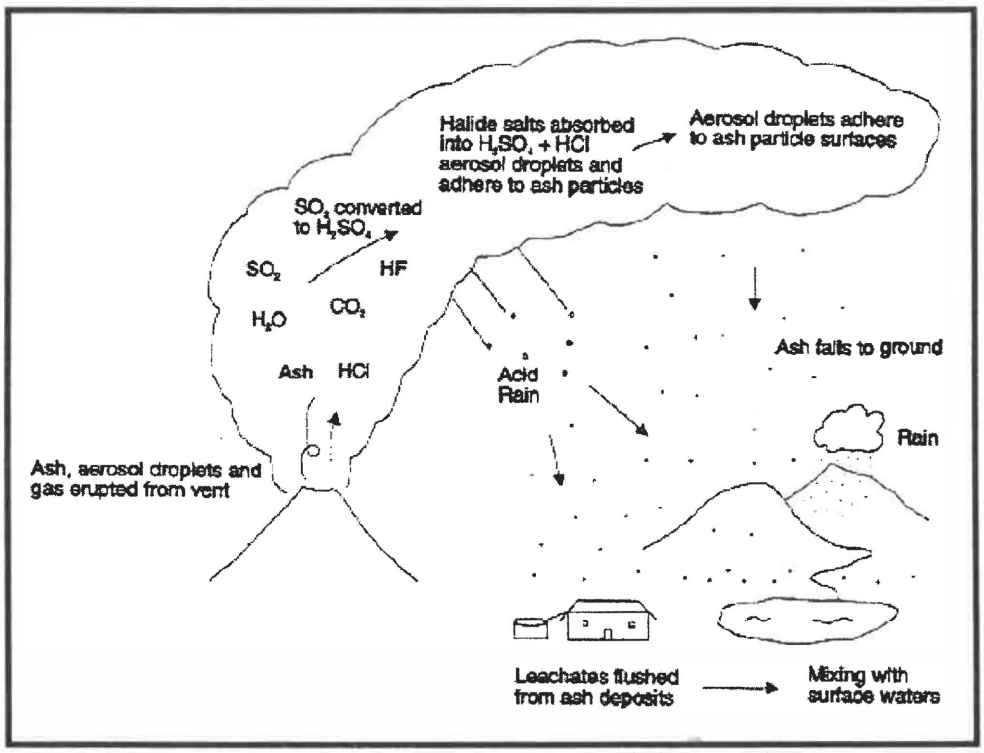

Figure 6.6: Development of acid rain from interaction of gases with the atmosphere. After www.maf.govt.nz (2004).

2) Interaction of gases with the atmosphere leading to the development of volcanic fog and/or acid rain (Fig. 6.6)

   - while the effect on livestock is not considered serious, acid rain can cause considerable damage to crops, machinery and other infrastructure (e.g. transmission lines) through corrosion (Neild *et al.*, 1998).

3) Uptake of the water-soluble plume gas species onto aerosol particles and ash, which then falls out onto pastures and forest.

- in the 1995 eruptions of Ruapehu, ash with even a moderate soluble chemical burden proved lethal to sheep and deer (Neild *et al.*, 1998).

6.4 *Public Safety*

The Te Maari Craters are located close to the Ketetahi Track and hut on the northern slopes of Tongariro. They are relatively close to the National Park boundary and as such are easily accessible to the public. This proximity increases the associated risk, as it would be very difficult to prevent the curious and "thrill-seeking" members of the public from going to have a look at an erupting volcano. The slow-moving nature of lava flows in this sort of eruption may deceive people into thinking they get close without realising the danger of sudden avalanches from the flow front. In Catania, Italy, the eruption of Mount Etna in 2002 caused two reactions in people; panic and intense curiosity. The desire to witness the eruption motivated many people to climb to the active vents or moving lava flows. This not only put people in immediate danger of bomb fallout, volcanic gases and aa lava flows, but also obstructed emergency services and created more problems, with tourists getting lost or injured. Alpine rescue teams had to then be deployed, putting even more people at risk. Many roadblocks were set up in order to prevent this but attempts were still made, creating queues of traffic, which further hampered emergency services (Barnard, 2004). Serious consideration needs to be given to how public access around the national park area could be managed during the next Tongariro eruptions.

6.5 *Economic Impacts*

The 1995-1996 eruptions of Mount Ruapehu provided the opportunity for a study of the economic impacts of a small volcanic eruption, as part of a wider investigation into the diverse effects of the eruption and people's perception of the eruption. The amount of ash fall experienced in the recent Ruapehu eruptions (Fig. 6.7) is comparable to that shown in the scenario for Te Maari Craters and provides a basis for assessing the

economic impacts of an eruption from Te Maari Craters. The results of a survey conducted soon after the 1996 eruptions show that major losses were experienced by those in the tourist industry, with various businesses losing between $100 - $3,000,000. Accommodation services, retail and those involved in water sports were also hit hard with losses ranging between $100 - $1,000,000 (Becker et al., 2001 & www.gns.cri.nz, 2004).

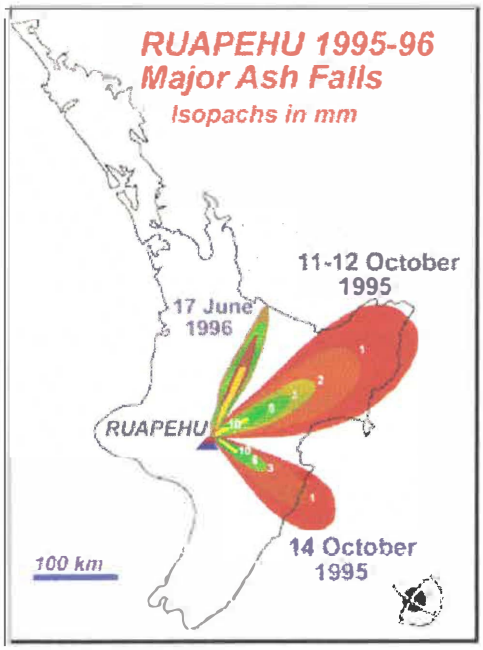

Figure 6.7: Isopach map of main tephras erupted from Mount Ruapehu, 1995-1996. (www.gns.cri.nz, 2004)

Further economic impacts that may be expected for this scenario include:

Electricity generation

- lost production if there is damage to the Rangipo power station through shutdown of Rangipo/Tokaanu Scheme and replacement and maintenance costs. In the 1995-1996 Ruapehu eruptions, electricity generation losses amounted to around $22 million dollars. About half of this was for repairs to two turbines that were damaged in the Rangipo power station (www.gns.cri.nz, 2004).

Aviation industry

it is difficult to estimate the cost to the aviation industry as many airports can be disrupted depending on plume height and wind directions, with cancelled or diverted flights, which can last for weeks. $24 million dollars was lost in cancelled flights alone during the Ruapehu eruption (www.gns.cri.nz, 2004).

Emergency services

there would be an urgent need for emergency services, due to fires, road accidents, clean-up etc. leading to extra staff and resources costs.

Agriculture

lost stock and production. During the Ruapehu eruptions there was $400,000 loss reported from lamb and ewe losses and the cauliflower crop loss in Gisborne (www.gns.cri.nz, 2004). This would also have secondary impacts with employment loss.

6.6 *Conclusions*

The dominant eruption style at the Te Maari Craters is vulcanian. The similarity of these eruptions to those of Ngauruhoe is the basis for an eruption scenario using a 100-1000 year return period event from Ngauruhoe for modelling the impacts of the next Te Maari event.

Tephra fall will be the most widespread hazard and have the biggest impact, especially on the largely agricultural communities of the central North Island. Ash fall would have adverse affects on most aspects of human life including, agriculture, forestry, infrastructure and health, not only during an eruption, but also in the short-term following the event.

The type of slow-moving, aa lava flows associated with this eruption type affects only a limited area, but can cause significant local impacts, such as fires and the destruction of vegetation and the generation of avalanches from the flow front.

Volcanic gases would have a direct impact only in areas close to the vent, but acid rain formation from volcanic gases causes considerable damage to crops, machinery and other infrastructure.

The location of the craters adds an additional hazard to public safety, with curious sightseers gaining access to the area following an eruption. They would not only put themselves in danger but also the rescue workers who have to go and save them if anything happens.

The economic impacts are widespread and can be long lasting depending on the duration and scale of the eruptions. Major losses will come from tourism, agriculture, electricity generation and the aviation industry, but the smaller communities and businesses will also be hit hard, probably resulting in closures and job losses, which can be devastating for small rural communities.

CHAPTER SEVEN

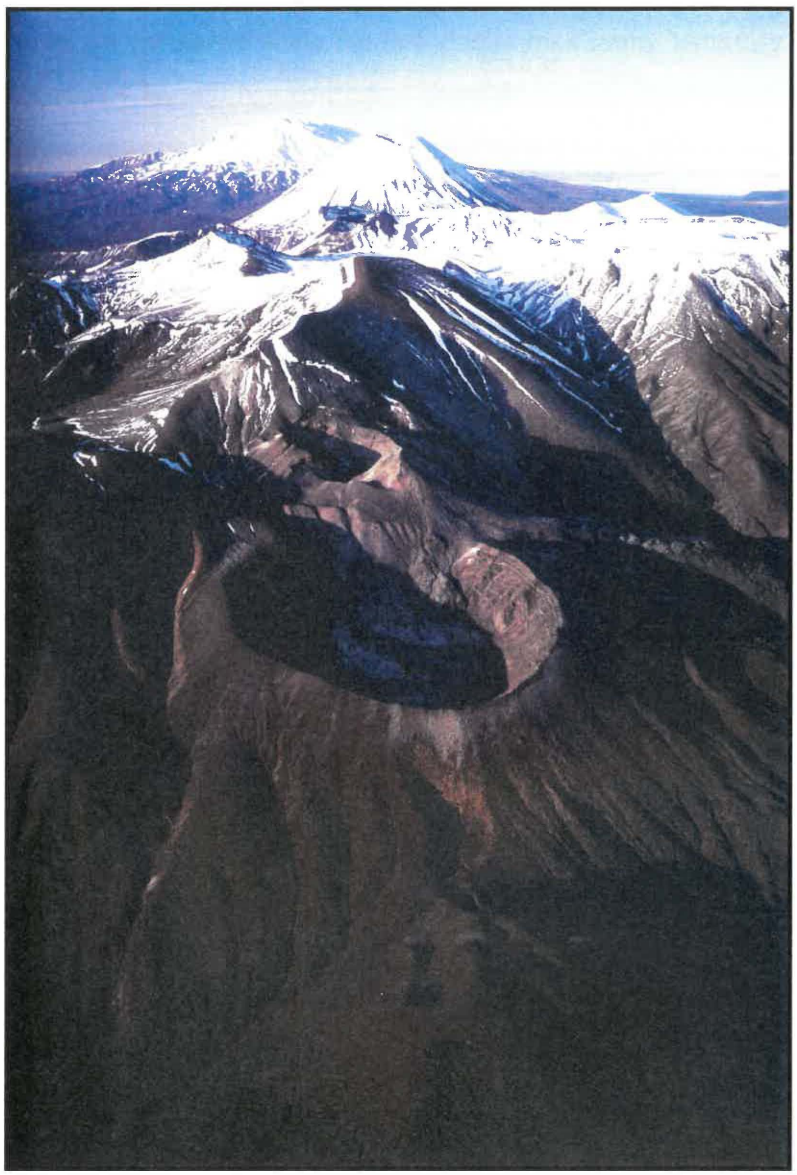

SUMMARY AND CONCLUSIONS

7.1 Introduction

The Te Maari Craters are located on the northern flanks of Mount Tongariro, in the Tongariro Volcanic Centre (TgVC). They represent one of at least seven vent systems that have been active on Tongariro since the last glacial maximum. Activity at Te Maari probably began about 14 ka and has continued through historic times, making it one of the most long-lived of the young eruptives on Tongariro (Hobden, 1997).

7.2 Field and Laboratory Characteristics

The Upper Te Maari Crater is the younger of the two larger craters and the most recently active, with the most recent ash eruptions (1892, 1896) and the c.1500 AD lava flow being sourced from here. It has a narrow, funnel-shaped structure. Three units can be distinguished in the upper crater: an upper unit of weakly consolidated, bedded, coarse andesite breccia, a lower unit of weakly consolidated, massive, very coarse breccia and a central structure of hydrothermally altered, massive, coarse breccia.

The breccia is unconsolidated, a brown/grey colour, weathered to red, containing sand to block sized, angular to subrounded clasts. It is poorly sorted with a fine-coarse ash-sized matrix. The clasts are medium grey, porphyritic, vesicular andesite. They are hypocrystalline and have a medium grainsize with crystals of subhedral and tabular plagioclase, pyroxene and opaques. These samples have an average crystallinity of 44% and an average vesicularity of 5-6%.

The Lower Te Maari Crater is the older of the two craters. It is a 500 m wide, 60 m deep flat-floored structure, which implies that some shallow collapse has occurred. There is also an ephemeral pool on the crater floor. The stratigraphy of the lower crater is comprised of multiple layers of jointed, massive andesite that has been exposed on the crater wall. There is an intrusion in the western wall with columnar and platy jointing

and an area of sulphurous hydrothermal activity. Ballistic blocks scattered around the rim of the crater, with a few displaying "breadcrust" textures and impact fractures are the only proximal pyroclastic facies associated with this crater.

There are two andesite rock types that display different characteristics in the Lower Te Maari Crater. The most abundant is a medium grey, medium-grained, vesicular, hypocrystalline, porphyritic andesite with crystals of subhedral plagioclase and pyroxene. The second andesite is light grey, moderately vesicular, fine medium-grained and porphyritic with crystals of subhedral, prismatic pyroxene and subhedral, tabular plagioclase. The groundmass is felted, intergranular and hyalopilitic. These samples have an average crystallinity of 40% and an average vesicularity of 6-7%.

The lava flows associated with these craters are thick, crystal-rich andesite, forming aa to blocky flows. There are 3-4 older flows, 3-4 km long, north of the craters that can be identified as originating from this area. The most recent lava flow has been dated at c.1500 AD by Topping (1974), and was erupted from the Upper Te Maari Crater. It is approximately 4 km long running downslope to the northwest and is comprised of multiple, overlapping lobes with some levee development. The thickness varies greatly from 80 m near the vent, to 20 m at the flow front. The overall surface texture is rubbly and vesicular, with angular to sub-angular blocks and a massive, less vesicular core.

The 1500 AD lava flow andesite is dark grey, coarse medium grained, vesicular, hypocrystalline and porphyritic, with abundant crystals of tabular subhedral plagioclase and pyroxenes and euhedral opaques and olivine. The matrix is felted and hyalopilitic with black glass weathering to red. These samples have an average crystallinity of 41% and an average vesicularity of 14%.

A small cluster of craters occurs directly north of Lower Te Maari Crater, lying on the outer slope of the crater wall. There are 4-5 pits with a shallow pool possibly infilling one. This area may be the source of the large post-glacial flows on the northern slopes below Te Maari.

There are a few outcrops of massive, jointed, medium grey, medium grainsized, vesicular, hypocrystalline and porphyritic andesite with subhedral to euhedral plagioclase and pyroxene and euhedral opaques, within the pits, and one outcrop on the eastern slopes. The matrix is hyalopilitic and felted with coarser sized plagioclase than any other of the Te Maari eruptives. These samples have an average crystallinity of 40% and an average vesicularity of 11-12%.

Apart from the hydrothermal area on the Lower crater wall, there are a few other small areas of steaming ground on the outer slopes of Upper Te Maari Crater and between the Upper and Lower crater. They are generally small cracks or fissures in the rock and are non-sulphurous.

There has not been substantial preservation of tephra deposits from any Te Maari Crater eruption. Pits dug proximal to the vent have revealed some coherent ash layers intercalated with soil and reworked deposits. The composition for most of the deposits coarse material is dominated by angular to subrounded, medium grey, non-vesicular, porphyritic andesite lithics and angular to subangular, dark, coarsely porphyritic, vesicular andesite with some angular to subrounded, red-brown to white, hydrothermally altered lithics and some angular to subangular, white sinter fragments. Averaging all the samples together gives a composition of 60% medium grey andesite, 33% hydrothermally altered andesite, 5% dark andesite and 2% sinter fragments.

The proximal primary ash samples found at the Te Maari Craters all generally display a normal distribution, with mean grainsizes between -1 phi and 1 phi and are well to poorly sorted.

7.3 Eruptive Processes and History

Previous work on the eruptives and history of Te Maari Craters has produced varying accounts of the timeline and products that can be attributed to them. Maps of the northern lava flows especially have evolved over time as more information is collected. Based on previous work done on the Te Maari Craters and others on the Tongariro Volcanic Centre, Lecointre *et al.,* (2004) produced a map with Topping's lava flow outlines and which also outlined older >14.7 ka flows.

The most recent work done by Tetsuo Kobayashi (Univ. of Kuyoshima), has correlated the agglutinates of North Crater with the sub-plinian fall, which suggests that the Rotoaira Lapilli is not from Te Maari, but is sourced from North Crater.

The eruptive style of the Te Maari Craters ranges from phreatic steam and ash and vulcanian eruptions to lava producing eruptions. The field evidence is of ballistic blocks and minor tephra deposits, but there is an absence of any proximal pyroclastic deposits, such as agglutinate or pumice, which implies that this has not been significantly explosive (sub-plinian). This also suggests the Rotoaira Lapilli cannot have originated from the Te Maari Craters. With no sub-plinian activity sourced from these craters it is likely the lower crater and the northern craters were partially formed through minor explosions through existing lava flows and from collapse due to shallow magma withdrawal.

The flows erupted from Te Maari have a total erupted volume of 0.4 km^3. Based on rheological and slope considerations, the 1500 AD lava flow had an emplacement velocity of 0.11 m s^{-1}, and may have been emplaced within 10.10 hours. A more reasonable emplacement time based on likely eruptive rates and the multi-lobe nature of the flow is in the order of a few days.

The breccia found in the Upper Te Maari Crater was emplaced during one of the lava-forming eruptions as a down-slope tapering, very coarse autobreccia apron. The similar

composition and crystallinity of the dense clasts to the 1500 AD lava flow indicates that the breccia was intimately associated with emplacement of this lava. Subsequent phreatic and phreatomagmatic explosions have excavated the upper crater's general morphology as seen today.

The geochronology of the Te Maari Craters can be summarised as follows:

~14 ka	- lava-producing eruptions
10-9.7 ka	– PM sequence (PM2 and PM6)
6.7-10 ka	- Lava-producing eruptions
1500 AD	- Youngest lava produced by Upper Te Maari Crater
1855-1896	- Phreatic/vulcanian activity (possibly to 1928)
2001	- Low frequency seismic events at shallow depth beneath craters

7.4 Volcanic Hazards

The dominant eruption style at the Te Maari Craters is vulcanian and lava-producing. The similarity of these eruptions to those of Ngauruhoe is the basis for an eruption scenario using a 100-1000 year return period event from Ngauruhoe for modelling the impacts of the next major Te Maari event.

Tephra fall will be the most widespread hazard and have the biggest impact, with adverse affects on most aspects of human life within the central North Island, including, agriculture, forestry, infrastructure and health, not only during an eruption, but also in the short-term following the event.

Aa lava flows associated with this eruption type affect only a limited area, but with significant local impacts, such as fires, destruction of vegetation and the generation of hot avalanches from the flow front.

Volcanic gases would have a direct impact only in areas close to the vent, but acid rain formation from volcanic gases causes considerable damage to crops, machinery and other infrastructure.

The location of the craters adds an additional hazard to public safety, with curious sightseers gaining access to the area following an eruption and placing themselves in danger.

The economic impacts are widespread and can be long lasting depending on the duration and scale of the eruptions, with major losses from tourism, agriculture, electricity generation and the aviation industry.

7.5 Suggestions for Further Work

- A more widespread and comprehensive search for proximal and distal deposits from Te Maari as part of a detailed study of the post-glacial eruptive history of Tongariro
- A more detailed analysis of the lava flows sourced from the Te Maari Craters, including: - geochemical analyses
  - dating of flows (searching for carbon at flow contacts)
  - numerical modelling of lava flow emplacement
  - more detailed mapping of flows to determine possible proto-Te Maari source vents.
- Further stratigraphic, geochemical and componentry analysis of the Rotoaira Lapilli to establish the source.

References

Barnard, S.T., 2004, Results of a reconnaissance trip to Mt. Etna, Italy: the effects of the 2002 eruption of Etna on the province of Catania, *Bulletin of the New Zealand Society for Earthquake Engineering, 37*, 47-61.

Becker, J., Smith, R., Johnston, D., Munro, A., 2001, Effects of the 1995-1996 Ruapehu eruptions and people's perceptions of volcanic hazards after the event, *The Australasian Journal of Disaster and Trauma Studies, 2001-1.*

Behncke, B. and Neri, M., 2003, The July-August 2001 eruption of Mt. Etna (Sicily), *Bulletin of Volcanology, 65*, 461-476.

Bibby, H.M., Caldwell, T.G., Davey, F.J., Webb, T.H., 1995, Geophysical evidence on the structure of the Taupo Volcanic Zone and its hydrothermal circulation, *Journal of Volcanology and Geothermal Research, 68,* 29-58.

Blake, S., Bruno, B.C., 2000, Modelling the emplacement of compound lava flows, *Earth and Planetary Science Letters, 184,* 181-197.

Blong, R.J., Volcanic Risk Assessment, in *Monitoring and Mitigation of Volcanic Hazards,* edited by R. Scarpa & R.I. Tilling, pp. 675-698, Springer-Verlag Berlin Heidelberg, Germany, 1996.

Blong, R.J., *Volcanic Hazards: A source book on the effects of eruptions,* 423 pp., Academic Press, Australia, 1984.

Bonadonna, C. & Houghton, B.F., Total grain-size distribution and volume of tephra fall deposits, *Bulletin of Volcanology,* Online Issue, 26 Jan. 2005.

Calvari, S., Neri, M., Pinkerton, H., 2002, Effusion rate estimations during the 1999 summit eruption on Mount Etna, and growth of two distinct lava flow fields, *Journal of Volcanology and Geothermal Research, 119,* 107-123.

Carrigan, C., Plumbing systems, in *Encyclopedia of Volcanoes,* edited by H. Sigurdsson, pp. 219-235, Academic Press, San Diego, 2000.

Cole, J.W., 1990, Structural control and origin of volcanism in the Taupo volcanic zone, New Zealand, *Bulletin of Volcanology, 52,* 445-459.

Cronin, S.J.; Hedley, M.J.; Neall, V.E.; Smith, R.G., 1998, Agronomic impact of tephra fallout from the 1995 and 1996 Ruapehu Volcano eruptions, New Zealand, *Environmental Geology, No.34 (1),* 21-30.

Davidson, J., Composite volcanoes, in *Encyclopedia of Volcanoes,* edited by H. Sigurdsson, pp. 663-681, Academic Press, San Diego, 2000.

Environment Waikato, *Volcanic Contingency Plan: For the Waikato Region,* 52pp., Environment Waikato Policy Series 1999/04, New Zealand, 1999.

Fagents, S.A. and Wilson, I., 1993, Explosive volcanic eruptions - VII. The ranges of pyroclasts ejected in transient volcanic explosions, *Geophysical Journal International, 113,* 359-370.

Fisher, R.V., Heiken, G., Hulen, J.B., *Volcanoes: Crucibles of Change,* 317pp., Princeton University Press, New Jersey, 1998.

Francis, P., *Volcanoes: A Planetary Perspective,* 443pp., Oxford University Press, New York, 1993.

Friedlander, B., 1898, Some Notes on the Volcanoes of the Taupo District, in *Transactions of the New Zealand Institute, 31,* 498-510.

Fudali, R.F. and Melson, W.G., 1972, Ejecta velocities, magma chamber pressure and kinetic energy associated with the 1968 eruption of Arenal volcano, *Bulletin Volcanologique, 15,* 383-401.

Gill, J.B., *Orogenic Andesites and Plate Tectonics,* 390pp., Springer-Verlag, Berlin-Heidelberg, 1981.

Gregg, D.R., 1960, Geology of the Tongariro Subdivision, *New Zealand Geological Survey, 40,* 9-102.

Grubensky, M.J., Smith, G.A., Geissman, J.W., 1998, Field and paleomagnetic characterization of lithic and scoriaceous breccias at Pleistocene Broken Top volcano, Oregon Cascades, *Journal of Volcanology and Geothermal Research, 83,* 93-114.

Hagerty, M., Benites, R., 2003, Tornillos beneath Tongariro Volcano, New Zealand, *Journal of Volcanology and Geothermal Research, 125*, 151-169.

Hickling, J., Clements, M., Weinstein, P., Woodward, A., 1999, Acute health effects of the Mount Ruapehu (New Zealand) volcanic eruption of June 1996, *International Journal of Environmental Health Research 9(2),* 97-107.

Hill, H., 1894, The volcanic outburst at Te Mari, Tongariro, in November, 1892, in *Transactions of the New Zealand Institute, 26,* 388-392.

Hill, H., 1891, Ruapehu and Ngauruhoe, in *Transactions of the New Zealand Institute, 24,* 603-625.

Hobden, B.J., Modelling magmatic trends in time and space: eruptive and magmatic history of Tongariro volcanic complex, New Zealand, Doctor of Philosophy thesis, University of Canterbury, 1997.

Hobden, B.J., Houghton, B.F., Geology of the Tongariro Volcano Traverse, in *State of the Arc: Processes and time scales in the genesis and evolution of arc magmas. Guide book for field excursions on Ruapehu and Tongariro volcanoes,* edited by R.C. Price, J.A. Gamble, and B.J. Hobden, 2000.

Hobden, B.J., Houghton, B.F., Nairn, I.A., 2002, Growth of a young, frequently active composite cone: Ngauruhoe volcano, New Zealand, *Bulletin of Volcanology, 64,* 392-409.

Hobden, B.J., Houghton, B.F., Davidson, J.P., Weaver, S.D., 1999, Small and short-lived magma batches at composite volcanoes: time windows at Tongariro volcano, New Zealand, *Journal of the Geological Society, London, 156,* 865-868.

Hobden, B.J., Houghton, B.F., Lanphere, M.A., Nairn, I.A., 1996, Growth of the Tongariro volcanic complex: new evidence from K-Ar age determinations, *New Zealand Journal of Geology and Geophysics, 39,* 151-154.

Ishihara, K., 1985, Dynamical analysis of volcanic explosion, *Journal of Geodynamics, 3,* 327-349.

Johnston, D.M., Nairn, I.A., Thordarson, T., Daly, M., *Volcanic Assessment for the Auckland Volcanic Field*, Auckland Regional Council, Technical Publication Number 79, 1997.

Kilburn, C.R.J., 2004, Fracturing as a quantitative indicator of lava flow dynamics, *Journal of Volcanology and Geothermal Research, 132,* 209-224.

Kilburn, C.R.J., Lava flows and flow fields, in *Encyclopedia of Volcanoes,* edited by H. Sigurdsson, pp. 291-305, Academic Press, San Diego, 2000.

Kilburn, R.J. and Guest, J.E., Aa lavas of Mount Etna, Sicily, in *Active Lavas,* edited by C.R.J. Kilburn & G. Luongo, pp. 73-106, UCL Press, London, 1993.

Linneman, S.R. & Borgia, A., The blocky andesitic lava flows of Arenal volcano, Costa Rica, in *Active Lavas,* edited by C.R.J. Kilburn & G. Luongo, pp. 73-106, UCL Press, London, 1993.

Morrissey, M. and Mastin, L.G., Vulcanian eruptions, in *Encyclopedia of Volcanoes,* edited by H. Sigurdsson, pp. 463-475, Academic Press, San Diego, 2000.

Nairn, I.A., Kobayashi, T., Nagakawa, M., 1998, The ~10 Ka multiple vent pyroclastic eruption sequence at Tongariro Volcanic Centre, Taupo Volcanic Zone, New Zealand: Part 1. Eruptive processes during regional extension, *Journal of Volcanology and Geothermal Research, 86,* 19-44.

Nairn, I.A. and Self, S., 1978, Explosive eruptions and pyroclastic avalanches from Ngauruhoe in February 1975, *Journal of Volcanology and Geothermal Research, 3,* 39-60.

Neild, J., O'Flaherty, P., Hedley, P., Underwood, R., Johnstone, D., Christenson, B., Brown, P., 1998, Impact of a Volcanic Eruption on Agriculture and Forestry in New Zealand, *MAF Policy Technical Paper 99/2.*

Potton, C., *Tongariro: A Sacred Gift: a centennial celebration of Tongariro National Park,* 192pp, Craig Potton Publishing, Nelson, NZ, 1995.

Schmincke, H., *Volcanism,* 324pp., Springer-Verlag Berlin Heidelberg, Germany, 2004.

Self, S., Wilson, L., Nairn, I.A., 1979, Vulcanian eruption mechanisms, *Nature, 277,* 440-443.

Self, S., 1975, Explosive activity of Ngauruhoe, 27-30 March 1974 (Note), *New Zealand Journal of Geology and Geophysics, Vol. 18, No. 1,* 189-195.

Smith, G.A., Grubensky, M.J., Geissman, J.W., 1999, Nature and origin of cone-forming volcanic breccias in the Te Herenga Formation, Ruapehu, New Zealand, *Bulletin of Volcanology, 61,* 64-82.

Topping, W.W., Some aspects of Quaternary history of Tongariro Volcanic Centre, Doctor of Philosophy thesis, Victoria University, Wellington, 1974.

Topping, W.W., 1973, Tephrostratigraphy and chronology of late Quaternary eruptives from the Tongariro volcanic centre, New Zealand, *New Zealand. Journal of Geology and Geophysics, 16,* 397-423.

Walker, G.P.L., Eruptions of andesitic volcanoes, in *Andesites: Orogenic andesites and related rocks,* edited by R.S. Thorpe, pp. 724, John Wiley & Sons, Chinchester, 1982.

Walsh, F.D., Hochstein, M.P., Bromley, C.J., 1998, The Tongariro geothermal system (NZ): Review of geophysical data, *Proceedings 20th NZ Geothermal Workshop,* 317–324.

Wilson, C.J.N., Houghton, B.F., McWilliams, M.O., Lanphere, M.A., Weaver, S.D., Briggs, R.M., 1995, Volcanic and structural evolution of Taupo Volcanic Zone, New Zealand: a review, *Journal of Volcanology and Geothermal Research, 68,* 1-28.

Wohletz, K. & Heiken, G., *Volcanology and Geothermal Energy,* 432pp., University of California Press, USA, 1992.

Wood, C.P. and Topping, W.W., Volcanoes and thermal areas south of Lake Taupo, in *Guide to Geophysics of the Volcanic and Geothermal Areas of the North Island, New Zealand,* edited by M.P. Hochstein and T.M. Hunt, pp. 93, The Royal Society of New Zealand, Wellington, 1980.

www.gns.cri.nz, 16/8/2004. Geological and Nuclear Sciences.

www.insights.co.nz, 25/9/2004. Forestry Insights.

www.maf.govt.nz, 25/9/2004. Ministry of Agriculture and Forestry.

APPENDIX I

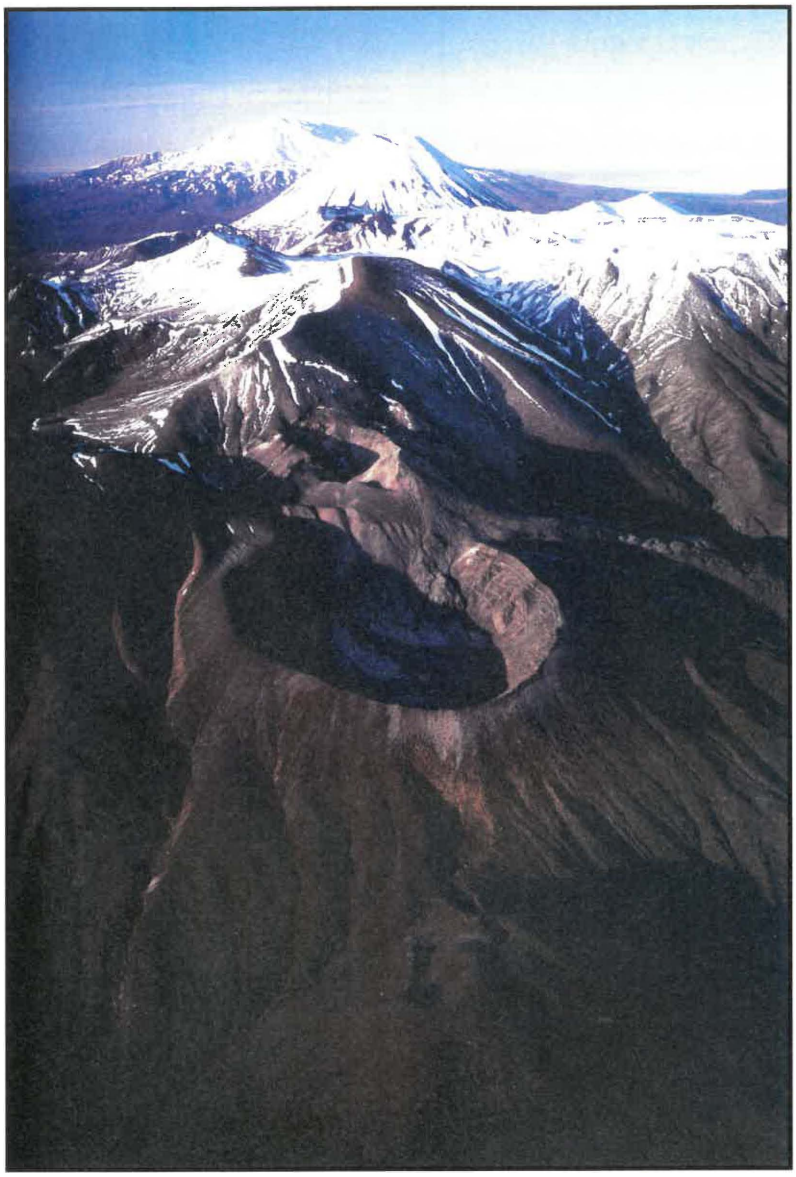

SAMPLE LOCATIONS AND GPS CO-ORDINATES

SAMPLE NO.	EASTING	NORTHING	DESCRIPTION
UC1	2740881	6229104	Upper crater, S wall
UC2	2740976	6229120	Upper crater, S wall
UC3	2741062	6229126	Upper crater, SE wall
UC4	2741019	6229182	Upper crater, E wall
UC5	2741014	6229250	Upper crater floor, hydrothermal unit
UC6/7	2740881	6229333	Upper crater, W wall, unconsolidated breccia – two clasts
UC8	2741043	6229272	Upper crater, E wall
UC9/10	2741143	6229346	Upper crater, eastern bedded breccia
26S10	2741477	6229818	Lower crater, E wall
26S12	2741471	6229860	Lower crater, E wall
LC1	2741309	6229677	Lower crater, SE wall
LC2	2741415	6229641	Lower crater, SE wall
LC3	2741409	6229734	Lower crater, E wall
LC4	2741460	6229875	Lower crater, E wall
LC5	2741381	6229998	Lower crater, E wall
LC6	2741205	6230113	Lower crater, N wall
LC7	2741134	6230092	Lower crater, N wall
LC8	2741076	6230066	Lower crater, NW wall
LC9	2740978	6230021	Lower crater, W wall
LC10	2740971	6229961	Lower crater W wall
LC11	2741011	6229968	Lower crater, W wall
LC12	No GPS signal		Lower crater, W wall
LC13	2741033	6229949	Lower crater, W wall
LC14	No GPS signal		Lower crater, big lava structure
LC15	2740966	6229806	Lower crater, SW wall
LC16	2740976	6229811	Lower crater, SW wall
LC 16	2740966	6229806	Lower crater, SW wall (mislabelled)
LC17	2740961	6229799	Lower crater, SW wall
LC18	2740926	6229798	Lower crater, SW wall
LC19	2740941	6229875	Lower crater, SW wall

SAMPLE NO.	EASTING	NORTHING	DESCRIPTION
RLF1	2740978	6229465	1500 AD lava flow, proximal
RLF2	2740943	6229508	1500 AD lava flow, proximal
RLF3	2740990	6229641	1500 AD lava flow, proximal
RLF4	2740839	6229563	1500 AD lava flow, proximal
RLF5	2740678	6229831	1500 AD lava flow, proximal
RLF6	2740394	6230151	1500 AD lava flow, medial
RLF7	2740306	6230454	1500 AD lava flow, medial
RLF8	2740306	6230454	1500 AD lava flow, medial
RLF9	2740260	6230570	1500 AD lava flow, medial
RLF10	2739970	6230333	1500 AD lava flow, medial
RLF11	2740033	6230302	1500 AD lava flow, medial
RLF12	2740220	6229778	1500 AD lava flow, proximal
RLF13	2740282	6229687	1500 AD lava flow, proximal
RLF14	2740396	6229612	1500 AD lava flow, proximal
RLF15	2740748	6229516	1500 AD lava flow, proximal
RLF16	2740780	6229722	1500 AD lava flow, proximal
LFF1	2740205	6232768	1500 AD lava flow, distal
LFF2	2740225	6232681	1500 AD lava flow, distal
LFF3	2740003	6232359	1500 AD lava flow, distal
EC1	2741478	6230492	Northern crater cluster, Pit 1
EC2	2741511	6230597	Northern crater cluster, Pit 2
EC3	2741534	6230473	Northern crater cluster, Pit3
EC4	2741637	6230503	Northern crater cluster, E slope
13/12Ash1	2741136	6229147	12 cm from surface, 1-2 cm thick
13/12Ash2	2741211	6229164	3 cm from surface, 8 cm thick
13/12Ash3	2741211	6229164	15 cm from surface, 2-3 cm thick
13/12Ash4	2741223	6229168	5 cm from surface, 0.5 cm thick
13/12Ash5	2741338	6229245	10 cm from surface, 1-2 cm thick
13/12Ash6	2741338	6229245	15 cm from surface, 6 cm thick
13/12Ash7	2741338	6229245	22 cm from surface, 2-3 cm thick
13/12Ash8	2741827	6229088	15 cm from surface, 3-4 cm thick
13/12Ash9	2742111	6229143	4-5 cm from surface, 2-3 cm thick
13/12Ash10	2741594	6229330	5 cm from surface, 2 cm thick
13/12Ash11	2741594	6229330	10 cm from surface, 1-2 cm thick

SAMPLE	EASTING	NORTHING	DESCRIPTION
13/12Ash12	2741594	6229330	22 cm from surface, 4-5 cm thick
13/12Ash13	2741439	6229361	5 cm from surface, 2-4 cm thick
13/12Ash14	2741338	6229449	8 cm from surface, 1-2 cm thick
13/12Ash15	2741338	6229449	13 cm from surface, 2-3 cm thick
13/12Ash16	2741338	6229449	20 cm from surface, 2-3 cm thick
Steamy area	2740934	6229530	
Steamy area	2740914	6229497	
Steamy area	2740945	6229515	
Steamy area	No GPS		Outer west wall of upper crater

Lava Flow Mapping GPS Co-ordinates

Plain = main flow **Bold** = breakaway lobes

	Elevation (m)	Easting	Northing
1.	1492	2740978	6229465
(Into lower crater)			
2.	**1493**	**2740941**	**6229470**
3.	**1492**	**2740938**	**6229482**
4.	**1488**	**2740932**	**6229487**
5.	**1486**	**2740934**	**6229530**
6.	**1470**	**2740943**	**6229508**
7.	**1451**	**2740971**	**6229596**
8.	**1441**	**2740989**	**6229632**
9.	**1435**	**2740990**	**6229641**
(Inner edge of main flow) (*outer edge below)			
10.	1449	2740839	6229563
11.	1414	2740789	6229630
12.	1391	2740745	6229681
13.	1369	2740699	6229793
14.	1346	2740678	6229831
(Two flow edges now one)			
15.	1313	2740562	6229912
16.	1294	2740478	6230025
17.	1274	2740414	6230115
18.	1273	2740394	6230217
19.	1251	2740404	6230217
20.	1221	2740306	6230454
21.	1181	2740260	6230570
(Halfway across flow)			
22.	1168	2740193	6230544

	Elevation (m)	Easting	Northing	
(Other side of flow, nearest hut)				
23.	1152	2739936	6230404	(+/- 20)
24.	1167	2739970	6230333	
25.	1152	2740033	6230302	(+/- 32)
26.	1221	2740116	6230140	(+/- 20)
27.	1261	2740213	6230051	(+/- 10)
28.	1269	2740201	6229915	
29.	1285	2740220	6229778	
30.	1293	2740280	6229740	
31.	**1291**	**2740266**	**6229702**	
32.	**1291**	**2740282**	**6229687**	
33.	**1290**	**2740348**	**6229658**	
34.	1285	2740387	6229705	
35.	**1307**	**2740381**	**6229646**	
36.	**1309**	**2740397**	**6229615**	
37.	**1312**	**2740396**	**6229612**	
38.	**1325**	**2740458**	**6229545**	
39.	1340	2740559	6229582	
40.	1347	2740629	6229561	
41.	1402	2740733	6229546	
42.	1408	2740748	6229516	
43.	1460	2740813	6229467	
*(Outer edge of main flow)				
1.	1411	2740858	6229620	
2.	1403	2740837	6229676	
3.	1395	2740760	6229711	
1.	1357	2740681	6229821	
(Even further outer edge)				
2.	1351	2740746	6229781	
3.	1354	2740788	6229733	
4.	1372	2740828	6229703	

APPENDIX II

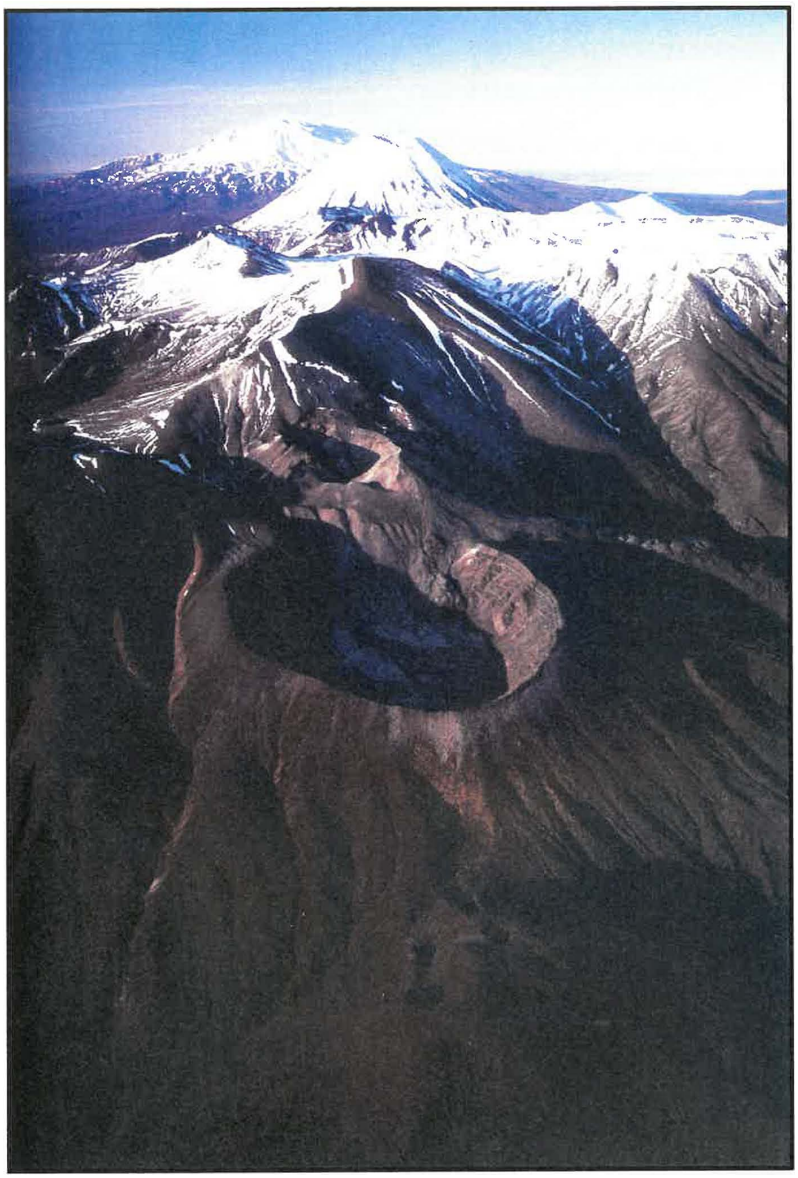

GRAINSIZE ANALYSIS

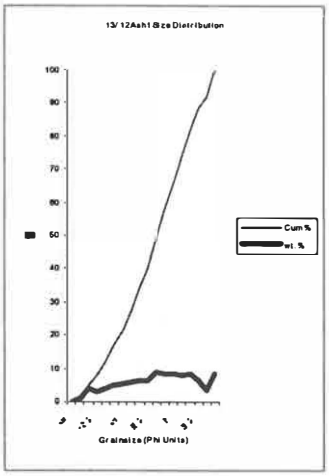

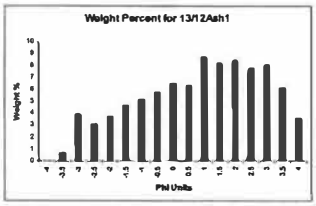

Grainsize Statistics:
Sample 13/12Ash1

Percentiles	***phi***
95	4.26
84	3.15
50	1.05
16	-1.54
5	-2.95

Mean 0.88

Sorting 2.26

phi	Wt. (g)	Wt. %	Cum.wt.%
-4	0.00	0.00	0
-3.5	3.07	0.74	0.738496
-3	16.66	4.01	4.746097
-2.5	13.06	3.14	7.88771
-2	15.85	3.81	11.70046
-1.5	19.73	4.75	16.44656
-1	21.80	5.24	21.6906
-0.5	24.42	5.87	27.56489
0	27.17	6.54	34.1007
0.5	26.31	6.33	40.42963
1	36.60	8.80	49.23384
1.5	34.53	8.31	57.54011
2	35.35	8.50	66.04364
2.5	32.54	7.83	73.87121
3	33.86	8.15	82.01631
3.5	25.58	6.15	88.16964
4	14.82	3.56	91.73462
>4	34.36	8.27	99.999
Total	415.71	100.00	

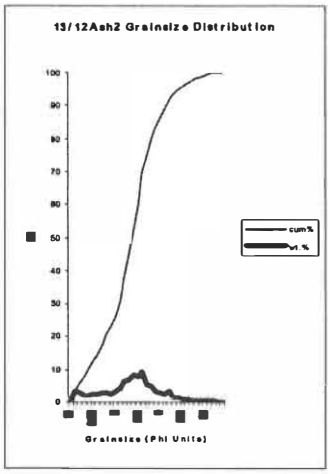

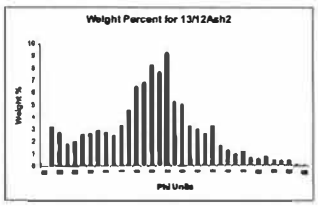

Grainsize Statistics:
Sample 13/12Ash2

Percentiles	***phi***
95	8.24
84	5.69
50	2.89
16	-0.79
5	-3.15

Mean 2.59

Sorting 3.34

phi	Wt. (g)	Wt. %	Cum.wt.%
-4	0	0.00	0.00
-3.5	5.46	3.21	3.21
-3	4.64	2.73	5.94
-2.5	3.02	1.78	7.72
-2	3.33	1.96	9.68
-1.5	4.3	2.53	12.20
-1	4.43	2.61	14.81
-0.5	4.97	2.92	17.73
0	4.67	2.75	20.48
0.5	4.26	2.51	22.99
1	5.57	3.28	26.26
1.5	7.7	4.53	30.79
2	11.11	6.53	37.33
2.5	11.6	6.82	44.15
3	13.94	8.20	52.35
3.5	13.07	7.69	60.03
4	15.75	9.26	69.30
4.5	8.99	5.29	74.59
5	8.55	5.03	79.61
5.5	5.49	3.23	82.84
6	5.05	2.97	85.81
6.5	4.49	2.64	88.45
7	5.47	3.22	91.67
7.5	2.74	1.61	93.28
8	2.10	1.23	94.52
8.5	1.62	0.95	95.47
9	1.95	1.14	96.62
9.5	1.12	0.66	97.27
10	0.98	0.57	97.85
10.5	1.25	0.73	98.58
11	0.75	0.44	99.02
11.5	0.68	0.40	99.42
12	0.67	0.39	99.82
12.5	0.20	0.12	99.93
13	0.11	0.07	99.99
Total	170.02	100.00	

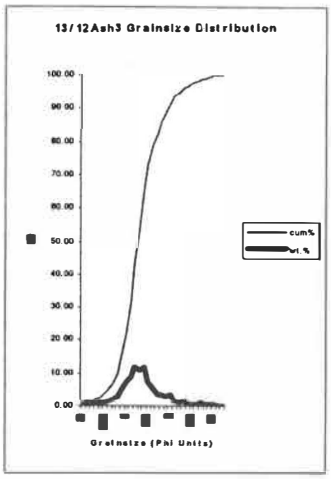

Grainsize Statistics:
Sample 13/12Ash3

Percentiles	***phi***
95	8.12
84	5.75
50	3.32
16	1.60
5	0.00

Mean 3.56

Sorting 2.27

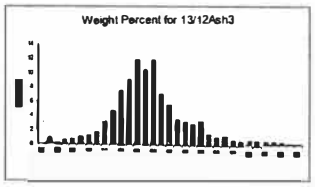

phi	Wt. (g)	Wt.%	Cum.wt.%
-3	0.00	0.00	0.00
-2.5	1.68	0.97	0.97
-2	0.46	0.26	1.23
-1.5	1.12	0.64	1.87
-1	1.41	0.81	2.68
-0.5	1.80	1.03	3.72
0	2.25	1.29	5.01
0.5	3.01	1.73	6.74
1	5.47	3.14	9.89
1.5	8.20	4.71	14.60
2	13.20	7.59	22.19
2.5	15.85	9.11	31.30
3	20.72	11.91	43.22
3.5	18.51	10.64	53.86
4	20.84	11.98	65.84
4.5	12.53	7.20	73.04
5	9.78	5.62	78.66
5.5	6.26	3.60	82.27
6	5.75	3.31	85.57
6.5	5.00	2.88	88.45
7	5.86	3.37	91.82
7.5	2.82	1.62	93.44
8	2.12	1.22	94.66
8.5	2.31	1.33	95.99
9	1.25	0.72	96.70
9.5	1.12	0.65	97.35
10	1.00	0.57	97.92
10.5	1.36	0.78	98.70
11	0.82	0.47	99.18
11.5	0.72	0.41	99.59
12	0.57	0.33	99.92
12.5	0.11	0.06	99.98
13	0.04	0.02	100.00
Total	173.94	100.00	

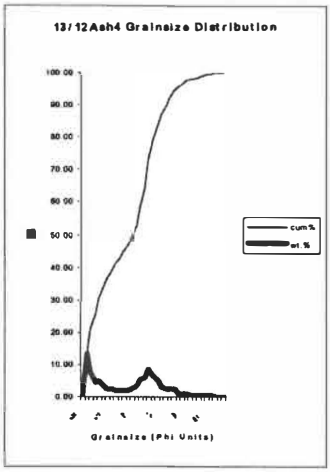

Grainsize Statistics:
Sample 13/12Ash4

Percentiles	***phi***
95	7.19
84	5.00
50	2.10
16	-3.32
5	-3.4

Mean 1.26

Sorting 3.68

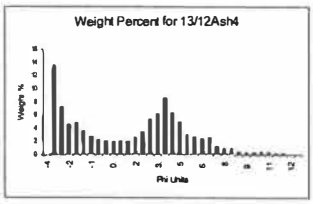

phi	Wt. (g)	Wt.%	Cum.wt.%
-4	0.00	0.00	0.00
-3.5	8.82	13.56	13.56
-3	4.80	7.38	20.94
-2.5	2.97	4.57	25.51
-2	3.13	4.81	30.32
-1.5	2.31	3.55	33.87
-1	1.72	2.64	36.52
-0.5	1.46	2.24	38.76
0	1.33	2.04	40.81
0.5	1.22	1.88	42.68
1	1.34	2.06	44.74
1.5	1.29	1.98	46.73
2	1.68	2.58	49.31
2.5	2.25	3.46	52.77
3	3.46	5.32	58.09
3.5	4.01	6.17	64.25
4	5.57	8.56	72.82
4.5	4.07	6.26	79.07
5	3.21	4.93	84.00
5.5	1.96	3.01	87.01
6	1.74	2.68	89.69
6.5	1.48	2.27	91.96
7	1.66	2.56	94.52
7.5	0.76	1.17	95.69
8	0.54	0.83	96.52
8.5	0.56	0.86	97.38
9	0.30	0.46	97.84
9.5	0.27	0.41	98.25
10	0.23	0.36	98.61
10.5	0.32	0.49	99.11
11	0.21	0.32	99.43
11.5	0.19	0.30	99.72
12	0.15	0.23	99.95
12.5	0.02	0.04	99.99
13	0.01	0.01	100.00
Total	65.04	100.00	

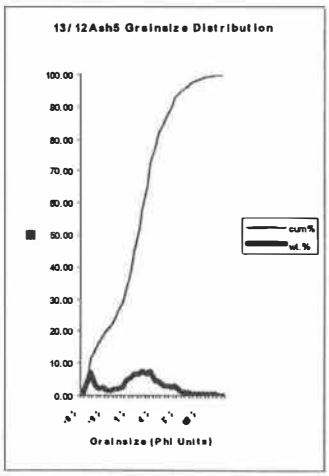

Grainsize Statistics:
Sample 13/12Ash5

Percentiles	***phi***
95	7.73
84	5.36
50	2.40
16	-2.55
5	-3.89

Mean 1.73

Sorting 3.74

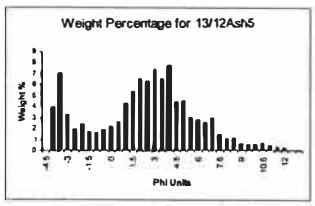

phi	Wt. (g)	Wt.%	Cum.wt.%
-4.5	0.00	0.00	0.00
-4	6.89	3.91	3.91
-3.5	12.54	7.12	11.03
-3	5.67	3.22	14.25
-2.5	3.46	1.96	16.22
-2	4.30	2.44	18.66
-1.5	3.03	1.72	20.38
-1	2.75	1.56	21.94
-0.5	3.30	1.87	23.82
0	3.87	2.20	26.01
0.5	4.63	2.63	28.64
1	7.58	4.30	32.95
1.5	9.56	5.43	38.38
2	11.55	6.56	44.93
2.5	11.17	6.34	51.28
3	12.99	7.38	58.65
3.5	11.48	6.52	65.17
4	13.61	7.73	72.90
4.5	7.81	4.43	77.34
5	7.93	4.50	81.84
5.5	5.24	2.98	84.81
6	4.92	2.80	87.61
6.5	4.39	2.49	90.10
7	5.23	2.97	93.07
7.5	2.52	1.43	94.50
8	1.86	1.06	95.56
8.5	1.98	1.12	96.68
9	1.04	0.59	97.28
9.5	0.93	0.53	97.81
10	0.82	0.47	98.27
10.5	1.08	0.62	98.89
11	0.68	0.38	99.27
11.5	0.61	0.34	99.62
12	0.51	0.29	99.91
12.5	0.12	0.07	99.98
13	0.04	0.03	100.00
Total	176.10	100.00	

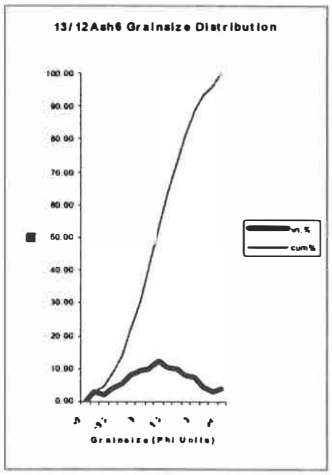

Grainsize Statistics:
Sample 13/12Ash6

Percentiles	***phi***
95	3.83
84	2.68
50	0.89
16	-0.84
5	-1.94

Mean 0.91

Sorting 1.75

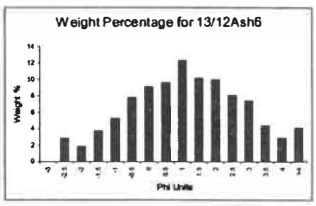

phi	Wt. (g)	Wt.%	Cum.wt.%
-3	0.00	0.00	0.00
-2.5	9.94	2.83	2.83
-2	6.43	1.83	4.67
-1.5	13.15	3.75	8.41
-1	18.53	5.28	13.69
-0.5	27.53	7.85	21.54
0	32.22	9.18	30.72
0.5	33.95	9.68	40.40
1	43.34	12.35	52.75
1.5	35.79	10.20	62.95
2	35.07	10.00	72.95
2.5	28.43	8.10	81.05
3	26.22	7.47	88.52
3.5	15.39	4.39	92.91
4	10.33	2.94	95.85
>4.5	14.55	4.15	99.99
Total	350.87	100.00	

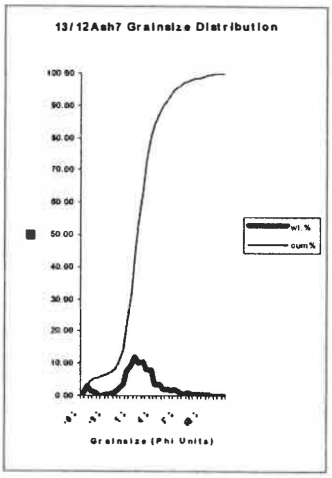

Grainsize Statistics:
Sample 13/12Ash7

Percentiles	***phi***
95	6.95
84	4.44
50	2.32
16	0.65
5	-3.24

Mean 2.47

Sorting 2.49

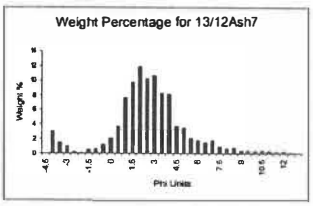

phi	Wt. (g)	Wt.%	Cum.wt.%
-4.5	0.00	0.00	0.00
-4	5.20	3.00	3.00
-3.5	2.59	1.49	4.50
-3	1.75	1.01	5.51
-2.5	0.35	0.20	5.71
-2	0.23	0.13	5.84
-1.5	0.87	0.50	6.34
-1	0.97	0.56	6.90
-0.5	2.01	1.16	8.06
0	3.71	2.14	10.20
0.5	6.47	3.73	13.94
1	13.35	7.70	21.64
1.5	17.00	9.81	31.45
2	20.58	11.88	43.33
2.5	17.85	10.30	53.63
3	18.49	10.67	64.30
3.5	14.32	8.26	72.56
4	14.10	8.14	80.70
4.5	6.45	3.72	84.42
5	6.07	3.50	87.92
5.5	3.58	2.07	89.99
6	3.14	1.81	91.81
6.5	2.68	1.55	93.36
7	3.15	1.82	95.17
7.5	1.56	0.90	96.07
8	1.20	0.69	96.77
8.5	1.37	0.79	97.56
9	0.76	0.44	97.99
9.5	0.69	0.40	98.39
10	0.59	0.34	98.73
10.5	0.76	0.44	99.17
11	0.47	0.27	99.44
11.5	0.43	0.25	99.69
12	0.40	0.23	99.92
12.5	0.10	0.06	99.98
13	0.05	0.03	100.00
Total	173.28	100.00	

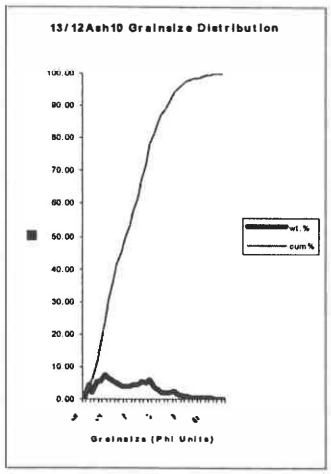

Grainsize Statistics:
Sample 13/12Ash10

Percentiles	***phi***
95	7.39
84	4.86
50	1.09
16	-2.05
5	-3.28

Mean 1.30

Sorting 3.35

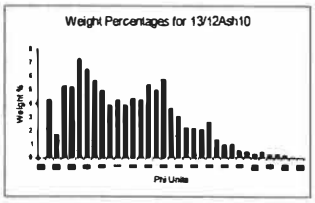

phi	Wt. (g)	Wt.%	Cum.wt.%
-4	0.00	0.00	0.00
-3.5	6.72	4.29	4.29
-3	2.79	1.78	6.07
-2.5	8.30	5.30	11.37
-2	8.21	5.24	16.61
-1.5	11.52	7.35	23.97
-1	10.28	6.56	30.53
-0.5	8.88	5.67	36.20
0	7.78	4.97	41.16
0.5	6.12	3.91	45.07
1	6.62	4.23	49.30
1.5	6.04	3.86	53.15
2	6.91	4.41	57.57
2.5	6.78	4.33	61.89
3	8.49	5.42	67.31
3.5	7.83	5.00	72.31
4	9.04	5.77	78.08
4.5	5.70	3.64	81.72
5	4.83	3.08	84.80
5.5	3.43	2.19	86.99
6	3.44	2.19	89.19
6.5	3.27	2.09	91.28
7	4.15	2.65	93.93
7.5	2.10	1.34	95.27
8	1.58	1.01	96.28
8.5	1.66	1.06	97.34
9	0.83	0.53	97.87
9.5	0.69	0.44	98.31
10	0.56	0.36	98.67
10.5	0.71	0.45	99.12
11	0.46	0.30	99.41
11.5	0.44	0.28	99.70
12	0.37	0.24	99.93
12.5	0.07	0.05	99.98
13	0.02	0.02	100.00
Total	156.64	100.00	

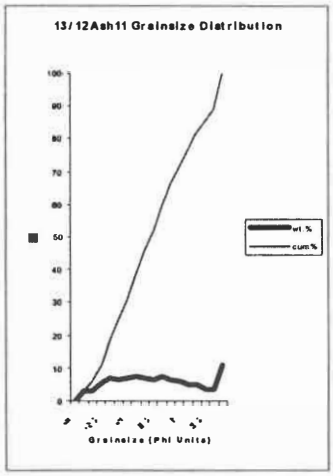

Grainsize Statistics:
Sample 13/12Ash11

Percentiles	***phi***
95	4.60
84	3.28
50	0.35
16	-2.14
5	-3.10

Mean 0.50

Sorting 2.52

phi	Wt. (g)	Wt. %	Cum.wt.%
-4	0.00	0.00	0.00
-3.5	4.19	2.85	2.85
-3	4.25	2.89	5.74
-2.5	7.84	5.34	11.08
-2	10.41	7.09	18.17
-1.5	9.19	6.26	24.42
-1	9.93	6.76	31.18
-0.5	10.60	7.21	38.40
0	10.22	6.96	45.35
0.5	9.63	6.55	51.91
1	11.16	7.60	59.50
1.5	9.65	6.57	66.07
2	8.58	5.84	71.91
2.5	7.28	4.96	76.86
3	7.38	5.02	81.89
3.5	5.38	3.66	85.55
4	5.27	3.59	89.14
>4	15.96	10.86	99.99
Total	146.92	100.00	

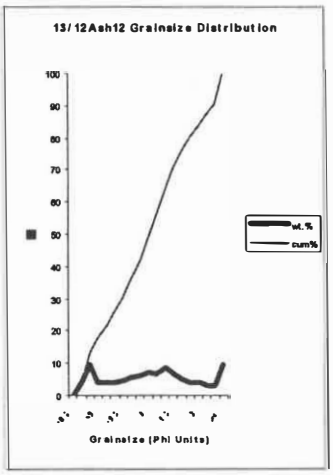

Grainsize Statistics:
Sample 13/12Ash12

Percentiles	***phi***
95	3.27
84	2.00
50	-0.28
16	-3.37
5	-3.97

Mean -0.55

Sorting 2.44

Phi	Wt. (g)	Wt. %	Cum.wt.%
-4.5	0.00	0.00	0.00
-4	10.10	3.90	3.90
-3.5	24.53	9.46	13.36
-3	10.95	4.22	17.58
-2.5	10.87	4.19	21.77
-2	11.02	4.25	26.02
-1.5	11.18	4.31	30.33
-1	14.20	5.48	35.81
-0.5	16.22	6.26	42.07
0	17.94	6.92	48.99
0.5	17.25	6.65	55.64
1	22.17	8.55	64.19
1.5	16.91	6.52	70.71
2	13.47	5.20	75.91
2.5	10.71	4.13	80.04
3	10.45	4.03	84.07
3.5	8.30	3.20	87.27
4	7.91	3.05	90.32
>4	25.10	9.68	100.00
Total	259.28	100.00	

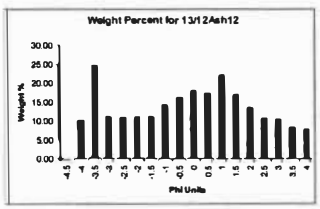

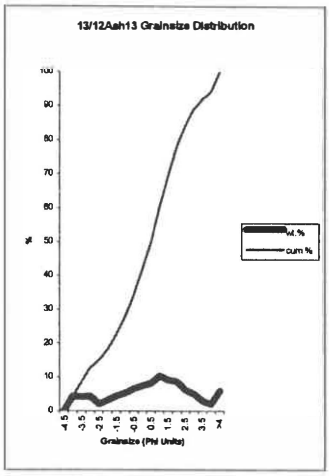

Grainsize Statistics:
Sample 13/12Ash13

Percentiles	***phi***
95	4.02
84	2.48
50	0.50
16	-2.32
5	-3.89

Mean	0.22
Sorting	2.40

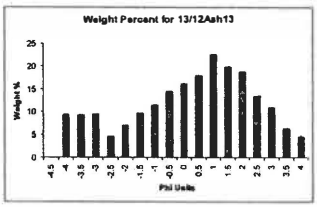

Phi	Wt. (g)	Wt. %	Cum.wt.%
-4.5	0.00	0	0
-4	9.34	4.29	4.29
-3.5	9.23	4.24	8.53
-3	9.39	4.31	12.84
-2.5	4.48	2.06	14.90
-2	6.99	3.21	18.11
-1.5	9.56	4.39	22.50
-1	11.43	5.25	27.75
-0.5	14.38	6.61	34.36
0	16.18	7.43	41.79
0.5	17.87	8.21	50.00
1	22.49	10.33	60.33
1.5	19.84	9.11	69.44
2	18.75	8.61	78.06
2.5	13.39	6.15	84.21
3	10.81	4.97	89.17
3.5	6.20	2.85	92.02
4	4.44	2.04	94.06
>4	12.93	5.94	99.99
Total	217.70	100.00	

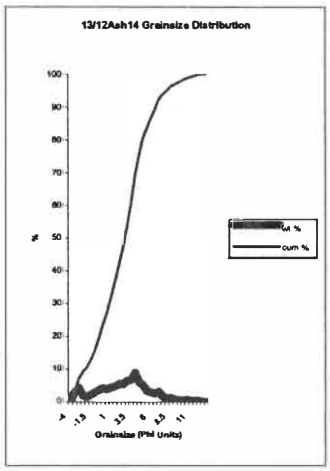

Grainsize Statistics:
Sample 13/12Ash14

Percentiles	***phi***
95	8.02
84	5.56
50	2.71
16	-0.96
5	-3.20

Mean	2.44
Sorting	3.33

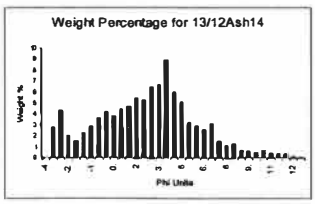

phi	Wt. (g)	Wt.%	Cum.wt.%
-4	0.00	0.00	0.00
-3.5	3.45	2.81	2.81
-3	5.29	4.30	7.11
-2.5	2.45	1.99	9.10
-2	1.84	1.50	10.60
-1.5	2.81	2.29	12.88
-1	3.53	2.87	15.75
-0.5	4.42	3.59	19.35
0	5.21	4.24	23.58
0.5	4.65	3.78	27.36
1	5.46	4.44	31.80
1.5	5.77	4.69	36.50
2	6.71	5.46	41.95
2.5	6.56	5.33	47.29
3	7.98	6.49	53.78
3.5	8.15	6.63	60.40
4	10.92	8.88	69.29
4.5	7.35	5.98	75.26
5	6.31	5.13	80.39
5.5	3.97	3.23	83.62
6	3.62	2.94	86.56
6.5	3.17	2.58	89.14
7	3.80	3.09	92.24
7.5	1.89	1.53	93.77
8	1.44	1.17	94.94
8.5	1.58	1.29	96.23
9	0.85	0.69	96.92
9.5	0.75	0.61	97.53
10	0.64	0.52	98.04
10.5	0.81	0.66	98.71
11	0.51	0.41	99.12
11.5	0.47	0.38	99.50
12	0.44	0.36	99.86
12.5	0.12	0.09	99.95
13	0.06	0.05	100.00
Total	122.97	100.00	

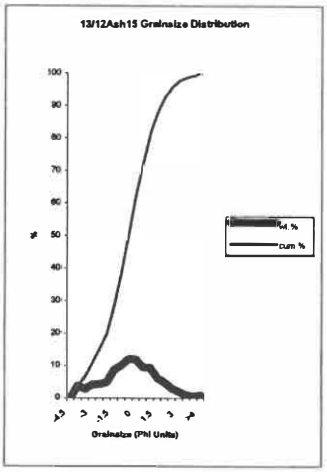

Grainsize Statistics:
Sample 13/12Ash15

Percentiles	***phi***
95	2.39
84	1.18
50	-0.53
16	-2.38
5	-3.76

Mean -0.58

Sorting 1.82

Phi	Wt. (g)	Wt. %	Cum.wt.%
-4.5		0.00	0.00
-4	13.95	3.80	3.80
-3.5	10.13	2.76	6.56
-3	15.09	4.11	10.68
-2.5	15.62	4.26	14.94
-2	17.76	4.84	19.78
-1.5	32.14	8.76	28.54
-1	37.20	10.14	38.68
-0.5	44.23	12.06	50.74
0	43.77	11.93	62.67
0.5	34.84	9.50	72.16
1	34.46	9.39	81.56
1.5	22.80	6.22	87.77
2	17.72	4.83	92.60
2.5	10.91	2.97	95.58
3	7.33	2.00	97.58
3.5	3.40	0.93	98.50
4	2.20	0.60	99.10
>4	3.29	0.90	99.99
Total	366.84	100.00	

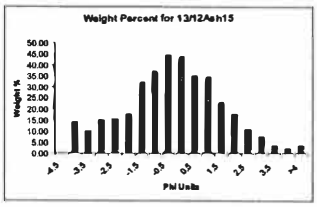

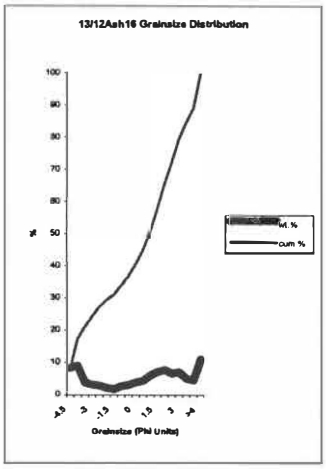

Grainsize Statistics:
Sample 13/12Ash16

Percentiles	***phi***
95	4.08
84	3.45
50	0.92
16	-4.06
5	-4.79

Mean 0.10

Sorting 3.22

Phi	Wt. (g)	Wt. %	Cum.wt.%
-4.5	17.91	8.28	8.28
-4	19.45	8.99	17.26
-3.5	8.20	3.79	21.05
-3	6.88	3.18	24.23
-2.5	6.28	2.90	27.13
-2	4.75	2.19	29.33
-1.5	3.86	1.78	31.11
-1	5.72	2.64	33.75
-0.5	6.56	3.03	36.78
0	8.32	3.84	40.63
0.5	9.36	4.32	44.95
1	13.07	6.04	50.99
1.5	15.34	7.09	58.08
2	16.68	7.71	65.79
2.5	14.35	6.63	72.42
3	15.14	7.00	79.42
3.5	10.90	5.04	84.45
4	9.85	4.55	89.00
>4	23.80	11.00	99.99
Total	216.42	100.00	

APPENDIX III

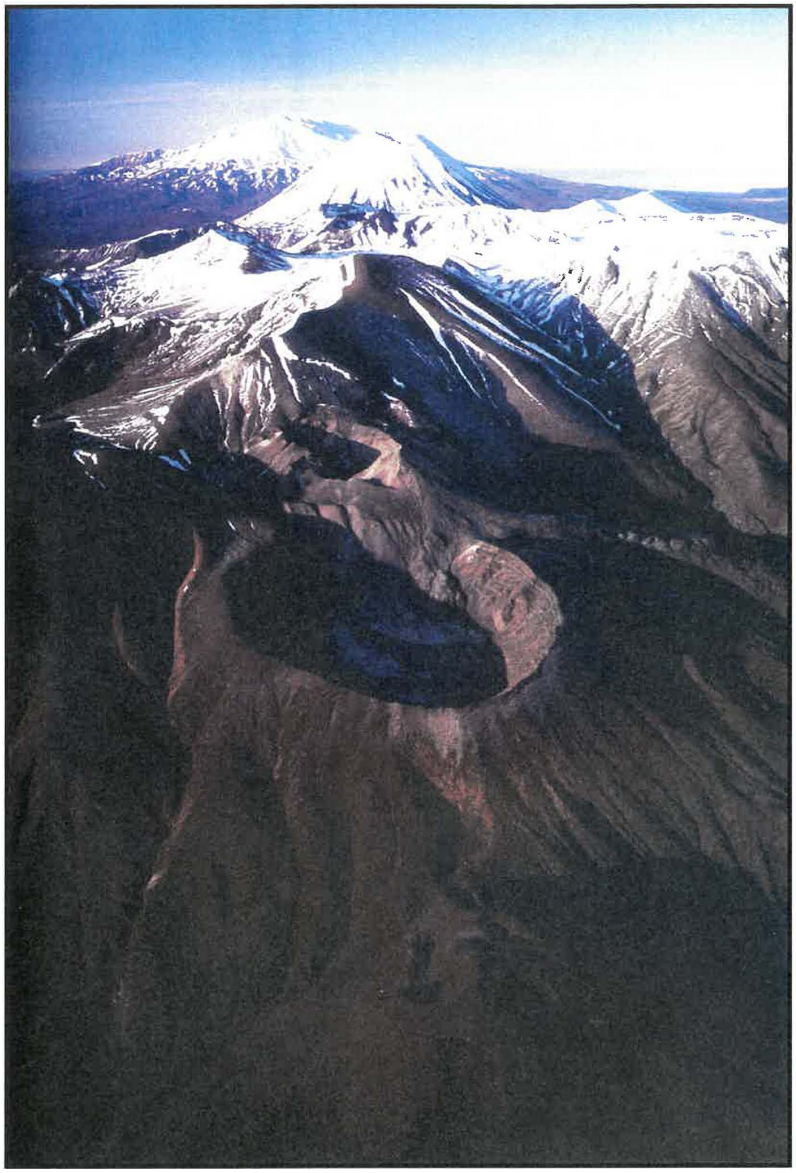

PETROGRAPHY DATA

LIST OF ABBREVIATIONS

Aug	Augite
Hyp	Hypersthene
Oliv	Olivine
Opaq	Opaques
Plag	Plagioclase
Pyx	Pyroxene
Xeno	Xenolith

SAMPLE LOCALITY	UC2 Upper Crater	UC3 Upper Crater	UC4 Upper Crater	UC5 Upper Crater	UC6 Upper Crater
HAND SPECIMEN					
Colour	White/brown/grey	Medium grey/brown	Orange/grey	Orange/yellow/white/purple	
Fabric	Porphyritic	Porphyritic	Porphyritic	Porphyritic	
Crystals visible	Plag, Pyx	Plag, Pyx	Plag, Pyx	Plag, Pyx	
Av. Crystal sizes	1-3 mm	2-3 mm	2-4 mm	2-3 mm	
Grainsize	Medium	Medium	Medium	Medium	Smaller clasts within unconsolidated breccia
Comments	Breccia clast	Breccia clast	Breccia clast	Hydrothermally altered	
THIN SECTION					
Groundmass	Intergranular, hyalopilitic, Plag laths, blebs Pyx	Intergranular, hyalopilitic, Plag laths, blebs Pyx	Intergranular, hyalopilitic, Plag laths, blebs Pyx	Intergranular, hyalopilitic, Plag laths, blebs Pyx	Intergranular, hyalopilitic, Plag laths, blebs Pyx
Phenocrysts	Plag > Hyp > Opaq > Aug > Xeno	Plag > Aug > Hyp > Opaq > Xeno	Plag > Hyp > Aug > Opaq > Xeno	Plag > Hyp > Aug > Opaq > Xeno	Plag > Hyp > Aug > Opaq
Shape	Subhedral to Euhedral	Subhedral to Euhedral	Subhedral to Euhedral	Subhedral to Euhedral	Subhedral to Euhedral
Proportion of crystals (%)	32 > 8 > 2.3 > 1.6 > 1.3	27.6 > 5.3 > 2.6 > 1.6 > 1.3	34.6 > 5 > 4 > 4 > 0.3	28.3 > 8.6 > 6 > 2 > 1	30 > 6.3 > 4.3 > 3.3
Proportion of vesicles	5.3%	5.6%	1.6%	5.3%	6.9%
Comments	Plag twinning, zoning Glomerocrystic	Plag twinning, zoning Glomerocrystic	Plag twinning, zoning Glomerocrystic	Plag twinning, zoning, rims	Plag twinning, zoning Glomerocrystic

SAMPLE LOCALITY	UC7 Upper Crater	UC8 Upper Crater	UC10 Upper Crater	26S10 Lower Crater	26S12 Lower Crater
HAND SPECIMEN					
Colour		Medium grey/orange	Red/brown	Medium grey	Medium grey
Fabric		Porphyritic	Porphyritic	Porphyritic	Porphyritic
Crystals visible		Plag, Pyx	Plag, Pyx	Plag, Pyx	Plag, Pyx
Av. Crystal sizes		2-3 mm	1-2 mm	2-3 mm	2-3 mm
Grainsize	Smaller clasts within	Medium	Medium	Medium	Medium
Comments	unconsolidated breccia	Breccia clast	Breccia		
THIN SECTION					
Groundmass	Intergranular, hyalopilitic, Plag laths, blebs Pyx	Intergranular, hyalopilitic, Plag laths, blebs Pyx	Intergranular, hyalopilitic, Plag laths, blebs Pyx	Intergranular, hyalopilitic, Plag laths, blebs Pyx	Intergranular, hyalopilitic, Plag laths, blebs Pyx
Phenocrysts	Plag > Aug > Hyp > Opaq > Xeno	Plag > Aug > Hyp > Opaq > Xeno	Plag > Hyp > Aug > Opaq	Plag > Hyp > Aug > Xeno	Plag > Hyp > Aug > Opaq > Xeno
Shape	Subhedral to Euhedral	Subhedral to Euhedral	Subhedral to Euhedral	Subhedral to Euhedral	Subhedral to Euhedral
Proportion of crystals (%)	30.3 > 6.3 > 2 > 2 > 3	25.3 > 5.6 > 5 > 3.3 > 3.3	25.6 > 7 > 5 > 3.3	33 > 5 > 3 > 0.3	25.3 > 6.6 > 5.3 > 2.3 > 0.6
Proportion of vesicles	4%	12.6%	2.6%	8%	3.6%
Comments	Plag twinning, zoning Glomerocrystic	Plag twinning, zoning Glomerocrystic	Plag twinning, zoning Glomerocrystic	Plag twinning, zoning Glomerocrystic	Plag twinning, zoning Glomerocrystic

SAMPLE LOCALITY	LC1 Lower Crater	LC2 Lower Crater	LC3 Lower Crater	LC4 Lower Crater	LC5 Lower Crater
HAND SPECIMEN					
Colour	Light grey	Medium grey	Medium grey	Medium grey	Medium grey
Fabric	Porphyritic	Porphyritic	Porphyritic	Porphyritic	Porphyritic
Crystals visible	Plag, Pyx	Plag, Pyx	Plag, Pyx	Plag, Pyx	Plag, Pyx
Av. Crystal sizes	1-3 mm	2-3 mm	2-3 mm	2-3 mm	2-3 mm
Grainsize	Fine to Medium	Medium	Medium	Medium	Medium
Comments					
THIN SECTION					
Groundmass	Intergranular, hyalopilitic, Plag laths, blebs Pyx	Intergranular, hyalopilitic, Plag laths, blebs Pyx	Intergranular, hyalopilitic, Plag laths, blebs Pyx	Intergranular, hyalopilitic, Plag laths, blebs Pyx	Intergranular, hyalopilitic, Plag laths, blebs Pyx
Phenocrysts	Plag > Aug > Hyp > Opaq > Xeno	Plag > Hyp > Aug > Opaq	Plag > Hyp > Aug > Xeno > Opaq	Plag > Hyp > Aug > Opaq	Plag > Hyp > Aug > Opaq > Xeno
Shape	Subhedral to Euhedral	Subhedral to Euhedral	Subhedral to Euhedral	Subhedral to Euhedral	Subhedral to Euhedral
Proportion of crystals (%)	29 > 4.6 > 4.6 > 2.3 > 0.3	32 > 8.3 > 3.6 > 1.3	22 > 6.3 > 2.6 > 2.6 > 1.3	23.3 > 6.6 > 4.3 > 2	31.6 > 7.6 > 2.6 > 2.6 > 0.3
Proportion of vesicles	5%	0%	3.3%	11.3%	3.3%
Comments	Plag twinning, zoning Glomerocrystic	Plag twinning, zoning Glomerocrystic	Plag twinning, zoning Glomerocrystic	Plag twinning, zoning Glomerocrystic	Plag twinning, zoning Glomerocrystic

SAMPLE LOCALITY	LC6 Lower Crater	LC7 Lower Crater	LC8 Lower Crater	LC9 Lower Crater	LC10 Lower Crater
HAND SPECIMEN					
Colour	Light grey	Medium grey	Light grey	Medium grey	Medium grey
Fabric	Porphyritic	Porphyritic	Porphyritic	Porphyritic	Porphyritic
Crystals visible	Plag, Pyx	Plag, Pyx	Plag, Pyx	Plag, Pyx	Plag, Pyx
Av. Crystal sizes	1-3 mm	2-3 mm	1-3 mm	2-3 mm	2-3 mm
Grainsize	Fine to Medium	Medium	Fine to Medium	Medium	Medium
Comments		Vesicular			
THIN SECTION					
Groundmass	Intergranular, hyalopilitic, Plag laths, blebs Pyx	Intergranular, hyalopilitic, Plag laths, blebs Pyx	Intergranular, hyalopilitic, Plag laths, blebs Pyx	Intergranular, hyalopilitic, Plag laths, blebs Pyx	Intergranular, hyalopilitic, Plag laths, blebs Pyx
Phenocrysts	Plag > Hyp > Aug > Opaq	Plag > Hyp > Opaq > Aug	Plag > Hyp > Aug > Xeno > Opaq	Plag > Hyp > Opaq > Aug	Plag > Hyp > Opaq > Aug > Xeno
Shape	Subhedral to Euhedral	Subhedral to Euhedral	Subhedral to Euhedral	Subhedral to Euhedral	Subhedral to Euhedral
Proportion of crystals (%)	30.6 > 5.6 > 3 > 2 > 0.3	27.6 > 6.6 > 2.3 > 2	23.3 > 8 > 3.6 > 2.6 > 0.6	33 > 5.6 > 2.6 > 1.6	32.6 > 6 > 2.3 > 1.3 > 0.3
Proportion of vesicles	5%	7.3%	3.5%	6.6%	4.6%
Comments	Plag twinning, zoning Glomerocrystic	Plag twinning, zoning Glomerocrystic	Plag twinning, zoning Glomerocrystic	Plag twinning, zoning Glomerocrystic	Plag twinning, zoning Glomerocrystic

SAMPLE LOCALITY	LC11 Lower Crater	LC12 Lower Crater	LC13 Lower Crater	LC14 Lower Crater	LC15 Lower Crater
HAND SPECIMEN					
Colour	Light grey	Medium grey	Light grey	Light grey	Medium grey
Fabric	Porphyritic	Porphyritic	Porphyritic	Porphyritic	Porphyritic
Crystals visible	Plag, Pyx	Plag, Pyx	Plag, Pyx	Plag, Pyx	Plag, Pyx
Av. Crystal sizes	2-3 mm	2-3 mm	1-3 mm	1-3 mm	2-3 mm
Grainsize	Medium	Medium	Fine to Medium	Fine to Medium	Medium
Comments					Vesicular
THIN SECTION					
Groundmass	Intergranular, hyalopilitic, Plag laths, blebs Pyx	Intergranular, hyalopilitic, Plag laths, blebs Pyx	Intergranular, hyalopilitic, Plag laths, blebs Pyx	Intergranular, hyalopilitic, Plag laths, blebs Pyx	Intergranular, hyalopilitic, Plag laths, blebs Pyx
Phenocrysts	Plag > Hyp > Opaq > Aug	Plag > Hyp > Aug > Opaq	Plag > Hyp > Opaq > Aug	Plag > Hyp > Aug > Opaq > Xeno	Plag > Hyp > Opaq > Aug
Shape	Subhedral to Euhedral	Subhedral to Euhedral	Subhedral to Euhedral	Subhedral to Euhedral	Subhedral to Euhedral
Proportion of crystals (%)	28.3 > 6.3 > 2.6 > 2	29.3 > 6 > 3.3 > 2.6	28 > 5 > 2.6 > 2.3	26 > 7.3 > 4.6 > 3 > 1.6	30.6 > 8 > 2.3 > 2
Proportion of vesicles	6%	7.6%	1%	1.6%	8.3%
Comments	Plag twinning, zoning Glomerocrystic	Plag twinning, zoning Glomerocrystic	Plag twinning, zoning Glomerocrystic	Plag twinning, zoning Glomerocrystic	Plag twinning, zoning Glomerocrystic

SAMPLE LOCALITY	LC16 Lower Crater	LC17 Lower Crater	LC18 Lower Crater	LC19 Lower Crater	LC10 Lower Crater
HAND SPECIMEN					
Colour	Medium grey	Medium grey	Light grey	Medium grey	Medium grey
Fabric	Porphyritic	Porphyritic	Porphyritic	Porphyritic	Porphyritic
Crystals visible	Plag, Pyx	Plag, Pyx	Plag, Pyx	Plag, Pyx	Plag, Pyx
Av. Crystal sizes	2-3 mm	2-3 mm	1-3 mm	2-3 mm	2-3 mm
Grainsize	Medium	Medium	Fine to Medium	Medium	Medium
Comments	Vesicular				Vesicular
THIN SECTION					
Groundmass	Intergranular, hyalopilitic, Plag laths, blebs Pyx	Intergranular, hyalopilitic, Plag laths, blebs Pyx	Intergranular, hyalopilitic, Plag laths, blebs Pyx	Intergranular, hyalopilitic, Plag laths, blebs Pyx	Intergranular, hyalopilitic, Plag laths, blebs Pyx
Phenocrysts	Plag > Hyp > Opaq > Aug > Xeno	Plag > Hyp > Aug > Opaq	Plag > Hyp > Opaq > Aug	Plag > Hyp > Opaq > Aug	Plag > Hyp > Aug > Opaq
Shape	Subhedral to Euhedral	Subhedral to Euhedral	Subhedral to Euhedral	Subhedral to Euhedral	Subhedral to Euhedral
Proportion of crystals (%)	31.3 > 6.3 > 2.6 > 2.3 > 0.3	28.3 > 8.6 > 3.3 > 2.6	25.6 > 5.3 > 3.3 > 1.6	33 > 5.6 > 2.6 > 1.6	25.6 > 8 > 3 > 3
Proportion of vesicles	14%	7.6%	7.3%	6.6%	15%
Comments	Plag twinning, zoning Glomerocrystic	Plag twinning, zoning Glomerocrystic	Plag twinning, zoning Glomerocrystic	Plag twinning, zoning Glomerocrystic	Plag twinning, zoning Glomerocrystic

SAMPLE LOCALITY	RLF1 1500 AD Lava Flow	RLF2 1500 AD Lava Flow	RLF3 1500 AD Lava Flow	RLF4 1500 AD Lava Flow	RLF5 1500 AD Lava Flow
HAND SPECIMEN					
Colour	Red/grey	Dark grey	Dark grey	Dark grey	Medium grey
Fabric	Porphyritic	Porphyritic	Porphyritic	Porphyritic	Porphyritic
Crystals visible	Plag, Pyx	Plag, Pyx	Plag, Pyx	Plag, Pyx	Plag, Pyx
Av. Crystal sizes	2-3 mm	2-4 mm	2- 5 mm	2-4 mm	2-3 mm
Grainsize	Medium	Medium	Medium	Medium	Medium
Comments	Vesicular		Vesicular		Vesicular
THIN SECTION					
Groundmass	Intergranular, hyalopilitic, Plag laths, blebs Pyx, Oliv	Intergranular, hyalopilitic, Plag laths, blebs Pyx, Oliv	Intergranular, hyalopilitic, Plag laths, blebs Pyx, Oliv	Intergranular, hyalopilitic, Plag laths, blebs Pyx, Oliv	Intergranular, hyalopilitic, Plag laths, blebs Pyx, Oliv
Phenocrysts	Plag > Aug > Hyp > Opaq	Plag > Aug > Hyp > Opaq > Xeno	Plag > Aug > Hyp > Opaq > Xeno	Plag > Hyp > Opaq > Aug	Plag > Aug > Xeno > Hyp > Opaq
Shape	Subhedral to Euhedral	Subhedral to Euhedral	Subhedral to Euhedral	Subhedral to Euhedral	Subhedral to Euhedral
Proportion of crystals (%)	31.6 > 4.6 > 4 > 3.6	30 > 5.3 > 5.3 > 4.3 > 0.3	29.6 > 9 > 7 > 4 > 0.3	33 > 5.6 > 2.6 > 1.6	28.3 > 8.6 > 7.3 > 4.6 > 3.3
Proportion of vesicles	17.3%	7.6%	12%	6.6%	11.6%
Comments	Plag twinning, zoning Glomerocrystic	Plag twinning, zoning Glomerocrystic	Plag twinning, zoning Glomerocrystic	Plag twinning, zoning Glomerocrystic	Plag twinning, zoning Glomerocrystic

SAMPLE LOCALITY	RLF6 1500 AD Lava Flow	RLF7 1500 AD Lava Flow	RLF8 1500 AD Lava Flow	RLF9 1500 AD Lava Flow	RLF10 1500 AD Lava Flow
HAND SPECIMEN					
Colour	Dark grey	Dark grey/red	Dark grey	Dark grey	Dark grey
Fabric	Porphyritic	Porphyritic	Porphyritic	Porphyritic	Porphyritic
Crystals visible	Plag, Pyx	Plag, Pyx	Plag, Pyx	Plag, Pyx	Plag, Pyx
Av. Crystal sizes	2-4 mm	2-5 mm	2-3 mm	2-4 mm	2-4 mm
Grainsize	Medium	Medium	Medium	Medium	Medium
Comments				Very weathered, rubbly surface	Vesicular
THIN SECTION					
Groundmass	Intergranular, hyalopilitic, Plag laths, blebs Pyx, Oliv	Intergranular, hyalopilitic, Plag laths, blebs Pyx, Oliv	Intergranular, hyalopilitic, Plag laths, blebs Pyx, Oliv	Intergranular, hyalopilitic, Plag laths, blebs Pyx, Oliv	Intergranular, hyalopilitic, Plag laths, blebs Pyx, Oliv
Phenocrysts	Plag > Aug > Opaq > Hyp	Plag > Aug > Hyp > Opaq > Oliv	Plag > Hyp > Aug > Opaq > Xeno	Plag > Hyp > Aug > Xeno > Opaq	Plag > Aug > Opaq > Hyp > Oliv > Xeno
Shape	Subhedral to Euhedral	Subhedral to Euhedral	Subhedral to Euhedral	Subhedral to Euhedral	Subhedral to Euhedral
Proportion of crystals (%)	25 > 6 > 3.3 > 2.6	25 > 6 > 4.6 > 2.6 > 1.4	26.6 > 7 > 4.6 > 4 > 0.3	26 > 5 > 4.3 > 4 > 1.6	22 > 5.6 > 3.6 > 2.6 > 2 > 0.3
Proportion of vesicles	6.6%	7.6%	10.3%	17%	17.3%
Comments	Plag twinning, zoning Glomerocrystic	Plag twinning, zoning Glomerocrystic	Plag twinning, zoning Glomerocrystic	Plag twinning, zoning Glomerocrystic	Plag twinning, zoning Glomerocrystic

SAMPLE LOCALITY	RLF11 1500 AD Lava Flow	RLF12 1500 AD Lava Flow	RLF13 1500 AD Lava Flow	RLF14 1500 AD Lava Flow	RLF15 1500 AD Lava Flow
HAND SPECIMEN					
Colour	Red	Dark grey/red	Dark grey	Dark grey	Dark grey
Fabric	Porphyritic	Porphyritic	Porphyritic	Porphyritic	Porphyritic
Crystals visible	Plag, Pyx	Plag, Pyx	Plag, Pyx	Plag, Pyx	Plag, Pyx
Av. Crystal sizes	2-4 mm	2-4 mm	2-5 mm	2-3 mm	2-4 mm
Grainsize	Medium	Medium	Medium	Medium	Medium
Comments	Vesicular and crumbly	Vesicular	Vesicular		Vesicular
THIN SECTION					
Groundmass	Intergranular, hyalopilitic, Plag laths, blebs Pyx, Oliv	Intergranular, hyalopilitic, Plag laths, blebs Pyx, Oliv	Intergranular, hyalopilitic, Plag laths, blebs Pyx, Oliv	Intergranular, hyalopilitic, Plag laths, blebs Pyx, Oliv	Intergranular, hyalopilitic, Plag laths, blebs Pyx, Oliv
Phenocrysts	Plag > Aug > Hyp > Opaq	Plag > Hyp > Aug > Opaq > Oliv > Xeno	Plag > Aug > Hyp > Opaq	Plag > Hyp > Aug > Opaq > Xeno	Plag > Aug > Hyp > Opaq > Xeno
Shape	Subhedral to Euhedral	Subhedral to Euhedral	Subhedral to Euhedral	Subhedral to Euhedral	Subhedral to Euhedral
Proportion of crystals (%)	14 > 3.6 > 3.3 > 3	28.6 > 4.3 > 3.3 > 2 > 1.2 > 0.3	17.6 > 4.3 > 4.3 > 2	30.6 > 7.6 > 5.3 > 1 > 0.6	22.3 > 5.3 > 4.6 > 1.6 > 0.3
Proportion of vesicles	29.3%	15.3%	19.2%	1.3%	21%
Comments	Plag twinning, zoning Glomerocrystic	Plag twinning, zoning Glomerocrystic	Plag twinning, zoning Glomerocrystic	Plag twinning, zoning Glomerocrystic	Plag twinning, zoning Glomerocrystic

SAMPLE LOCALITY	RLF16 1500 AD Lava Flow	LFF1 1500 AD Lava Flow	LFF2 1500 AD Lava Flow	LFF2 1500 AD Lava Flow	LFF3 1500 AD Lava Flow
HAND SPECIMEN					
Colour	Dark grey/red	Dark grey	Dark grey	Dark grey	Medium grey
Fabric	Porphyritic	Porphyritic	Porphyritic	Porphyritic	Porphyritic
Crystals visible	Plag, Pyx	Plag, Pyx	Plag, Pyx	Plag, Pyx	Plag, Pyx
Av. Crystal sizes	2-4 mm	2-4 mm	2-5 mm	2-5 mm	2-4 mm
Grainsize	Medium	Medium	Medium	Medium	Medium
Comments	Vesicular				
THIN SECTION					
Groundmass	Intergranular, hyalopilitic, Plag laths, blebs Pyx, Oliv	Intergranular, hyalopilitic, Plag laths, blebs Pyx, Oliv	Intergranular, hyalopilitic, Plag laths, blebs Pyx, Oliv	Intergranular, hyalopilitic, Plag laths, blebs Pyx, Oliv	Intergranular, hyalopilitic, Plag laths, blebs Pyx, Oliv
Phenocrysts	Plag > Xeno > Hyp > Opaq > Aug	Plag > Aug > Hyp > Opaq > Oliv	Xeno > Plag > Aug > Hyp > Opaq > Oliv	Plag > Aug > Hyp > Oliv >Opaq	Plag > Aug > Oliv > Hyp > Opaq
Shape	Subhedral to Euhedral	Subhedral to Euhedral	Subhedral to Euhedral	Subhedral to Euhedral	Subhedral to Euhedral
Proportion of crystals (%)	20.3 > 16.3 > 5.3 > 5.3 > 2.6	24 > 7.6 > 3.6 > 2 > 1.3	13.6 > 11.6 > 6.6 > 3.3 > 3.3 > 1	19.6 > 8 > 2.3 > 2 > 1.3	19 > 8.6 > 3 > 2.3 > 1.3
Proportion of vesicles	23%	5%	9.3%	15.3%	17%
Comments	Plag twinning, zoning Glomerocrystic	Plag twinning, zoning Glomerocrystic	Plag twinning, zoning Glomerocrystic	Plag twinning, zoning Glomerocrystic	Plag twinning, zoning Glomerocrystic

SAMPLE LOCALITY	EC1 Northern Craters	EC2 Northern Craters	EC3 Northern Craters	EC4 Northern Craters	
HAND SPECIMEN					
Colour	Medium grey	Dark grey	Medium grey	Medium to Dark grey	
Fabric	Porphyritic	Porphyritic	Porphyritic	Porphyritic	
Crystals visible	Plag, Pyx	Plag, Pyx	Plag, Pyx	Plag, Pyx	
Av. Crystal sizes	2-4 mm	2-4 mm	2-3 mm	2-3 mm	
Grainsize	Medium	Medium	Medium	Medium	
Comments		Vesicular	Vesicular		
THIN SECTION					
Groundmass	Intergranular, hyalopilitic, Plag laths, blebs Pyx	Intergranular, hyalopilitic, Plag laths, blebs Pyx	Intergranular, hyalopilitic, Plag laths, blebs Pyx	Intergranular, hyalopilitic, Plag laths, blebs Pyx	
Phenocrysts	Plag > Hyp > Aug > Opaq	Plag > Hyp > Aug > Opaq	Plag > Hyp > Aug > Opaq	Plag > Hyp > Aug > Opaq	
Shape	Subhedral to Euhedral	Subhedral to Euhedral	Subhedral to Euhedral	Subhedral to Euhedral	
Proportion of crystals (%)	26.3 > 6.6 > 5 > 2	31.6 > 5 > 3.6 > 2	23.3 > 5.3 > 2.6 > 1.3	32.3 > 6.3 > 4 > 1.3	
Proportion of vesicles	6%	12.6%	19.6%	8%	
Comments	Plag twinning, zoning Glomerocrystic	Plag twinning, zoning Glomerocrystic	Plag twinning, zoning Glomerocrystic	Plag twinning, zoning Glomerocrystic	

APPENDIX IV

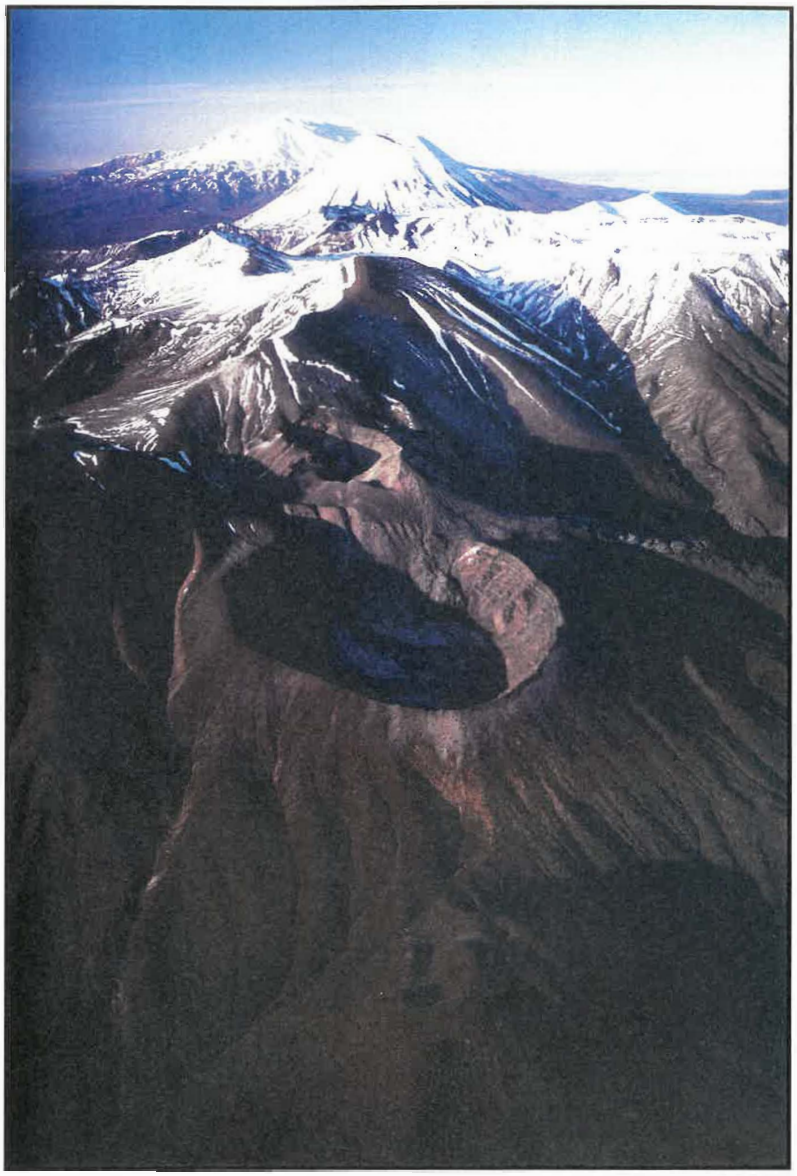

LOWER CRATER SAMPLE SITES

Lower Te Maari Crater sample sites (LC)

Southwest wall

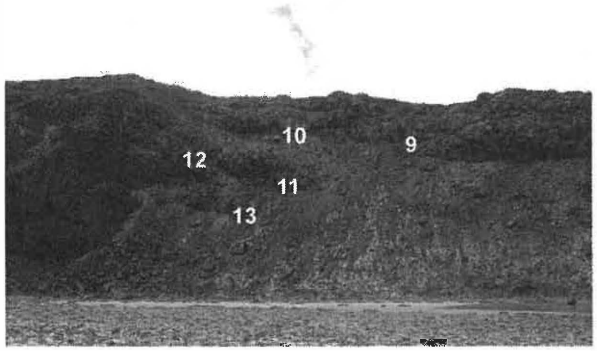

West wall

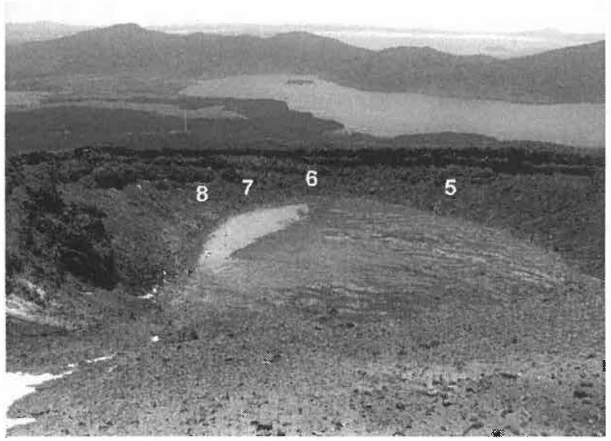

North wall

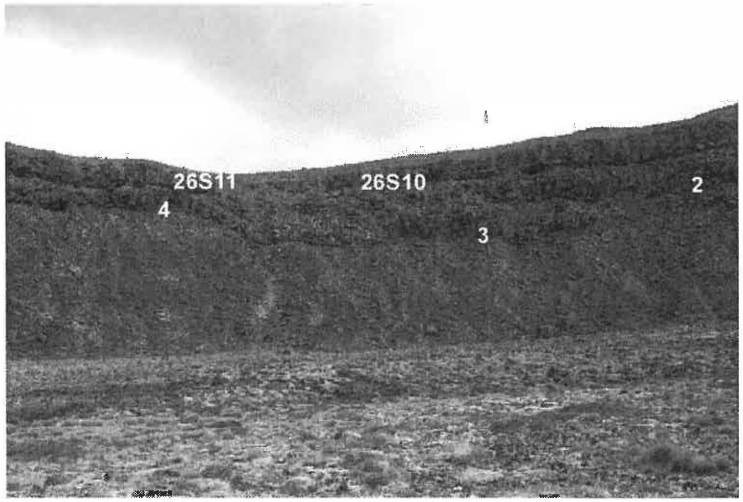

East wall

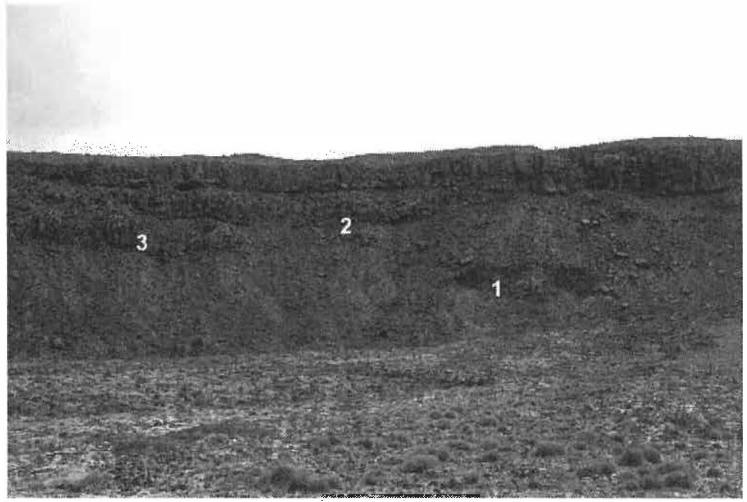

Southeast wall

APPENDIX V

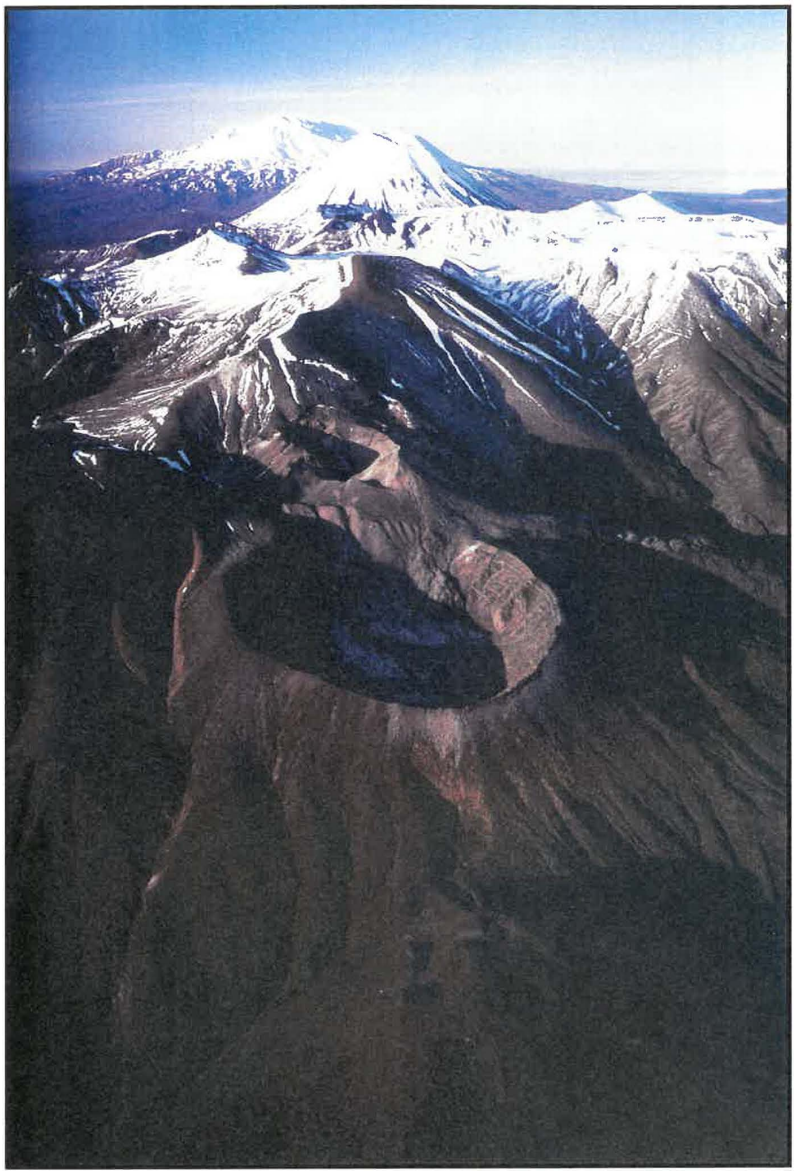

HYDROTHERMAL LOCATIONS


N
Legend
Steamy Areas
0 0.05 0.1 0.2 Kilometres